AD_____

Award Number: DAMD17-99-1-9213

TITLE: Developing Novel Anticancer DNA-binding Drugs to Disrupt ETS-mediated Transcription Associated With Breast Cancer: Use of the c-fos Serum Response Element as a Model System

PRINCIPAL INVESTIGATOR: Christine M. White

CONTRACTING ORGANIZATION: Health Research Incorporated
Buffalo, New York 14263

REPORT DATE: June 2002

TYPE OF REPORT: Annual Summary

PREPARED FOR: U.S. Army Medical Research and Materiel Command
Fort Detrick, Maryland 21702-5012

REPORT DOCUMENTATION PAGE

Form Approved
OMB No. 074-0188

1. AGENCY USE ONLY (Leave blank)	2. REPORT DATE	3. REPORT TYPE AND DATES COVERED
	June 2002	Annual Summary (15 May 99 - 14 May 02)

4. TITLE AND SUBTITLE
Developing Novel Anticancer DNA-binding Drugs to Disrupt ETS-mediated Transcription Associated With Breast Cancer: Use of the c-fos Serum Response Element as a Model System

5. FUNDING NUMBERS
DAMD17-99-1-9213

6. AUTHOR(S)
Christine M. White

7. PERFORMING ORGANIZATION NAME(S) AND ADDRESS(ES)
Health Research Incorporated
Buffalo, New York 14263

E-Mail: chrissyberry99@hotmail.com

8. PERFORMING ORGANIZATION REPORT NUMBER

9. SPONSORING / MONITORING AGENCY NAME(S) AND ADDRESS(ES)
U.S. Army Medical Research and Materiel Command
Fort Detrick, Maryland 21702-5012

10. SPONSORING / MONITORING AGENCY REPORT NUMBER

11. SUPPLEMENTARY NOTES

12a. DISTRIBUTION / AVAILABILITY STATEMENT
Approved for Public Release; Distribution Unlimited

12b. DISTRIBUTION CODE

13. Abstract ***(Maximum 200 Words)***

Disregulated transcription factor (TF)-mediated activation of gene expression can play a key role in oncogenesis, especially in breast cancer. Preventing TF/DNA interactions using small molecule DNA-reactive agents may decrease oncogenic gene expression and potentially halt cancer development. Our goal is to improve DNA-binding drugs' abilities to inhibit specific TF/DNA interactions using the human c-fos promoter's serum response element (SRE) as a target. In an effort to improve drug effectiveness, the novel minor groove-binding fluorescent microgonotropens (FMGTs) were developed. These A/T selective bisbenzimidazole-based agents have polyamine tails that contact DNA's phosphodiester backbone, allowing them to bind with very high affinity. We explored the potential of these agents to inhibit TF/DNA complex formation in a series of increasingly complex assays in the c-fos model and assessed whether their ability to contact both grooves makes them more effective than classical minor groove-binding drugs. Analyzing these agents using a well-defined gene regulatory element has provided insight into the relationship between their chemical structure and biological activities. Notably, our studies revealed that one agent, L2, was the only FMGT to inhibit endogenous c-fos gene expression. L2 is therefore a promising lead candidate for future drug design studies.

14. Subject Terms

Breast Cancer	DNA-binding drugs	DNA
Oncogenic gene expression	Anticancer drugs	
Ets transcription factors	c-fos	

15. NUMBER OF PAGES
56

16. PRICE CODE

17. SECURITY CLASSIFICATION OF REPORT	18. SECURITY CLASSIFICATION OF THIS PAGE	19. SECURITY CLASSIFICATION OF ABSTRACT	20. LIMITATION OF ABSTRACT
Unclassified	Unclassified	Unclassified	Unlimited

Table of Contents

Introduction

Disregulated gene expression, which may contribute to the development and progression of various diseases, including breast cancer, often occurs at the level of transcription. This aberrant transcription may result from the inappropriate binding of transcription factors (TFs) to their target DNA sequences in gene promoters (1). For example, overexpression of certain *ets* family TFs, such as PEA3 and ESX, is associated with early stage breast cancer development and the upregulation of Her2/Neu, a receptor tyrosine kinase overexpressed in nearly 30% of breast cancer cases (2, 3). Disrupting specific TF/DNA complexes on key growth-controlling genes may inhibit cancer development and progression and is therefore a desirable first step in the design of therapeutically useful agents (4). While classical DNA-binding drugs, such as the A/T selective minor groove binders distamycin or Hoechst 33342, can inhibit TF/DNA complex formation through steric hindrance and deformation of the DNA helix, such agents lack specificity (5, 6). Since they bind to many sites on DNA, they inhibit general transcription and disrupt other template related activities, leading to significant toxicity in both normal and cancer cells. Our studies focus on evaluating DNA-binding drugs as inhibitors of TF/DNA complex formation in order to identify agents with enhanced sequence selectivity, potency and cellular activity; a key step in using such agents to understand and modify regulation of gene expression or even as an ultimate basis for the development of therapeutics. We chose the well-defined human c-fos serum response element (SRE) as a model system to study drug effects on TF/DNA complexes and resultant transcription and to develop paradigms for drug targeting in increasingly complex assay environments. The binding of serum response factor (SRF) to an A/T rich site and the subsequent recruitment of the *ets* TF Elk-1 to a GGA core sequence provide the opportunity to study drug effects on these TFs separately or the resulting ternary complex as a whole (see manuscript 1 in Appendix III) (7). In an effort to improve drug potency, the novel, rationally designed DNA-binding microgonotropens (MGTs) were developed in collaboration with Dr. Thomas C. Bruice at the University of Santa Barbara, California (8, 9). These agents have an A/T selective, minor groove-binding polypyrrole or bisbenzimidazole backbone attached to a major groove-associating polyamine tail (see Fig. 1 in Appendix II). The c-fos SRE model was used to explore the potential of these agents as inhibitors of TF/DNA complex formation and assessed whether their ability to contact both grooves makes them more effective than their classical minor groove-binding parent compounds, Hoechst 33342 and Hoechst 33258 (see manuscript 3 in Appendix V). The inability of this generation of compounds to inhibit gene expression in whole cells led to the creation of new MGTs in which polyamine tails were linked to N-methyl pyrrole moieties (see manuscript 4 in Appendix VI). One compound, **L2**, possessed enhanced potency and cellular activity. Our systematic evaluation provides insight into structure/activity relationships that can potentially be used to make further, strategic improvements to the chemical design of the MGTs and make them more effective inhibitors of gene expression.

Summary of Research and Training

Background / Aims:

The SRE of the human c-fos promoter provides a well-characterized system that can be used to develop paradigms for selective targeting of oncogenic gene promoters with small molecule DNA-binding agents. The binding of SRF and Elk-1 to A/T rich and mixed sequences, respectively, and their mode of binding to DNA (primary interactions in the major groove coupled with minor groove contacts) are amenable to our drug targeting strategies and allow us to study drug effects on more than one TF in a single system in increasingly complex environments. Ultimately, such knowledge may be used to disrupt aberrant TF-driven gene expression in breast cancer.

The aims set forth in my original proposal were:

AIM 1: Evaluate the ability of DNA-binding drugs to disrupt TF complex formation on the SRE. Prevention or disruption of TF/DNA complexes under simple conditions consisting of purified TFs, DNA, and drug are quantitated using electrophoretic mobility shift assays (EMSAs), while DNA footprinting studies assess where the drugs bind.

AIM 2: Evaluate the ability of DNA-binding drugs to inhibit c-fos driven gene expression in cell-free transcription assays. Drugs are added to a linearized plasmid in the presence of a nuclear extract and radiolabeled nucleotides. The resulting radiolabeled transcript that is produced can be quantitated using autoradiography and densitometry. The presence of a higher amount of DNA with greater sequence complexity as well as additional proteins provides a more complex assay environment.

AIM 3: Evaluate the ability of DNA-binding drugs to inhibit gene expression from the c-fos promoter in a cellular system. Cells are transiently transfected with a luciferase reporter plasmid in addition to SRF and Elk-1 expressing constructs before being treated with drugs. Inhibition of gene expression is analyzed by quantitating luciferase activity. The intact, cellular environment provides the most rigorous conditions – the full complement of cellular proteins and DNA in its native, histone bound conformation in the nucleus.

****Alterations to original aims****: Deviations from these original aims and the statement of work are addressed on page 10.

Materials and Methods/Protocol Development:

The SRE of the human c-fos promoter was first established as a model system to study, understand, and develop paradigms for drug targeting of TF/DNA complexes in cell-free and cellular assays. The details of this work have been published (see manuscript 1 in Appendix III). In brief, the ability of DNA-binding drugs to inhibit TF complex formation on the SRE was assessed in EMSAs. The c-fos promoter-driven cell-free transcription assay analyzed drug effects in a more complicated environment. Effects of agents on endogenous c-fos expression in whole cells were assessed using Northern blot assays. Cytotoxicity and RNA synthesis assays determined how drugs affected cells in general. The IC_{50} values (the concentration of drug needed to inhibit the observed activity by 50%) were used to compare drug potencies in each assay.

We also wished to determine if drugs could disrupt other DNA-template activities in a nuclear environment and whether this activity correlated to the EMSA or cell-free transcription assay results. Therefore, in addition to these methods, an additional assay was established to assess

drug effects on topoisomerase II (topo II) activity in isolated nuclei. As an enzymatic mediator of DNA topology, topo II associates with DNA and nicks both strands, becoming covalently bound to the free DNA ends in a "cleavable complex." After cellular DNA is labeled with [^{14}C]-thymidine and nuclei are isolated, covalent topo II/DNA complexes are induced by the epipodophyllotoxin VM-26 (10). These cleavable complexes are then precipitated in the presence of sodium dodecyl sulfate and quantitated through scintillation counting. In the presence of minor groove-binding agents such as Hoechst 33342, cleavable complex formation is inhibited (11). This assay provides a more complex environment than cell-free assays, but barriers to drug uptake do not exist and DNA-template effects can therefore be measured directly. Detailed protocols for this and the aforementioned assays are provided in the attached manuscripts in Appendices III and V.

In my last summary, I reported on the evaluation of a series of classical DNA-binding drugs with contrasting sequence selectivities and modes of binding. This work, which furthered understanding on how the DNA-binding characteristics of drugs influence their ability to inhibit transcription, has since been published in *Biochemistry* (see Appendix III). The c-fos model is now being employed to analyze novel, rationally-designed DNA-binding agents as described below.

Summary of Findings and Results:

Part 1: Evaluation of classical DNA-binding drugs and establishment of the c-fos SRE as a model system. To our knowledge, this was the first study to systematically analyze the ability of drugs possessing different sequence selectivities and modes of binding to target two different TF binding motifs in increasingly complex assays. The commercially available compounds chromomycin, Hoechst 33342, and nogalamycin were chosen for analysis (see manuscript 1 in Appendix III). Our findings demonstrated how the DNA-characteristics of these agents were related to their biological effects on a particular gene and also provided a standard to which novel compounds could be compared. Findings from this study include:

- **Drug potencies in EMSAs were not predictive for potencies in the remaining assays.** The order of potency in the EMSAs was: nogalamycin > Hoechst 33342 > chromomycin. For the cell-free transcription assay, Northern blot analyses of endogenous c-fos expression, cytotoxicity studies, and assessments of total cellular RNA synthesis, the order of potency was: chromomycin > nogalamycin > Hoechst 33342.

- **The potency of a DNA-binding compound does not depend solely upon its sequence preference or mode of binding.**
While Hoechst 33342, an A/T rich binder, was predicted to be a potent inhibitor of SRF/DNA interactions, it had a high IC_{50} value compared to the other compounds. Surrounding base pairs may influence DNA conformation and affect the ability of an agent to efficiently recognize and bind its target.

- **Chromomycin was the most potent inhibitor of endogenous c-fos gene expression and also worked the most quickly.**
A 40% inhibition of c-fos expression was achieved after just 40 minutes, suggesting that chromomycin rapidly enters cells.

- **The effects of these agents on gene expression may be associated with their toxicity.**

The IC_{50} values for the cytotoxicity, total RNA synthesis and Northern blot assays were similar (See Appendix III, manuscript 1, Table 1) suggesting that the toxic effects of the agents stem from their non-specific inhibition of the expression of many different genes.

Part 2: Evaluation of the fluorescent microgonotropens (FMGTs).

Most TFs, including SRF and Elk-1, primarily interact with the major groove of DNA but may gain increased specificity through minor groove contacts (12, 13). With their ability to approach the helix from the opposite groove and alter DNA conformation, minor groove-binding drugs can inhibit major groove-binding TFs from binding their target sites (14). However, drugs that contact both grooves with high affinity have the potential to more effectively inhibit a wider range of TFs. The MGTs, developed by the Bruice lab, were designed with this goal in mind. They consist of minor groove-binding backbones equipped with major groove-associating functional groups. The first MGTs were based on a polypyrrole structure, similar to distamycin (see Fig. 1 in Appendix II). Polyamine tails extending from the central pyrrole electrostatically interact with the phosphodiester backbone of DNA, allowing these compounds to bind with affinities equal to or greater than those of TFs and resulting in significant bending of the helix (8). These agents were orders of magnitude more potent than distamycin in inhibiting the E2F1 TF from binding to its target promoter site. This success spurred investigation of whether other minor groove-binding agents could be equipped with major groove-binding moieties and whether such additions improved their ability to inhibit TF/DNA interactions. The bisbenzimidazole backbone of the Hoechst family of A/T selective minor groove-binding drugs was therefore attached equipped with polyamine tails to yield FMGTs (structures are shown in Appendix V, manuscript 3, Fig. 2) (9, 15). These agents are capable of forming 2:1 complexes on DNA with up to five fold higher affinity than Hoechst 33258. FMGTs with polyamine tails of varying lengths and degrees of branching were synthesized and evaluated for their ability to inhibit TF/DNA interactions using the c-fos model. Notable findings from this published study include:

- **The potencies of FMGT-1, FMGT-2 and FMGT-3 in inhibiting TF complex formation in EMSAs were approximately an order of magnitude greater than their parent compounds Hoechst 33342 and 33258.**

  The order of binding affinity on 5 contiguous A/T bp as determined in chemical studies was: FMGT-2 > FMGT-5 = FMGT-1 ~ FMGT-3 >> Hoechst 33258.
  Their order of potency in inhibiting ternary complex formation on the SRE was:
  FMGT-2 > FMGT-1 ~ FMGT-3 > FMGT-5 > Hoechst 33342 = Hoechst 33258.
  The order of absolute polyamine tail length for these compounds is:
  FMGT-5 > FMGT-3 > FMGT-2 > FMGT-1.
  The degree of polyamine tail branching is:
  FMGT-5 > FMGT-3 > FMGT-1 > FMGT-2.

Binding affinity alone therefore fails to explain the EMSA results. The findings suggest that a minimum polyamine tail length is required for contacting the phosphodiester backbone, but further increases in length or branching may interfere with the abilities of FMGTs to inhibit TF complexes. The helical distortions caused by FMGTs, their ability to form higher order complexes, and their ability to contact both grooves may all contribute to the ability of these agents to be more effective inhibitors of TF complex formation than the Hoechst compounds.

- **FMGT-1 and FMGT-2 were able to inhibit c-fos promoter-driven cell-free transcription in a more complicated environment consisting of more proteins and additional DNA with**

greater sequence complexity. However, these agents were equipotent to the Hoechst compounds in this assay.

Higher amounts of DNA with greater sequence variation may provide additional lower affinity binding sites for the agents and therefore act as a drug "sink". Alternatively, additional proteins may be interfering with drug binding. A decrease in drug potency as assay conditions become more complex has been seen in several systems and was therefore expected (16-18). However, the relative loss of potency of the FMGTs compared to Hoechst compounds was not. While we had hoped that equipping the bisbenzimidazoles with major groove-binding tails would overcome this limitation, it appears that the ratio of improvement between drugs in EMSAs is not easily maintained in more complex environments.

- **All of the compounds inhibited topo II activity in isolated nuclei.**

However, there was a lack of correlation between the potencies of FMGTs in these assays and in the EMSAs and cell-free transcription assays. This suggests that characteristics that make the FMGTs good inhibitors of TF complex formation may differ from those needed to inhibit other DNA related activities, especially those which require processive movement of a protein along the DNA, as in the case of topo II.

- **The FMGTs were unable to decrease endogenous c-fos expression in NIH3T3 cells.**

Additional studies demonstrated that they were also unable to cause cell death, even after a three day continuous exposure. This may stem from poor cellular permeability or poor nuclear localization.

Part 3: Characterization of the A/T selective minor groove binder, Hoechst 33377.

In addition to evaluating the FMGTs as summarized above, we collaborated with the Bruice lab in analyzing an additional bisbenzimidazole compound, Hoechst 33377 (see Appendix IV, manuscript 3). Very few studies of Hoechst 33377 have been performed. The Bruice lab was interested in characterizing it more fully because of its potential to recognize longer DNA sequences. We therefore analyzed Hoechst 33377 in a series of cellular experiments, including a cytotoxicity assay, its ability to inhibit endogenous c-fos expression in NIH3T3 cells, and visualization of its cellular localization through fluorescence microscopy. These studies complemented the DNA-binding affinity, stoichiometry, and sequence recognition analyses carried out by the Bruice lab. Notable findings include:

- **Chemical analyses carried out by the Bruice lab revealed that Hoechst 33377:**
  -- can bind dsDNA in 2:1 stoichiometries in an antiparallel, side-by-side arrangement, similar to distamycin.
  -- requires at least 4 contiguous A/T bp for binding.
  -- exhibited higher sequence selectivity than Hoechst 33342 or Hoechst 33258 in that it preferentially stabilized duplexes lacking 5'-TpA-3' steps.

Our evaluations using cellular assays demonstrated the following:

- **Hoechst 33377 localized to nuclei of live NIH3T3 cells and exhibited a speckled staining pattern similar to Hoechst 33342.**

The increase in fluorescence exhibited by Hoechst 33377 upon binding to nucleic acids facilitated its visualization in cells using fluorescence microscopy.

- **Northern blot analysis demonstrated that following a 16 h exposure, Hoechst 33377 inhibited endogenous c-fos transcription in NIH3T3 cells by 50% at 4 μM.**

- **Following a three day continuous exposure, the LD_{50} of Hoechst 33377 in NIH3T3 cells was 3.4 μM.**

The ability of Hoechst 33377 to downregulate gene expression may be contributing to its ability to cause cell death.

Part 4: Analysis of bisbenzimidazole/tripyrrole MGTs.

The FMGTs analyzed in Appendix II exhibited enhanced inhibition of TF/DNA complex formation, attesting to the potential of equipping minor groove binding compounds with major groove-contacting functional groups. However, their failure to maintain potency in more complex assays indicated that further exploration of this drug design strategy and refinement of the agents were needed. The Bruice lab therefore synthesized another group of MGTs in which pyrrole moieties were linked to bisbenzimidazoles in *meta* to the terminal phenyl ring (see Appendix VI, manuscript 4). Polypropylamine tails were then added to each of the pyrroles. Different structural analogs, as shown in Figure 1 of manuscript 4, were analyzed in order to determine how structure and activity relate. To note, the Bruice lab found that equipping bisbenzimidazoles with polyamine tails resulted in a dramatic increase in DNA binding affinity and also endowed these compounds with the ability to better distinguish between 5 and 9 A/T bp sites. These agents were tested using the battery of assays established for the c-fos model, including analysis of their cytotoxicity and effects on topo II activity as described above. Our findings include:

- **Agents lacking polyamine side chains were poor inhibitors of TC formation in EMSAs.**

The simple bisbenzimidazole Hoechst 33342, used in this study as a representative A/T rich minor groove binder, and the **L1** compound, which possesses three polypyrrole subunits, but no polyamine side chains, were both about two orders of magnitude less potent than the most effective compound, **L2**. This bisbenzimidazole agent possesses three pyrrole subunits equipped with polyamine tails. Equipping bisbenzimidazoles with tripyrroles alone, while increasing DNA binding affinity, is apparently not enough to impart greatly improved TF/DNA complex inhibitory properties.

- **The order of potency in the cell-free transcription assay was identical to that in the EMSAs, but drastic decreases in effectiveness were observed.**

The order of potency was: **L2** > **L3** > **L4** > Hoechst 342 > **L5** > **L1.** Higher levels of each compound were needed to achieve the same level of inhibition in the cell-free transcription assay compared to the EMSAs, however. For example, 26-fold higher levels of **L3** were needed to achieve equivalent inhibition in the former assay compared to the latter. To note, **L2**, the most effective compound in the EMSAs, inhibited cell-free transcription at submicromolar levels and was still an order of magnitude more effective than Hoechst 33342.

- **L2 inhibited topo II activity significantly less than cell-free transcription**. At 2 μM **L2**, cell free transcription was inhibited completely, but there was no effect on topo II. Drug characteristics that result in good inhibition of TF complexes may therefore be different from those needed to inhibit the activity of topo II. Additional modification of these compounds may lead to the development of agents that can selectively target desired DNA template functions.

• **L2 was the only MGT to inhibit endogenous c-fos gene expression in NIH3T3 cells.** Following a 16 hour exposure to 10 μM **L2**, over 50% inhibition of c-fos transcription was achieved. This suggests that **L2** is able to enter cells, reach the nucleus and inhibit gene expression.

Comments on deviations from the original "Statement of Work":
During the course of the project, progress in certain areas led to deviations from the goals originally outlined in my submitted grant.

• Our studies increasingly focused on biological characterization of the novel DNA-binding drugs, such as the FMGTs. The binding and chemical characteristics of these compounds were determined in greater detail by our collaborators in the Bruice lab. Therefore, we found little need to investigate where and how these agents bind using DNA footprinting as noted in *Aim 1.*

• We first presumed that transient transfections were needed to evaluate drug effects on gene expression in whole cells, as outlined in *Aim 3.* However, the serum inducibility of the endogenous c-fos gene and the robustness of its expression in NIH3T3 cells made transfections unnecessary. Less manipulation of the cells was beneficial since it eliminated complications in evaluating drug effects following transfections.

• In an effort to better characterize the biological activity of novel DNA-binding drugs, we established two additional methods not outlined in the original *Statement of Work.* The topo II activity assay evaluates drug effects on the DNA template in isolated nuclei. Additionally, the use of fluorescence microscopy facilitated the characterization of Hoechst 33377.

• In my original grant, I outlined plans to evaluate a second series of novel DNA-binding agents using the c-fos model: the sequence specific polyamides developed by Dr. Peter Dervan of the California Institute of Technology. These agents continue to be studied by other members of the Beerman lab, especially in regards to their effects on the *ets* binding site on the Her-2/Neu promoter. However, their minimal cellular activity has prompted more extensive studies of what parameters affect their intracellular localization. Problems regarding cellular uptake of these agents were not resolved during my training period, and I was therefore unable to evaluate them using the c-fos model.

Training:

This project allowed me to learn a wide array of methods for the molecular and cellular characterization of DNA-binding drugs. More importantly, my training period honed my data evaluation and presentation skills. Writing the enclosed manuscripts was particularly helpful in this regard, and I also learned how to communicate effectively with scientific journals during the publication process.

My collaboration with the Bruice lab was especially instructive. It gave me the opportunity to directly apply my findings in the strategic design of agents and allowed me to gain more extensive knowledge on drug chemistry. My open dialogue with the Bruice lab prompted me to think more critically about my own work and allowed me to pursue more extensive studies on the biological and pharmacological characteristics of novel DNA-binding drugs.

Key Research Accomplishments

1. Established the human c-fos promoter's SRE as a model system to evaluate the effectiveness of DNA-binding compounds.

A series of commercially available DNA-binding drugs with varying sequence selectivities and modes of binding (chromomycin, Hoechst 33342, and nogalamycin) were analyzed for their ability to inhibit TF/DNA interactions at the SRE in increasingly complex assay environments.

- Analyzed ability of drugs to inhibit the following TF/DNA complex formation in EMSAs:
  -- SRF complexes
  -- Elk-1 complexes
  -- SRF + Elk-1 (ternary complex): both forward and reverse EMSAs.
- Analyzed ability of drugs to inhibit c-fos promoter-driven cell-free transcription.
- Assessed the ability of drugs to inhibit endogenous c-fos expression in NIH3T3 cells
- Determined the cytotoxicity of these compounds in NIH3T3 cells.
- Evaluated the ability of the agents to inhibit total RNA synthesis as measured by [^{3}H]-uridine incorporation.

2. Completed evaluation of a series of novel, rationally designed FMGTs using the c-fos model.

Results obtained from the analysis of five FMGTs (designated 1, 2, 3 and 5) with polyamine tails of varying lengths and degrees of branching were compared to those obtained for their parent compounds, Hoechst 33342 and Hoechst 33258.

- Analyzed ability of drugs to inhibit TF/DNA complex formation in EMSAs, c-fos promoter-driven cell-free transcription, and endogenous c-fos expression in NIH3T3 cells as described above.
- Determined the ability of these agents to inhibit topo II-mediated cleavable complex formation in isolated nuclei.

3. Evaluated the biological activity of Hoechst 33377.

Little work has previously been done to characterize Hoechst 33377. Our evaluation of its biological activity complemented the chemical analyses carried out by the Bruice lab

- Visualized the localization of Hoechst 33377 in live NIH3T3 cells and compared its staining pattern to the extensively studied Hoechst 33342.
- Investigated the effects of Hoechst 33377 on endogenous c-fos expression in cells.
- Evaluated the cytotoxic effect of Hoechst 33377 in NIH3T3 cells.

4. Analyzed the ability of novel, rationally designed bisbenzimidazole/pyrrole MGTs to inhibit TF complex formation using the c-fos model.

While the FMGTs exhibited enhanced potency as TF complex inhibitors compared to their unmodified parent compounds in simple assays such as EMSAs, they lost potency as assay conditions became more complex and had no effect in whole cells. Bisbenzimidazoles were therefore linked to pyrrole subunits equipped with polyamine tails in an effort to further increase DNA binding affinity and effectiveness in whole cells. A series of these MGTs were analyzed to gain better insight into structure/activity relationships.

- Analyzed ability of drugs to inhibit TF/DNA complex formation in EMSAs, c-fos promoter-driven cell-free transcription, and endogenous c-fos expression in NIH3T3 cells as described above. Also assessed their cytotoxic potential.

- Determined the ability of these agents to inhibit topo II-mediated cleavable complex formation in isolated nuclei.

Reportable Outcomes

Manuscripts:

One original and two copies of each of the manuscripts below have been enclosed.

White, C.M., Heidenreich, O., Nordheim, A., and Beerman, T.A. Evaluation of the effectiveness of DNA-binding drugs to inhibit transcription using the c-fos serum response element as a target. *Biochemistry* 39: 12262-12273 (2000).

Satz, A.L., **White, C.M.**, Beerman, T.A., and Bruice, T.C. Double-Stranded DNA binding characteristics and subcellular distribution of a minor groove binding diphenylether bisbenzimidazole. *Biochemistry* 40: 6465-6474 (2001).

White, C.M., Satz, A.L., Bruice, T.C., and Beerman, T.A. Inhibiting transcription factor/DNA complexes using fluorescent microgonotropens (FMGTs). *Proc. of the Natl. Acad. of Sci.* 98 (19): 10590-10595 (2001).

White, C.M., Satz, A.L., Gawron, L.S., Bruice, T.C., and Beerman, T.A. Inhibiting transcription factor/DNA complexes using fluorescent microgonotropens (FMGTs). *Biochim Biophys Acta*: 1574(1):100-8 (2002).

Abstracts:

White, C.M., Heidenreich, O., Nordheim, A., and Beerman, T.A. Evaluating the effectiveness of DNA-binding drugs to inhibit transcription using the c-fos serum response element as a target. Sigma Xi Research Competition. Buffalo, New York, 2000.

White, C.M., Satz, A.L., Bruice, T.C., and Beerman, T.A. Developing novel minor groove-binding agents to disrupt gene expression: Microgonotropens as inhibitors of transcription factor/DNA complex formation. American Association for Cancer Research National Meeting. New Orleans, Louisiana, 2001.

Degrees obtained that are supported by this award:

Ph.D., Molecular Pharmacology, awarded by the State University of New York at Buffalo. Officially conferred February, 2002.

Employment / Research opportunities applied for and received based on the training supported by this award:

Near the end of my training period, I applied for several post-doctoral positions at the following universities: Harvard University, University of Pittsburgh, and Johns Hopkins University. I accepted a postdoctoral fellowship in the laboratory of Dr. Bert Vogelstein in the Oncology Department of Johns Hopkins' School of Medicine.

Conclusions

Inhibiting the expression of a gene that plays an essential role in the development or progression of breast cancer has great therapeutic implications. Improving the ability of small-molecule DNA-binding drugs to selectively prevent TF complex formation is one strategy that can be used to accomplish this goal. This project has provided a coherent and rational approach for developing improved drug targeting paradigms for small molecule DNA reactive agents. Such agents may also be extremely useful tools for investigating the molecular mechanisms of cancer development.

The SRE of the human c-fos promoter proved to be a useful and effective model system to analyze the ability of DNA-binding drugs to inhibit TF/DNA interactions. Previous studies of DNA-binding agents rarely evaluated drug effects on more than one TF, and many focused on simple cell-free assays, such as EMSAs. In contrast, to our knowledge, our studies were the first in which agents were used to target more than one TF in a series of increasingly complex assays. Evaluating drugs in this way provides an immediate measure of how well the drugs are able to maintain potency under more rigorous conditions.

The SRE was found to be particularly well suited to such a series of analyses for many reasons. The availability of components (such as plasmids encoding the recombinant TFs and probes for the Northern blot assays) facilitated the development of the model. The A/T rich and mixed sequence motifs of the SRE could be targeted by a wide variety of both classical and novel DNA-binding drugs. Additionally, the strong and rapid inducibility of endogenous c-fos gene expression and the lack of pre-existing c-fos mRNA before serum induction aided in easy evaluation of drug effects in whole cells. The analysis of classical DNA-binding drugs with varying sequence selectivities and modes of binding as described in manuscript 1 served not only to establish the c-fos model as a useful analytical tool, but also provided a standard to which other drugs could be compared.

Our analysis of the novel FMGTs using the c-fos SRE model was the first to determine the biological effects of these agents. Our studies demonstrated the potential of adding major groove-binding functional groups to minor groove-binding bisbenzimidazoles to enhance their effectiveness as inhibitors of TF/DNA complex formation. Previous work showed that equipping a tripyrrole moiety with a major groove-binding tail significantly increased its DNA-binding affinity and potency in inhibiting TF/DNA interactions (8, 19). Our evaluation of the FMGTs demonstrates that this concept can be applied to other minor groove-binding compounds, thereby confirming proof-of-principle and expanding the potential number of compounds that can functionalized with major groove-binding groups. However, while the FMGTs were more potent than classical Hoechst compounds in cell-free EMSAs, they were unable to affect endogenous c-fos gene expression. Problems with the cellular permeability of small molecules designed to target DNA is not uncommon, as evidenced by the poor uptake of triplex forming oligonucleotides and peptide nucleic acids in other studies (20, 21).

The studies of Hoechst 33377 demonstrated that the unique side-by-side binding mode of this agent appears to impart a rare ability to distinguish between certain A/T rich sites. The lipophilic phenyl group on this compound may contribute to its ability to penetrate cell membranes and localize to the nucleus. Its chemical characteristics, combined with its biological effects in whole cells, may make Hoechst 33377 a potentially useful starting compound in the development of other sequence selective agents.

Efforts to further improve the potency and cellular effectiveness of the FMGTs led to the rational design of a second set of MGTs possessing bisbenzimidazole backbones equipped with pyrrole/polyamine subunits. Like their predecessors, these MGTs simultaneously contact both

grooves of DNA, but the structural alterations employed by the Bruice lab produced compounds with higher binding affinities (subpicomolar K_as) and the ability to distinguish between 5 and 9 A/T bp. Our evaluations using the c-fos model demonstrated that equipping bisbenzimidazoles with phosphodiester-contacting functional groups leads to increased inhibitory effectiveness by orders of magnitude in cell-free assays and also results in the first demonstration of MGT cellular activity. Notably, **L2** was the first MGT to inhibit endogenous gene expression in intact cells. **L2** is a suitable and promising candidate for future drug design studies.

References

1. Papavassiliou, A. G. Transcription factors: Structure, function, and implication in malignant growth, Anticancer Res. *15:* 891-894, 1995.
2. Benz, C. C., O'Hagan, R. C., Richter, B., Scott, G. K., Chang, C. H., Xiong, X. H., Chew, K., Ljung, B. M., Edgerton, S., Thor, A., and Hassell, J. A. HER2/Neu and the Ets transcription activator PEA3 are coordinately upregulated in human breast cancer, Oncogene. *15:* 1513-1525, 1997.
3. Chang, C., Scott, G. K., Kuo, W., Xiong, X., Suzdaltseva, Y., Park, J. W., Sayre, P., Erny, K., Collins, C., Gray, J. W., and Benz, C. C. ESX: A structurally unique Ets overexpressed early during human breast tumorigenesis, Oncogene. *14:* 1617-1622, 1997.
4. Hurst, H. C. Transcription factors as drug targets in cancer, Eur J Cancer [A]. *32A:* 1857-1863, 1996.
5. Broggini, M. and D'Incalci, M. Modulation of transcription factor--DNA interactions by anticancer drugs, Anticancer Drug Des. *9:* 373-87., 1994.
6. Chiang, S. Y., Welch, J., Rauscher, F. J., 3rd, and Beerman, T. A. Effects of minor groove binding drugs on the interaction of TATA box binding protein and TFIIA with DNA, Biochemistry. *33:* 7033-40, 1994.
7. Treisman, R. The serum response element, Trends Biochem Sci. *17:* 423-6, 1992.
8. Bruice, T. C., Houng, Y. M., Gong, X. H., and Lopez, V. Rational design of substituted tripyrrole peptides that complex with DNA by both selective minor-groove binding and electrostatic interaction with the phosphate backbone, Proc Natl Acad Sci USA. *89:* 1700-1704, 1992.
9. Satz, A. L. and Bruice, T. C. Synthesis of a fluorescent microgonotropen (FMGT-1) and its interactions with the dodecamer d(CCGGAATTCCGG), Bioorg Med Chem Lett. *9:* 3261-6, 1999.
10. Chen, G. L., Yang, L., Rowe, T. C., Halligan, B. D., Tewey, K. M., and Liu, L. F. Nonintercalative antitumor drugs interfere with the breakage-reunion reaction of mammalian DNA topoisomerase II, J Biol Chem. *259:* 13560-6., 1984.
11. Woynarowski, J. M., Sigmund, R. D., and Beerman, T. A. DNA minor groove binding agents interfere with topoisomerase II mediated lesions induced by epipodophyllotoxin derivative VM-26 and acridine derivative m-AMSA in nuclei from L1210 cells, Biochemistry. *28:* 3850-5., 1989.
12. Pellegrini, L., Tan, S., and Richmond, T. J. Structure of serum response factor core bound to DNA, Nature. *376:* 490-8, 1995.
13. Mo, Y., Vaessen, B., Johnston, K., and Marmorstein, R. Structure of the elk-1-DNA complex reveals how DNA-distal residues affect ETS domain recognition of DNA, Nat Struct Biol. *7:* 292-7., 2000.
14. Dorn, A., Affolter, M., Muller, M., Gehring, W. J., and Leupin, W. Distamycin-induced inhibition of homeodomain-DNA complexes, The EMBO Journal. *11:* 279-286, 1992.
15. Satz, A. L. and Bruice, T. C. Synthesis of fluorescent microgonotropens (FMGTs) and their interactions with dsDNA, Bioorg Med Chem. *8:* 1871-80., 2000.
16. Chiang, S. Y., Azizkhan, J. C., and Beerman, T. A. A comparison of DNA-binding drugs as inhibitors of E2F1- and Sp1-DNA complexes and associated gene expression, Biochemistry. *37:* 3109-3115, 1998.

17. Chiang, S. Y., Burli, R. W., Benz, C. C., Gawron, L., Scott, G. K., Dervan, P. B., and Beerman, T. A. Targeting the Ets binding site of the HER2/neu promoter with pyrrole-imidazole polyamides, J Biol Chem, 2000.
18. White, C. M., Heidenreich, O., Nordheim, A., and Beerman, T. A. Evaluation of the effectiveness of DNA-binding drugs To inhibit transcription using the c-fos serum response element as a target, Biochemistry. *39:* 12262-73., 2000.
19. Chiang, S. Y., Bruice, T. C., Azizkhan, J. C., Gawron, L., and Beerman, T. A. Targeting E2F1-DNA complexes with microgonotropen DNA binding agents, Proc Natl Acad Sci USA. *94:* 2811-6, 1997.
20. Wickstrom, E. Strategies for administering targeted therapeutic oligodeoxynucleotides, Trends Biotechnol. *10:* 281-7., 1992.
21. Nielsen, P. E. Peptide nucleic acids as therapeutic agents, Curr Opin Struct Biol. *9:* 353-7., 1999.

Appendix I: Abbreviations

A	Adenine
bp	Base pair(s)
C	Cytosine
EMSA	Electrophoretic mobility shift assay
FMGT	Fluorescent microgonotropen
G	Guanine
h	Hour(s)
IC_{50}	Concentration of drug needed to inhibit the observed activity by fifty percent
LD_{50}	Concentration of drug needed to kill fifty percent of cells in a cytotoxicity assay
MGT	Microgonotropen
Oligo	Oligonucleotide
PNA	Peptide nucleic acid
SRE	Serum response element
SRF	Serum response factor
T	Thymine
TF	Transcription factor
Topo	Topoisomerase
μM	Micromolar

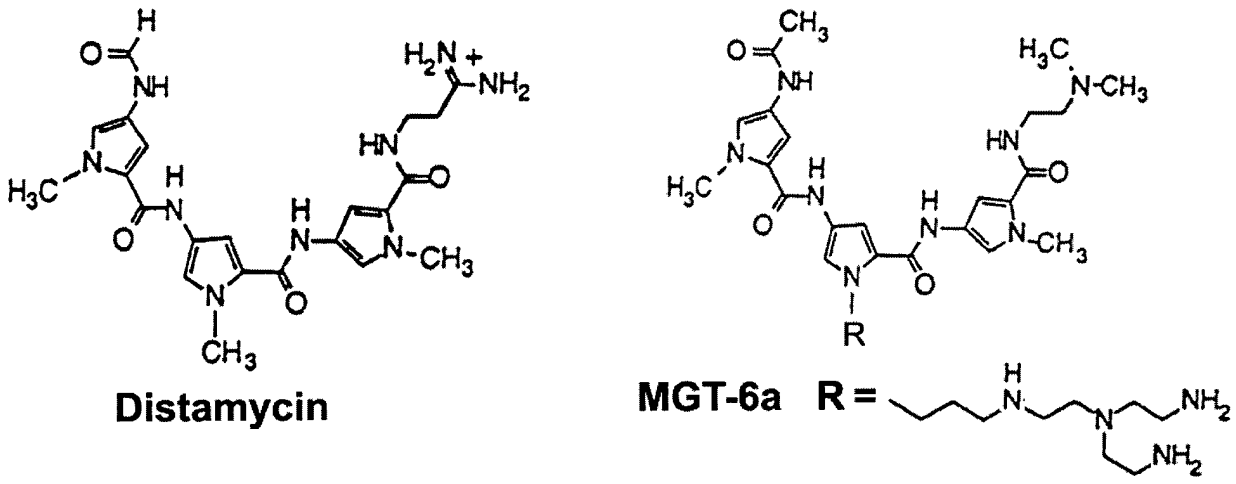

FIGURE 1: Structures of distamycin and a first generation microgonotropen, MGT-6a.

Both agents bind selectively to A/T rich sequences in the minor groove, but the polyamine tail of MGT-6a allows it to electrostatically contact the phosphodiester backbone of DNA in the major groove.

Evaluation of the Effectiveness of DNA-Binding Drugs To Inhibit Transcription Using the c-fos Serum Response Element as a Target†

Christine M. White,‡ Olaf Heidenreich,§ Alfred Nordheim,§ and Terry A. Beerman*,‡

Department of Pharmacology and Therapeutics, Roswell Park Cancer Institute, Elm and Carlton Streets, Buffalo, New York 14263, and Institut für Zellbiologie, Abteilung Molekularbiologie, Universität Tübingen, D-72076 Tübingen, Germany

Received June 21, 2000; Revised Manuscript Received August 7, 2000

ABSTRACT: Previous work has demonstrated that sequence-selective DNA-binding drugs can inhibit transcription factors from binding to their target sites on gene promoters. In this study, the potency and effectiveness of DNA-binding drugs to inhibit transcription were assessed using the c-fos promoter's serum response element (SRE) as a target. The drugs chosen for analysis included the minor groove binding agents chromomycin A_3 and Hoechst 33342, which bind to G/C-rich and A/T-rich regions, respectively, and the intercalating agent nogalamycin, which binds G/C-rich sequences in the major groove. The transcription factors targeted, Elk-1 and serum response factor (SRF), form a ternary complex (TC) on the SRE that is necessary and sufficient for induction of c-fos by serum. The drugs' abilities to prevent TC formation on the SRE in vitro were nogalamycin > Hoechst 33342 > chromomycin. Their potencies in inhibiting cell-free transcription and endogenous c-fos expression in NIH3T3 cells, however, were chromomycin > nogalamycin > Hoechst 33342. The latter order of potency was also obtained for the drugs' cytotoxicity and inhibition of general transcription as measured by [^{3}H]uridine incorporation. These systematic analyses provide insight into how drug and transcription factor binding characteristics are related to drugs' effectiveness in inhibiting gene expression.

Drugs that bind to DNA can act as template poisons by inhibiting interactions between cellular proteins and their DNA targets. The activity of RNA polymerases, DNA polymerases, and topoisomerases I and II can all be affected by drug treatment of their DNA templates (*1*−*3*). Our studies focus on evaluating DNA reactive agents as inhibitors or disruptors of transcription factor (TF)[1] binding to target sequences in gene promoters and their resultant effects on gene expression. Successful initiation of transcription requires specific binding of TFs to their cognate promoter sequences (reviewed in *4*). Interfering with these specific TF/DNA interactions may therefore lead to decreased expression of a target gene of interest. The ability to selectively prevent TFs from binding to desired DNA targets has implications in the study of the molecular regulation of gene expression and, ultimately, in the development of therapeutics (reviewed in *5*).

DNA-binding agents can be classified according to both their mode of binding as well as their sequence preference. Members of the reversible minor groove binding family (MGBs), such as distamycin, netropsin, and the Hoechst compounds, exhibit preferential binding to A/T tracts at least 4 base pairs long (reviewed in *6*). Their curved structure allows them to interact favorably with base pairs on the floor and wall of the minor groove via hydrogen bonds and van der Waal forces. The sequence selectivity of these agents may be influenced by subtle, sequence-dependent variations in DNA structure. The inherent differences in groove width and flexibility that result from neighboring base pair effects are factors that influence these agents' ability to optimally recognize and bind to a particular sequence (reviewed in *7*). This generally holds true for other drugs as well. Anticancer antibiotics, such as chromomycin A_3 and mithramycin, are MGBs that prefer G/C-rich elements. Unlike the A/T-selective MGBs, which primarily widen the minor groove, chromomycin can unwind the double helix by about 11° and cause more extensive DNA structural alterations (*8*).

Intercalators, such as nogalamycin, doxorubicin, and hedamycin, possess aromatic moieties that are inserted between base pairs, resulting in unwinding and extension of the DNA helix. Their binding is therefore more disruptive to DNA structure than MGBs. While intercalators generally prefer binding to wider-grooved G/C-rich sequences, their binding selectivity may be influenced by surrounding base pairs, as has been demonstrated for nogalamycin (*9*). Footprinting studies have shown that this agent selectively binds to regions of alternating purines and pyrimidines, and notably prefers 5′TpG steps (*10*). Nogalamycin is also

† This study was supported in part by National Cancer Institute Grant CA16056 (to T.A.B.), American Cancer Society Grant RPG-96-034-04-CDD (to T.A.B.), US Army Medical Research Grant BC980100 (to C.M.W.), and DFG Grant 120/7-3 (to A.N.).

* To whom correspondence should be addressed. Phone: (716) 845-3443; Fax: (716) 845-8857; E-mail: Terry.Beerman@RoswellPark.org.

‡ Roswell Park Cancer Institute.

§ Universität Tübingen.

[1] Abbreviations: SRE, serum response element; SRF, serum response factor; TC, ternary complex; TF, transcription factor; MGB, minor groove binding drug; EMSA, electrophoretic mobility shift assay; bp, base pair(s).

10.1021/bi001427l CCC: $19.00
Published on Web 09/14/2000

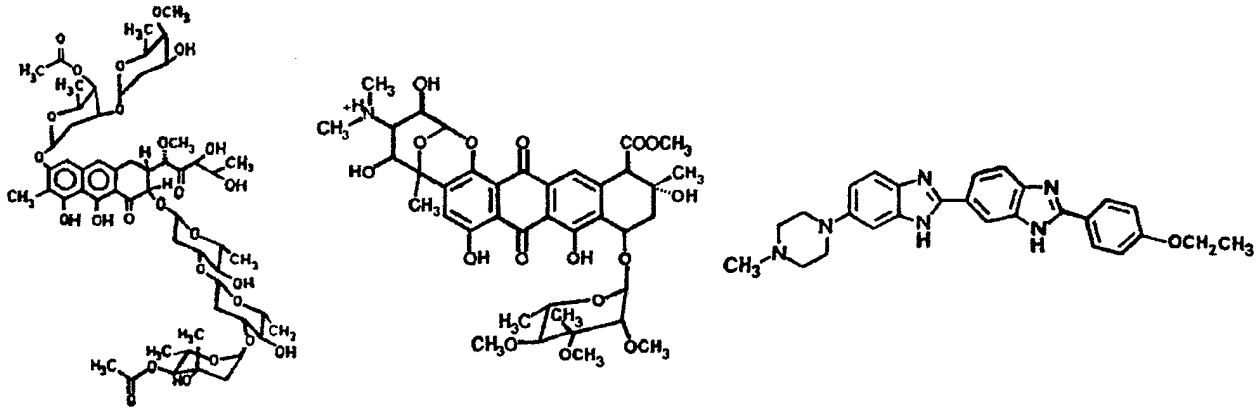

FIGURE 1: Structures of chromomycin A_3, nogalamycin, and Hoechst 33342.

somewhat unique because of its extremely slow dissociation kinetics, which likely stem from its characteristic threading mode of intercalation (*11*).

There has been considerable interest in targeting TFs using each of these drug classes. TFs can be classified into families according to their conserved DNA-binding domains. While TFs in each family can recognize and bind to specific consensus sequences, their precise recognition of promoter sites is often dependent on the composition and conformation of neighboring DNA base pairs. Electrophoretic mobility shift assays (EMSAs) using a variety of TF and DNA targets have established the potential of DNA-binding drugs as selective disruptors of target gene function. These previous studies have demonstrated that inhibition of TF/DNA complexes by DNA-binding drugs in vitro is more effective if the TFs and drugs analyzed share binding selectivities and characteristics. For example, the MGB distamycin is a potent inhibitor of TATA box binding protein (TBP) association with its A/T-rich target sequence in the minor groove (*12*). Distamycin's distortion of DNA groove conformation has also been implicated in its ability to disrupt TFs bound to A/T-rich sites in the major groove, such as homeodomain peptides (*13*).

Further investigations have suggested a relationship between the ability of drugs to disrupt TF binding to DNA in the simpler EMSAs and their ability to inhibit cell-free transcription under more complex conditions using a nuclear lysate. Distamycin was an effective inhibitor of both TBP complex formation in EMSAs as well as TBP-driven cell-free transcription (*14*). Mithramycin and chromomycin inhibited the binding of nuclear factors to G/C-rich Sp-1-binding sites on the long terminal repeat (LTR) of the HIV-1 promoter and were also able to inhibit HIV-1 LTR-directed transcription in a cell-free system (*15*). In such studies, higher drug concentrations were often needed to observe inhibition of transcription. In regards to novel drug development, these studies emphasize the need to maximize drug effectiveness in simpler systems before proceeding with testing in more complex assays or whole cells.

Evaluating DNA reactive compounds and developing paradigms for drug targeting in increasingly complex assay environments will help to improve drug specificity and potency. The c-fos promoter's serum response element (SRE) (reviewed in *16*) has characteristics that make it appropriate for this type of drug evaluation. The c-fos gene, which has been rigorously studied and characterized due to its importance in growth control, is an immediate-early response gene that is tightly regulated at the level of transcription (*17*). The SRE is necessary and sufficient for the rapid and transient induction of c-fos by serum (*18*). Two transcription factors bind to adjacent sites in this promoter sequence and mediate c-fos expression. A homodimer of SRF binds to the CArG box, an A/T-rich region (*19*). SRF binding is required for efficient recruitment of the ternary complex factor Elk-1 to its *ets* motif immediately upstream (*20*) (see Figure 2). Like other members of the *ets* family, Elk-1 binds to an invariant GGA core sequence in the major groove of DNA, but makes contacts with the phosphate backbone of unique flanking nucleotides in the minor groove (*21*). The TC, consisting of SRF and Elk-1, is constitutively bound to the SRE. Activation of this complex and upregulation of transcription are achieved as part of the cellular response to serum. Activation of signal transduction pathways by growth factors results in the phosphorylation of these factors by various kinases, most notably members of the mitogen-activated protein kinase (MAPK) family (*22, 23*).

The A/T-rich and mixed sequences present in the SRE are well suited for the study of a wide variety of DNA reactive agents. Also, the fact that Elk-1 contacts both grooves makes it an interesting target for drugs that bind in one groove or the other. Moreover, using this sequence as a target allows drug effects on more than one TF to be studied in a single system. Another advantage is that in addition to EMSAs and cell-free transcription assays, use of the c-fos SRE allows drug effects on endogenous c-fos mRNA production to be assessed. The rapid and transient expression of c-fos that follows serum induction provides a facile way of determining immediate or short-term drug effects on transcription in whole cells.

Here, we investigate the effectiveness of drugs as inhibitors of TF/DNA interactions in increasingly complex systems using the c-fos SRE as a target. Representative agents from the drug classes discussed above were chosen based upon their contrasting sequence preferences, and modes of DNA-binding (drug structures are shown in Figure 1). The MGBs chromomycin and Hoechst 33342, which do not radically distort DNA, have G/C- and A/T-rich preferences, respectively. They were compared to nogalamycin, which has less

sequence specificity but which causes greater helical distortion. The agents' abilities to affect TF/DNA interactions in vitro were evaluated in EMSAs, a simple system consisting of purified proteins and short oligonucleotides. The cell-free transcription assay, which uses a nuclear lysate to drive transcription from a plasmid, was used to analyze the drugs' effects in a more complicated environment. Finally, effects of these agents on endogenous c-fos expression in whole cells were assessed using Northern blots. Cytotoxicity and RNA synthesis assays also provided insight into how these agents were affecting cells in general.

MATERIALS AND METHODS

Drugs. Stocks of 5 mM chromomycin A_3 (Sigma, St. Louis, MO) and 5 mM nogalamycin (Pharmacia Upjohn Corp.) were prepared in dimethyl sulfoxide. A 20 mM stock of Hoechst 33342 (Aldrich Chemical Co.) was prepared in distilled water. All drugs were stored in the dark at −20 °C and diluted into water immediately before use.

Oligonucleotides. Two 24-mer oligonucleotides and their complementary strands were synthesized by the Biopolymer facility at Roswell Park Cancer Institute (Buffalo, NY) and purified on a Poly-Pak column. The first oligo (5′-ACACAGGATGTCCATATTAGGACA-3′), designated "SRE", contained the −301 to −324 sequence of the human c-fos promoter SRE. The second oligo (5′-GATACCGGAAGTCCATATTAGGAC-3′), designated "E74", was similar, but contained the high-affinity *ets*-binding site from the E74 *Drosophila* promoter (underlined), based on the consensus sequence published by Urness et al. (*24*). Oligos were reannealed according to Lee et al. (*25*). These double-stranded oligos were 5′-end-labeled with [γ-^{32}P]ATP (10 mCi/mL) and T4 Polynucleotide Kinase. Unincorporated nucleotides were removed using a Sephadex G-25 microspin column (Amersham Pharmacia Biotech).

Protein Purification. pILASRF, a plasmid encoding the SRF protein with an N-terminal His-tag, was developed in the Nordheim laboratory (Institut fuer Zellbiologie, Universitaet Tuebingen, Tuebingen, Germany). Expression of this protein and its purification were achieved following the protocol by Heidenreich et al. (*26*), but with two changes. First, the bacterial pellet was resuspended in PBS and lysed using three freeze/thaw cycles. The lysate was sonicated and pelleted at 10000*g* for 25 min at 4 °C before being combined with Ni−NTA beads (Qiagen, Inc.). Second, after transfer to a column, the beads were initially rinsed 4 times with 2 column volumes of PBS. pAS278, a plasmid encoding full-length Elk-1 with a C-terminal His-tag (*27*), was generously provided by Dr. Andrew Sharrocks (University of Newcastle, Newcastle upon Tyne, England). Following expression in BL21-pLysS bacteria, the protein was purified under native conditions using Ni−NTA beads, following manufacturer's instructions (Qiagen).

Electrophoretic Mobility Shift Assays. In general, experiments were performed as follows: drug, radioactively end-labeled oligo, and binding buffer were combined and allowed to incubate at room temperature for 30 min. Purified transcription factors were diluted into binding buffer. Following addition of purified protein(s), the reactions were allowed to incubate an additional 30 min at room temperature before being electrophoresed on a 5% polyacrylamide gel. These incubation times were based on time course experiments that established 30 min as sufficient time to achieve equilibrium of complex formation. Specifically, for the Elk-1 EMSAs, a binding buffer containing 25 mM Hepes−KOH, pH 7.9, 10 mM $MgCl_2$, 10 mM EDTA, 10 mM spermidine, 10 mM dithiothreitol, 7.5 μg/μL bovine serum albumin, and 20% glycerol was used. Ten nanograms of purified Elk-1 was added to 1 nM ^{32}P-end-labeled E74 oligo in these reactions. For the SRF EMSAs, the binding buffer contained 10 mM Tris-HCl, pH 7.5, 50 mM NaCl, 1 mM EDTA, 0.05% milk, 10 mM DTT, and 5% glycerol. Twenty-five nanograms of purified SRF was added to 1 nM ^{32}P-end-labeled SRE in these reactions. For ternary complex formation, the SRF binding buffer was used. Twenty-five nanograms of SRF and 6.25 ng of Elk-1 were added to 1 nM ^{32}P-end-labeled SRE. In samples containing chromomycin, Mg^{2+} was added to a final concentration of 10 mM in the binding reactions. For all EMSAs, a 5% native polyacrylamide gel was pre-run at room temperature at 200 V in 0.5× TBE buffer (44.6 mM Tris base, 44.5 mM boric acid, and 10 mM EDTA). Reactions were loaded onto the gel and electrophoresed for a maximum of 2 h. Adequate separation of free and complexed DNA on the Elk-1 and SRF MSAs was achieved by as little as 30 min of electrophoresis. Dried gels were exposed to Kodak Biomax Scientific Imaging film. Quantitation of free and complexed DNA was carried out by scanning the resulting autoradiogram on a computing laser densitometer (Molecular Dynamics) and analyzing the results with the manufacturer's ImageQuant program. Fifty percent inhibition of complex formation by the drugs (IC_{50}) was calculated by comparing drug-treated samples to controls. Where specified, purified proteins were added to the oligo before drug. These "reverse" experiments were electrophoresed as detailed above.

Cell Culture. Murine NIH3T3 fibroblast cells were obtained from the American Type Culture Collection and cultured in Dulbecco's modified Eagle's medium (DMEM) containing high glucose (4500 mg/mL) and sodium pyruvate (110 mg/mL) and supplemented with 10% calf serum. Cells were maintained at 37 °C and 5% CO_2.

NIH3T3 Nuclear Lysate Preparation for Cell-Free Transcription. NIH3T3 cells were grown in 175 cm^2 flasks until approximately 60% confluent before being starved overnight in starvation media (DMEM containing 0.5% calf serum). In general, a minimum of 10 flasks was needed to see adequate lysate activity. Cells were induced by adding induction media (DMEM with 15% calf serum) for 30 min, rinsed with room temperature PBS, and scraped into ice-cold PBS. Nuclear lysates were then prepared essentially as described by Blake et al. (*28*). All centrifugations were performed at 4 °C. In brief, cells were pelleted by centrifugation, washed, and repelleted in 5 pellet volumes of Buffer A [10 mM 4-(2-hydroxyethyl)-1-piperazineethanesulfonic acid (Hepes)/KOH, pH 7.9, 0.1 mM EDTA, 0.1 mM EGTA, 10 mM KCl, 0.75 mM spermidine, 0.15 mM spermine, 1 mM dithiothreitol (DTT)], and then allowed to swell on ice in the same volume of Buffer A for approximately 20 min. Cells were dounced on ice until 95% cell lysis was achieved, and then centrifuged until 31000*g* was reached. As soon as this speed was obtained, the centrifuge was turned off and the rotor was allowed to come to a halt. The pelleted nuclei were

resuspended in Buffer C [20 mM Hepes/KOH, pH 7.9, 20% glycerol, 0.2 mM EDTA, 2 mM EGTA, 0.75 mM spermidine, 0.15 mM spermine, 2 mM DTT, and 1 mM phenylmethanesulfonyl fluoride (PMSF)] to a final minimum concentration of 5×10^8 nuclei/mL. An equal volume of Buffer C + NaCl (same composition as buffer C, but with 0.75 M NaCl) was then added dropwise, with swirling. The lysate was rocked at 4 °C for 30 min, and then centrifuged at 214000*g* for 45 min. Supernatants were pooled, loaded into a Slide-A-Lyzer dialysis cassette (Pierce) with a 10 000 molecular weight cut-off, and dialyzed against 500 volumes of buffer D (20 mM Hepes/KOH, pH 7.9, 100 mM KCl, 20% glycerol, 0.2 mM EDTA, 0.2 mM EGTA, 12.5 mM $MgCl_2$, 2 mM DTT, and 1 mM PMSF) at 4 °C for 3 h, with a buffer change after the first 1.5 h. Dialyzed extract was cleared by a 15 min spin at 31000*g*. Aliquots of the resulting supernatant were immediately frozen on dry ice and stored at −80 °C.

Cell-Free Transcription Assay. The template, pFosLuc19, containing a human c-fos promoter fragment (−711 to −3) upstream of a luciferase reporter gene, was developed in the Nordheim laboratory. Digestion of this plasmid with *Sph*I prior to use in the assay yields a transcript approximately 750 bases in length. For drug studies, 0.5 μg of this plasmid was combined with drug and 5 μL of Buffer D for a total volume of 9 μL, and allowed to incubate 30 min at 30 °C. Approximately 15 μg of NIH3T3 nuclear lysate was added, the total volume was brought to 19 μL with Buffer D, and the reaction was allowed to incubate for 15 min at 30 °C. The subsequent reaction and transcript purification steps were carried out as described by Chiang et al. (*29*). A T3 transcript of pGEM4z (Promega), 250 bases long, was used as an internal control. Quantitation following autoradiography was as described for the EMSAs, and the visualized transcripts were normalized to the internal controls.

Whole Cell Drug Treatment and Northern Blot Analysis. For typical drug treatments prior to Northern blot analysis, 2.5×10^5 NIH3T3 cells were plated in 60 mm dishes and allowed to grow for 48 h until approximately 60% confluent. Growth medium was removed, the cells were rinsed with PBS, and starvation medium (DMEM containing 0.5% calf serum) was added. Appropriate dilutions of drugs were made into sterile water, and 20 μL of these dilutions was added directly to the plates. Solvent controls in which no drug was added were also prepared. Cells were generally starved for 16 h at the growth conditions detailed above. Induction of c-fos was accomplished by adding calf serum directly to the plates to a final concentration of 15%, followed by incubation at 37 °C for 30 min.

RNA Isolation/Northern Blot Analysis. Following serum induction of NIH3T3 cells, total RNA was isolated using TRIzol (GIBCO BRL). In brief, 20 μg of total RNA was loaded onto 1.5% denaturing agarose gel (2.2 M formaldehyde, 40 mM MOPS, pH 7.0, 10 mM sodium acetate, and 10 mM EDTA) and electrophoresed in 1× MOPS buffer (40 mM MOPS, 10 mM sodium acetate, and 10 mM EDTA) at 80 V for 4.5 h. The gel was rinsed in ddH_2O, and the RNA was transferred to GeneScreen (NEN Life Science Products) overnight. Following UV cross-linking of the RNA, the membrane was pre hybridized for 1 h at 60 °C in pre-hybe buffer [0.5 M sodium phosphate, pH 7.2, 7% SDS, 1 mM EDTA, 1% bovine serum albumin (BSA)]. A plasmid containing 4.8 kb of the murine c-fos coding sequence, pGEM4z-Fos (Loftstrand Labs, Ltd.), was linearized with *Hin*dIII before being radioactively labeled using a DecaPrime II kit (Ambion Inc.) and [α-^{32}P]dCTP (10 mCi/mL) for use as a probe. A phagemid containing the coding sequence for human glyceraldehyde-3-phosphate dehydrogenase (G3) (American Type Culture Collection) was also linearized with *Hin*d III and similarly labeled. Hybridization with the radiolabeled probes was overnight at 60 °C. Membranes were washed twice with wash buffer A (40 mM sodium phosphate, pH 7.2, 5% SDS, 1 mM EDTA, and 0.5% BSA) and twice with wash buffer B (20 mM sodium phosphate, pH 7.2, 1% SDS, and 1 mM EDTA) at 60 °C (each wash was for 20 min). The blot was exposed in a phosphorimager cassette (Molecular Dynamics) and scanned with a Molecular Dynamics phosphorimager.

Cytotoxicity Assay: Colony Formation Using NIH3T3 Cells. A total of 1×10^5 NIH3T3 cells were plated in 35 mm dishes and allowed to grow for 48 h until approximately 50% confluent. Growth medium was removed, and 1 mL of fresh medium containing the desired drug concentration was added. Following a 4 h drug exposure, the cells were trypsinized, serially diluted, and replated into 60 mm dishes. The total number of cells plated per dish ranged from 1×10^4 to 1×10^2. Cells were incubated at normal growth conditions for 10 days. The medium was then removed, and the cells were stained using 2 mL of methylene blue staining solution (7 mg/mL methylene blue in 70% EtOH) per dish for 30 min. Following removal of the staining solution, the dishes were rinsed in lukewarm water and air-dried. Colonies, designated as groups of 50 or more cells, were counted under a stereo microscope. Plating efficiencies were calculated by dividing the number of colonies by the total number of cells plated. Relative plating efficiencies for the drug treatments were then calculated by dividing the plating efficiencies of the drug-treated samples by the plating efficiencies of the controls.

RNA Synthesis ([^{3}H]Uridine Incorporation Assay). A total of 6.6×10^5 NIH3T3 cells were plated in 60 mm dishes and allowed to grow for 48 h until approximately 85% confluent. Drugs were diluted appropriately and added directly to the growth medium for a 4 h exposure under normal growth conditions. Then 2 μCi of [5-^{3}H]uridine (15 mCi/mmol) and unlabeled uridine to a final concentration of 50 μM were added to each dish. Following a 30 min pulse, the cells were rinsed with cold PBS, and then each dish was scraped into 1 mL of ice-cold 0.5 M perchloric acid (PCA) to begin precipitation of nucleic acids; 0.5 mL of the resuspension was transferred to prechilled eppendorf tubes, 1 mL of cold 0.5 M PCA was added, and the tubes were incubated on ice for 30 min. The samples were pelleted at 2800 rpm at 4 °C and washed 2 times in 0.4 M PCA before 0.5 mL 0.5 M PCA was added. The tubes were then heated to 70 °C for 1 h, and the counts in 0.5 mL were measured on a scintillation counter.

RESULTS

c-fos Components. The c-fos SRE sequence targeted in this study is shown in Figure 2A. This sequence is located approximately 300 bp upstream of the c-fos transcription

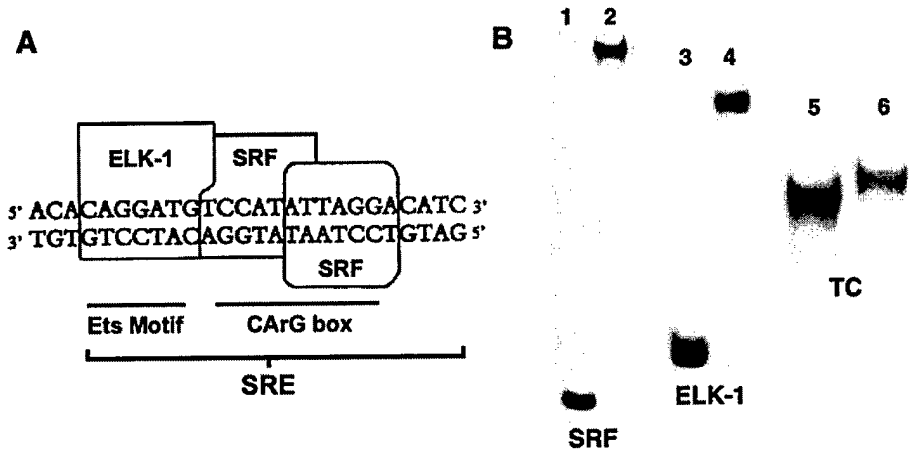

FIGURE 2: Components of the c-fos promoter. (A) TFs bound to the human c-fos promoter's SRE. Binding of the homodimer of SRF is required for the recruitment of Elk-1. Together, these TFs make up the ternary complex (TC). (B) Binding of SRF and Elk-1 to radiolabeled probes in EMSAs. ^{32}P-labeled oligonucleotides were incubated with purified proteins for 30 min at room temperature before being electrophoresed on a 4% polyacrylamide gel and autoradiographed. The 24 bp oligonucleotides contained sequences from the c-fos SRE or the *Drosophila* E74 promoter. Lane 1, free SRE probe; lanes 2 and 5, SRE plus SRF protein; lane 3, free E74 probe; lane 4, E74 plus Elk-1 protein; lane 6, SRE plus SRF and Elk-1 forms the TC. In lanes 5 and 6, the gel was electrophoresed longer to maximize shift differences. The free SRE probe ran off the gel under these conditions.

initiation site. Binding sites for the ternary complex factor Elk-1 and the homodimer of SRF are indicated. The TC is formed when binding of SRF to the CArG box recruits Elk-1 to the *ets* motif immediately upstream. SRF and Elk-1 were expressed as 6-Histidine-tagged proteins in bacteria and purified for use in the EMSAs as described in detail under Materials and Methods. While the SRE can be used to study drug effects on SRF binding and ternary complex formation on the SRE, it cannot be used to assess drug effects on Elk-1 binding alone, since this protein cannot bind to the SRE without SRF present (*30*). However, it can bind to the high-affinity *ets* motif in the *Drosophila* E74 promoter (*31*). Therefore, we made use of this promoter to study drugs' influence on Elk-1 association with DNA. Recombinant proteins were combined with 24 bp radiolabeled oligonucleotides containing the targeted promoter regions, and the complexes were electrophoresed on a polyacrylamide gel. Free SRE and E74 probe was successfully shifted by the addition of SRF or Elk-1 alone (Figure 2B, compare lanes 1 and 3 with lanes 2 and 4). In lanes 5 and 6, the gel was electrophoresed longer in order to maximize the difference in shift evident when SRF and Elk-1 were combined to form the TC (lane 6) as compared to SRF alone (lane 5). Under these conditions, the free probe ran off the gel. In subsequent experiments, where the complexes were electrophoresed under standard conditions as in Figure 2B (lanes 1−4), we noted that the TC was still distinguishable from the SRF complex on the basis of a slight difference in mobility (see Figure 3A, compare lanes 8 and 10 with lane 9).

Inhibition of TF Binding to the SRE in EMSAs. The ability of drugs to prevent TF binding to their specific promoter sites was assessed using the components of the SRE system. Three drugs were chosen on the basis of their different binding properties. The structures of chromomycin and Hoechst 33342, minor groove binding agents with G/C and A/T preferences, respectively, and nogalamycin, an intercalating drug that prefers G/C-rich regions, are shown in Figure 1. When incubated with the radiolabeled probes prior to protein addition, these drugs prevented TF binding in a dose-dependent manner. Representative results are shown in Figure 3A for chromomycin. As the amount of chromomycin added to the E74 promoter decreases in lanes 3−7, the amount of Elk-1 complexed with the probe increases back to control levels (lanes 1 and 2, no drug addition). Chromomycin also yields a dose-dependent inhibition of the TC as seen in lanes 11−15, as compared to controls in lanes 8 and 10. Similar inhibition was also achieved for SRF complex formation (data not shown).

Quantitation of the free and shifted DNA in drug-treated samples, and comparison to non-drug-treated controls, allowed percent inhibition of complex formation to be calculated. Representative dose−response curves for chromomycin (Figure 3B) show that this agent exhibits different potencies on the three TF complexes analyzed. The Elk-1 complex is by far the most sensitive to this drug, exhibiting a steep dose−response curve that plateaus by 10 μM. Formation of the SRF complex is less sensitive and yields a more gently sloping curve that starts to level off around 30 μM. When Elk-1 and SRF are combined to form the TC, the dose−response curve falls between those obtained for the individual factors, but retains the rather steep increase of the Elk-1 curve.

The drug concentration needed to inhibit complex formation by 50% (IC_{50}) was determined from dose−response curves plotted for each agent analyzed and used to compare the drugs' effectiveness in preventing TF binding (Figure 3C). Hoechst 33342 exhibited a trend similar to that observed for chromomycin: it was not particularly potent in preventing the SRF complex from forming, but was much more effective in inhibiting TC formation. Notably, Hoechst 33342 was approximately twice as potent as chromomycin in preventing TC formation. Unfortunately, the effects of Hoechst 33342 on Elk-1 complexes could not be determined, since binding of this drug to the E74 probe alone resulted in its retention in the well of the gel and excessive smearing, making quantitation impossible. Of the three drugs tested, nogalamycin was by far the most potent agent; IC_{50}s for all complexes fell well below 5 μM. Its inhibition profile differed from chromomycin in that SRF, rather than Elk-1, was the most sensitive target. Like chromomycin, however,

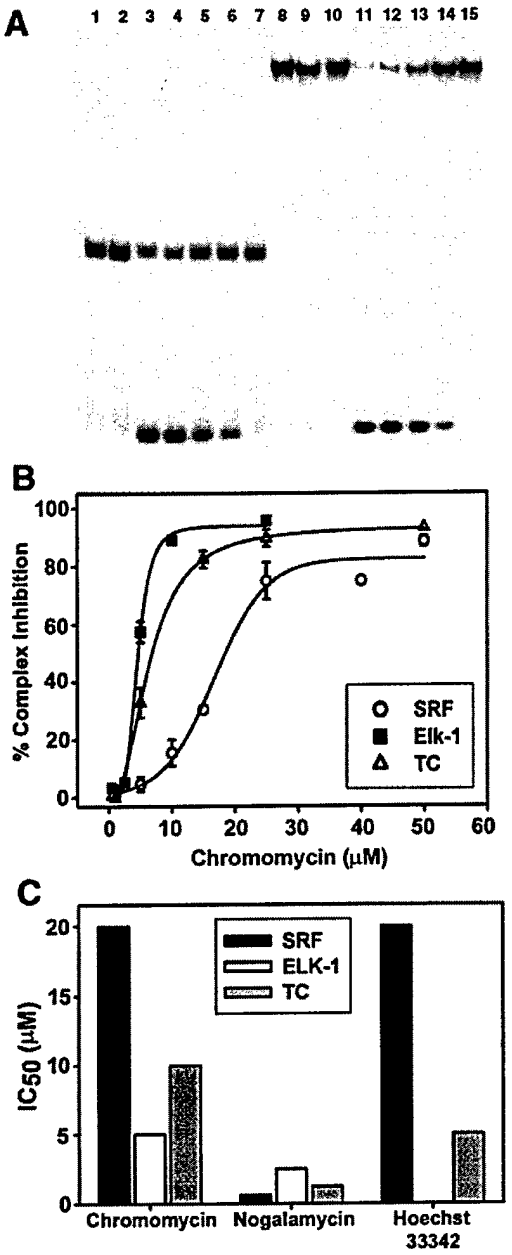

FIGURE 3: Effect of drugs on preventing complex formation in EMSAs. (A) Chromomycin's effect on Elk-1 and SRF complex formation. Increasing amounts of drug were incubated with the probes for 30 min before addition of purified proteins and electrophoresis as described in Figure 2. Lanes 1−7 contain Elk-1 complexes. Lanes 1−2, Elk-1 complex controls, no drug; lanes 3−7 contain 50, 25, 10, 5, and 1 μM chromomycin, respectively. Lanes 8 and 10−15 contain TC bound to the SRE. Lanes 8 and 10, TC controls, no drug; lane 9, SRF complex control, no drug; lanes 11−15 contain 100, 50, 25, 10, and 1 μM chromomycin, respectively. (B) Quantitation of chromomycin's inhibition of complex formation. Percent probe shifted in each drug treatment was compared to non-drug-treated controls to yield percent complex inhibition for SRF (○), Elk-1 (■), and TC (△). Results are the mean of four experiments (mean value ± standard error). (C) Comparison of drugs' potency in preventing complex formation in the EMSAs. Drug concentrations needed to prevent each complex formation by 50% (IC_{50}s) were calculated using graphs as shown in panel B.

the IC_{50} for TC inhibition fell between the IC_{50}s for the individual factors' complexes. In addition to its higher potency and unique inhibition profile in comparison to the MGBs, nogalamycin possessed another distinct characteristic. Reverse assays, in which each of the drugs was added after the TC was already formed on the SRE, demonstrated that only nogalamycin required significantly higher concentrations to disrupt complex formation (data not shown).

Drug Effects on c-fos Promoter-Driven Cell-Free Transcription. Upon observing different potencies among the drugs in the EMSAs, we wished to determine if similar levels of effectiveness could be maintained in a more complex, cell-free environment containing additional nuclear proteins and larger amounts of DNA with greater sequence complexity. The cell-free transcription assay makes use of a linearized plasmid containing the c-fos promoter. Upon addition of nuclear lysate from serum-induced NIH3T3 cells and the proper mix of nucleotides, the c-fos promoter drives the production of a transcript of a known length of 750 bp (Figure 4A, control lanes 3 and 8 marked by asterisks, top arrow). Preincubation of the plasmid with drug before nuclear lysate addition results in a dose-dependent inhibition of transcript production, as is seen for representative results following chromomycin treatment (lanes 1, 2, and 4−7). At 7.5 μM chromomycin (lanes 1 and 2), transcript appearance is abolished. At lower drug concentrations (5 and 2.5 μM in lanes 4−5 and 6−7, respectively), the intensity of the transcript is diminished, but there is no change in transcript size. The lack of detectable shorter transcripts suggests that transcriptional elongation is not being affected by the drug treatment. Quantitation of the bands followed by normalization to a 250 bp internal standard (Figure 4A, bottom arrow), and comparison to controls, yields percent inhibition of transcription. Dose−response curves, as seen in the representative graph for chromomycin in Figure 4B, were plotted for each drug treatment. The IC_{50}s for this assay were then used to compare the drugs in Figure 4C. Chromomycin and nogalamycin showed a level of potency that was only about 3 times higher than Hoechst 33342. The trend evident in the EMSAs, where an unusually high level of chromomycin was required to inhibit TC formation, therefore did not hold true in the cell-free transcription assays. While the IC_{50}s for nogalamycin and Hoechst 33342 increased approximately 4-fold from inhibition of the TC to inhibition of cell-free transcription, the respective IC_{50}s for chromomycin's inhibition actually decreased by a factor of 2.5.

Use of Northern Blots To Measure c-fos mRNA Induction. After observing that the drugs' potencies in the EMSAs and cell-free transcription assays were comparable, we next wished to assess the drugs' effectiveness in inhibiting c-fos expression in whole cells using Northern blots. The serum inducibility of the c-fos gene and its quick mRNA turnover (*17*) are advantageous in analyzing drug effects on endogenous c-fos transcription because complications arising from preexisting levels of c-fos mRNA are minimized. Optimal conditions established for c-fos induction in NIH3T3 cells are shown in Figure 5A. Unsynchronized, logarithmically growing cells have undetectable levels of c-fos mRNA (Figure 5A, lane 1). Inducing these cells with 15% serum for 30 min results in its detectable upregulation (lane 2). Starving the cells overnight (16 h) in media containing 0.5% serum downregulates c-fos (lane 3), and a subsequent 30 min induction of these cells with serum results in optimal expression (lane 4), as determined in time course studies (data not shown). The housekeeping gene, glyceraldehyde-3-

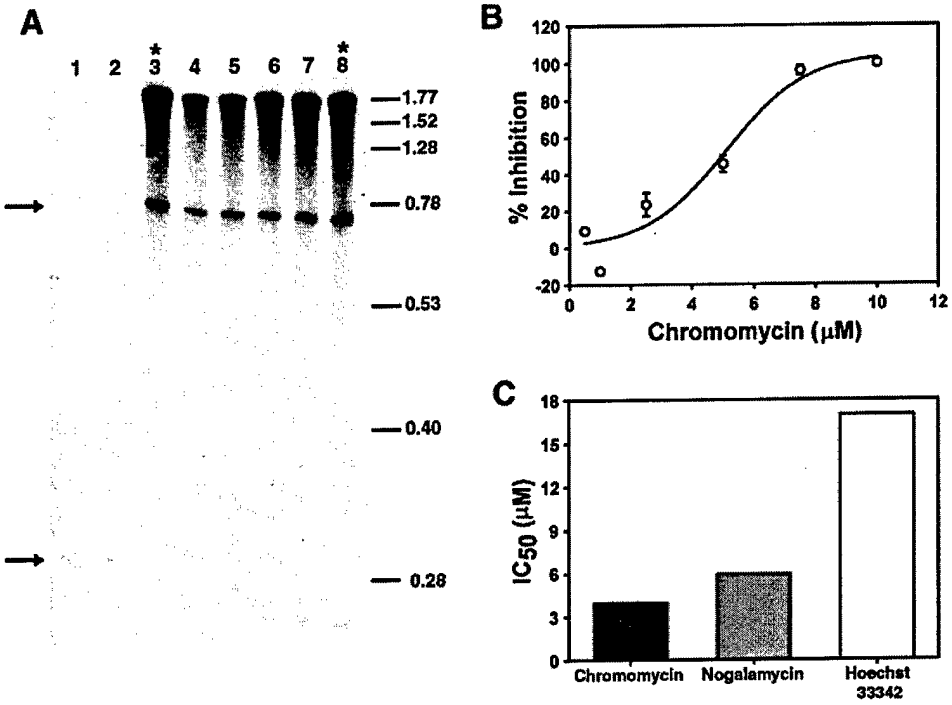

FIGURE 4: Effect of drugs on cell-free c-fos promoter-driven transcription (A) Chromomycin's effect on cell-free transcription. *Sph*I-linearized pFosLuc, a plasmid containing the human c-fos promoter upstream of a luciferase gene, was incubated with varying concentrations of drug for 30 min. Nuclear lysate from serum-induced NIH3T3 cells was then added for 15 min before the addition of nucleotides and [^{32}P]CTP. After a 1 h incubation, the resultant RNA transcripts were isolated and electrophoresed on a 4% denaturing polyacrylamide gel. Top arrow: the expected pFosLuc transcript at approximately 750 bases; lower arrow, internal control: a T3 transcript from pGEM4z at approximately 250 bases. Lanes 1−2, 4−5, and 6−7 contain 7.5, 5, and 2.5 μM chromomycin, respectively. Lanes 3 and 8, marked by asterisks: controls, with no drug treatment. Positions of size markers in a typical RNA ladder, in kilobases, are indicated. (B) Quantitation of chromomycin's inhibition of cell-free transcription. As in Figure 3B, comparison of drug-treated samples to controls yielded percent inhibition of transcription. Results are the mean of three experiments (mean ± standard error). (C) Comparison of drugs' effectiveness as inhibitors of cell-free transcription. IC_{50}s for each agent were calculated from graphs as shown in panel B.

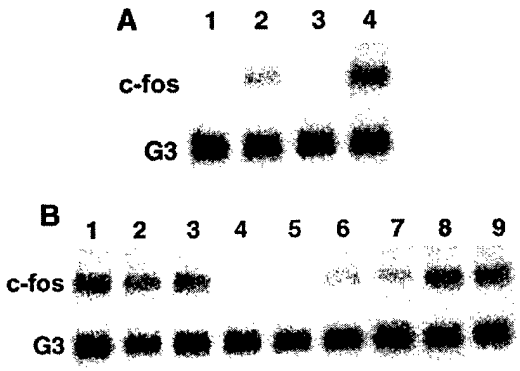

FIGURE 5: Representative Northern blot results. (A) Characteristics of c-fos expression in NIH3T3 cells. Following various treatments, 20 μg total RNA was electrophoresed on formaldehyde-containing agarose gels, transferred to a nylon membrane, and hybridized with radiolabeled probes for c-fos and G3. Lanes 1−2, normally growing cells; lanes 3−4, 16 h starvation in 0.5% serum; lanes 2 and 4, cells induced by raising serum concentration to 15% for 30 min. (B) Representative results on c-fos expression following exposure of NIH3T3 cells to chromomycin. After cells were starved for 16 h, drug was added for 1 h, and then cells were induced for 30 min as in (A). Lanes 1−3, controls, no drug treatment; lanes 4−5, 6−7, and 8−9 were exposed to 1, 0.5, and 0.25 μM chromomycin, respectively.

phosphate dehydrogenase (G3), is used in these blots as a loading control.

Analysis of Drug Effects on c-fos Expression in Whole Cells. For drug treatments, cells were starved for 16 h, exposed to varying drug concentrations for 1 h, and subsequently induced with serum. Chromomycin, as shown in Figure 5B, was capable of decreasing absolute c-fos mRNA levels in a dose-dependent manner (lanes 4−9), as compared to non-drug-treated controls (lanes 1−3). An approximately 30% decrease in c-fos expression is noted at only 0.5 μM (lanes 6 and 7), and the message is almost completely eliminated with a 1 μM treatment (lanes 4 and 5). There is no significant effect on G3 mRNA after a 1 h treatment at any drug concentration. In addition, as was noted in the cell-free transcription assay, there were no detectable levels of shorter transcripts following drug exposure.

Nogalamycin and Hoechst 33342 were analyzed in the above manner to see if they were also capable of inhibiting c-fos expression. Quantitation of the resulting hybridized signals allowed dose−response curves to be plotted (Figure 6). From these curves, it is evident that the drugs differ in their effectiveness: a 1 h exposure to 1 μM chromomycin results in 80% inhibition of c-fos expression, compared to no substantial inhibition for nogalamycin or Hoechst 33342 at the same concentration (compare panels A to B and C). At 2.5 μM Hoechst 33342 or nogalamycin, expression is inhibited approximately 40%, compared to greater than 95% inhibition for chromomycin. Chromomycin is therefore about an order of magnitude more potent than nogalamycin or Hoechst 33342 in inhibiting c-fos expression after a 1 h treatment. This is in contrast to the results obtained in the cell-free transcription assay, where chromomycin and nogala-

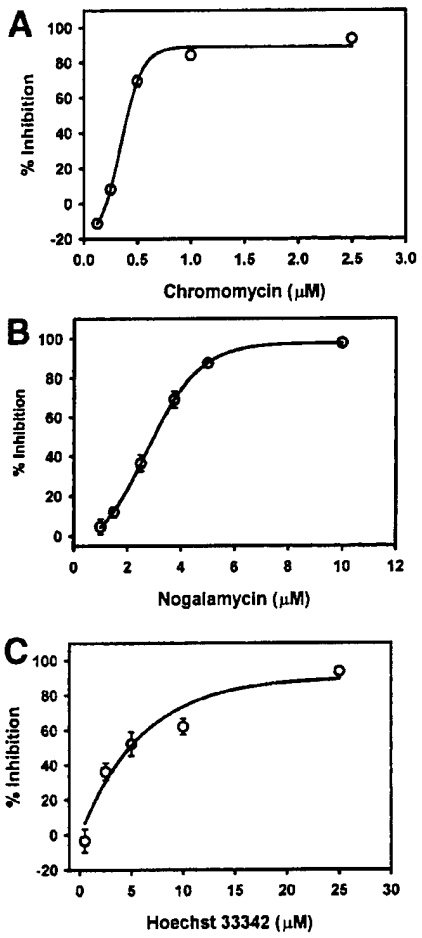

FIGURE 6: Quantitation of drugs' effects on endogenous c-fos expression in NIH3T3 cells following 1 h exposures. Cells were starved for 16 h before being exposed to a range of drug concentrations, in μM, for 1 h and induced with 15% serum for 30 min as described in Figure 5. Total RNA was analyzed in Northern blots through hybridization to radiolabeled c-fos and G3 probes, and the blots were visualized following autoradiography. Quantitation of the bands and comparison of the drug-treated lanes to controls yielded percent inhibition for each drug: (A) chromomycin; (B) nogalamycin; and (C) Hoechst 33342. Results are the mean of five experiments (mean ± standard error). The IC_{50}s calculated from these graphs are presented in Figure 8.

mycin exhibited similar potencies that were only 3 times greater than Hoechst 33342.

Chromomycin's Effects on c-fos Expression over a Shorter Time Course. After observing very effective inhibition of c-fos expression following exposure of cells to low levels of chromomycin after only 1 h, we wished to further characterize this drug's effect during shorter exposures. NIH3T3 cells were therefore starved for 16 h in low-serum media before being exposed to 1 μM chromomycin for various times (0−60 min). For the zero time point, drug was added to cells immediately before serum induction. Cells were then induced for 30 min before RNA isolation as discussed above. A concentration of 1 μM was chosen for this time course because of its substantial effect on c-fos expression (~80% inhibition after a 1 h exposure). As seen in Figure 7, there is a slight induction of c-fos mRNA after a 15 min exposure to chromomycin, but inhibition begins by 30 min and increases fairly rapidly to reach nearly 80% after an hour.

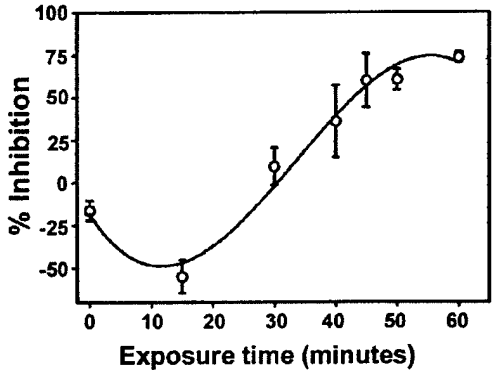

FIGURE 7: Chromomycin's inhibition of endogenous c-fos expression in NIH3T3 cells over time. Cells were starved for 16 h before being exposed to 1 μM chromomycin for various lengths of time. They were then induced with 15% serum for 30 min. Analysis using Northern blots and quantitation was carried out as previously described in Figure 6. Results are the mean of three experiments (mean ± standard error).

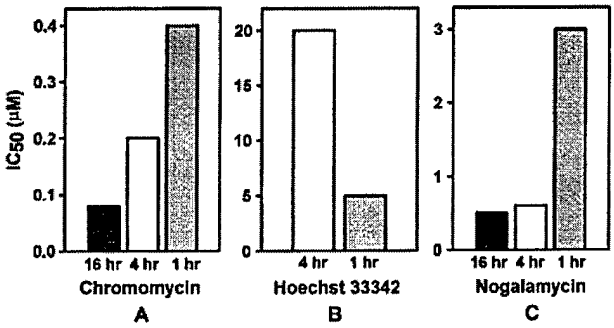

FIGURE 8: Effect of time on drug inhibition of endogenous c-fos expression. One hour drug exposures (gray bars) following 16 h starvation of NIH3T3 cells were performed as described in Figure 5. The 4 h exposures (white bars) were also performed after the cells were starved 16 h. For the 16 h exposures, (black bars), cells were starved and exposed to drug simultaneously. Northern blot analysis following hybridization to c-fos and G3 probes and subsequent quantitation yielded IC_{50} values. These values are plotted for each time point for (A) chromomycin, (B) Hoechst 33342, and (C) nogalamycin.

Drugs' Abilities To Inhibit c-fos Expression Over Time. Clearly, chromomycin is a rapid inhibitor of c-fos expression, but is this effect maintained over time to result in a continued decrease in expression? Longer exposures of 4 and 16 h were carried out to determine if each drug was able to maintain its effectiveness in the cellular environment. Like the 1 h time points, the 4 h drug exposures followed a 16 h overnight starvation period. However, for 16 h treatments, cells were starved and exposed to drug concurrently. The IC_{50} values were then used to compare the time course results as well as to compare drugs to one another. For chromomycin (Figure 8A), there was a continued increase in drug potency over time. That is, less drug was needed to obtain 50% inhibition of c-fos expression following a 16 h exposure compared to a 1 h exposure. Interestingly, Hoechst 33342 yielded a pattern of inhibition that was completely opposite. While a 16 h exposure to Hoechst 33342 yielded no consistent inhibition (not shown), the drug was more effective at shorter time points, with the IC_{50} dropping 4-fold between 4 and 1 h (Figure 8B). The pattern exhibited by nogalamycin (Figure 8C) was similar to that obtained for chromomycin. However, 5 times more drug was needed to obtain an

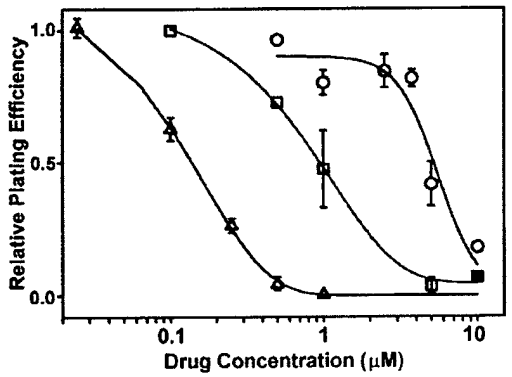

FIGURE 9: Cytotoxic effect of drugs on NIH3T3 cells. Cells were exposed to a range of drug concentrations for 4 h before being serially diluted, replated, and grown for 10 days. The cells were then stained and fixed in a solution of methylene blue and ethanol. Groups of more than 50 cells were deemed colonies and counted under a stereo microscope. Plating efficiencies were calculated by dividing the number of colonies by the number of cells plated. Relative plating efficiencies were then calculated by dividing the plating efficiency of each drug treatment by the control plating efficiency. The results shown for chromomycin (△), nogalamycin (□), and Hoechst 33342 (○) are the mean of three experiments (mean ± standard error).

equivalent level of inhibition at 1 h as compared to 4 h, after which more time did not result in any substantial further increases in drug effectiveness.

Drugs' Effects on Cell Survival and RNA Synthesis. The Northern blot results demonstrated that the drugs chosen are capable of affecting endogenous c-fos expression in a dose- and time-dependent manner. However, the complexity of the cellular environment necessitates that these results be interpreted in the context of the agents' other biological activities and whole cell effects. Therefore, to further characterize the drugs' effects in whole cells, NIH3T3 cells were exposed to a range of drug concentrations for 4 h before being plated in a colony formation assay. The colonies formed after 10 days of growth were counted and used to calculate relative plating efficiencies for each drug treatment as compared to non-drug-treated controls (Figure 9). Chromomycin was found to be the most toxic agent, causing 50% cell death at only 0.125 μM. The amount of Hoechst 33342 required to obtain the same level of toxicity (4.5 μM) was over an order of magnitude greater. Nogalamycin's toxicity fell between these values, with an IC_{50} of 1 μM. The cytotoxicity of these compounds may be reflected by their ability to shut down general transcription in cells, since they are capable of binding to many regions on DNA. To get a sense of how general transcription was being affected, RNA synthesis in NIH3T3 cells, as quantitated by [^{3}H]uridine incorporation, was measured following 4 h drug exposures (data not shown). The IC_{50}s from this assay are summarized in Table 1, along with IC_{50}s for the 4 h drug treatments in the cytotoxicity and Northern blot assays. The order of potency for drugs in the cellular assays was chromomycin > nogalamycin > Hoechst 33342. For all agents, similar drug concentrations were needed to achieve equivalent levels of activity in each assay.

Table 1: IC_{50} Values for Selected Whole Cell Assays[a]

drug	cytotoxicity	c-fos mRNA synthesis	total RNA synthesis
chromomycin	0.125	0.2	0.1
nogalamycin	1.0	0.6	0.5
Hoechst 33342	4.5	20	7.5

[a] Concentrations of drug, in μM, needed to inhibit the measured activity by 50%. The values for each assay, as described under Materials and Methods, were obtained after exposing NIH3T3 cells to drug for 4 h.

DISCUSSION

This study has compared and contrasted the ability of various classes of DNA-binding agents to inhibit TF/DNA interactions and resultant gene expression using a defined target gene promoter sequence, the c-fos SRE. To our knowledge, this is the first study that systematically analyzes the effectiveness of drugs possessing different sequence selectivities and modes of DNA binding to target two different TF-binding motifs in increasingly complex assays. The drugs' abilities to inhibit TF binding to target sequences in EMSAs were compared to their potencies in inhibiting cell-free transcription as well as their abilities to inhibit cellular gene expression. The drugs selected for analysis, chromomycin, nogalamycin, and Hoechst 33342, exhibited different potencies in each assay. Interesting differences were also noted when the drugs' effectiveness was compared between assays. These variations may stem from many factors including the DNA-binding characteristics of the compounds as well as their overall stability in cells.

In the EMSAs, the overall order of decreasing potency for inhibiting SRF and Elk-1 complexes was nogalamycin > Hoechst 33342 > chromomycin. Potential binding sites for nogalamycin, consisting of alternating purines and pyrimidines, are located near the *ets* motif of the Elk-1 binding site and in the CArG box of the SRF binding site. As an intercalator that makes contacts in both the major and minor grooves (*32*), and in comparison to the MGBs, nogalamycin dissociates from DNA very slowly (*11*), favoring more effective inhibition of TF binding under equilibrium conditions. It was anticipated that since SRF is required for Elk-1 binding, the IC_{50}s for inhibition of TC and SRF binding would be equivalent. However, 2 times more nogalamycin was needed to inhibit TC formation by 50% as compared to SRF binding. Structural studies and circular permutation analyses have shown that binding of a homodimer of SRF bends DNA 72° (*33*), while DNA bound to the TC has increased flexibility and is bent approximately 50° (*34*). This alteration in DNA conformation upon Elk-1 binding and its effects on neighboring DNA structure may therefore influence a drug's ability to optimally recognize and bind its target sequences.

In contrast to nogalamycin, chromomycin was more potent in inhibiting TC formation as compared to SRF binding but exhibited the highest potency in inhibiting Elk-1 complexes. While the E74 oligo used in the EMSAs contains four contiguous G/C base pairs in the *ets* motif that may be an appropriate chromomycin binding site (5′-CCGG-3′), the SRE lacks such a sequence. However, this drug was still able to prevent SRF and TC binding with lower potency, suggesting that if a consensus sequence is not available, the drug will associate with other sequences by default. Similar results have been obtained using chromomycin to inhibit TBP association with its A/T-rich binding site (*35*). The higher concentration of chromomycin required to inhibit TC forma-

tion as compared to Elk-1 complex formation may be due to SRF's stabilization of Elk-1 binding. Analogous results were seen in previous evaluations of drug effects on TBP binding. When TBP's binding was stabilized by addition of TFIIA, higher concentrations of distamycin were needed to disrupt complex formation (*12*).

Analysis of Hoechst 33342's inhibition of Elk-1 complexes was limited by well retention of the oligo when complexed to drug, regardless of whether protein was present (data not shown). This effect has been seen previously in our lab with other drug/oligonucleotide combinations. Despite its A/T preference, Hoechst 33342 was not a potent inhibitor of SRF binding to the A/T-rich CArG box on the SRE. Sequence selection studies have demonstrated that other bisbenzimidazole-based drugs, such as Hoechst 33258, greatly prefer some A/T sites over others, and surrounding sequences appear to influence the drug's affinity and optimal binding ability (*36*). In particular, the presence of 5′TpA steps greatly decreases the affinity of this Hoechst dye for DNA (*37*). The two 5′TpA steps present in the CArG box may therefore be contributing to the low potency observed in the SRF complex analysis. Given its high IC_{50} value, it is possible that Hoechst 33342 is binding to the target oligo by default, much like chromomycin.

When EMSA analyses using the TC were carried out, drugs never solely inhibited Elk-1 binding, which would have resulted in the appearance of the SRF complex. This suggests that these agents are generally disruptive and that they apparently alter the conformation of the DNA through bending or groove widening so that neither TF is able to bind. This is supported by previous studies that investigated long-range effects of drug binding on DNA. For example, the MGB distamycin can alter DNA allosterically up to 100 bp away from its binding site (*38*). Furthermore, the alterations in local DNA structure following binding of distamycin or the intercalator actinomycin produce changes in DNase I cleavage patterns at flanking sites (*39*).

In reverse EMSAs, where drug was added to preformed TF/DNA complexes, only nogalamycin required higher concentrations to achieve equivalent levels of TC inhibition. The equilibrium conditions required to inhibit complex formation were therefore altered, since more drug was needed to disrupt the TC if it was added after the proteins were bound. Dissociation studies carried out for the TC showed that this complex was stably bound for over 2 h under assay conditions (data not shown). SRF and Elk-1 primarily contact the SRE in the major groove. Since nogalamycin binds in a similar manner, the drug's association with DNA may be hindered by the presence of TFs at or near its binding site. In contrast, drugs such as chromomycin or Hoechst 33342 may be more effective in inhibiting TF binding to the major groove in reverse assays because they can approach DNA from the opposite, minor groove (*35*).

Drug activity was maintained in a more complex milieu of nuclear proteins and plasmid DNA in the cell-free transcription assay. IC_{50}s obtained in this assay were not substantially different from the EMSA IC_{50}s for TC inhibition, but the order of potency was chromomycin > nogalamycin > Hoechst 33342. As noted in Figure 4C, there was only a 4-fold decrease in potency for nogalamycin and Hoechst 33342 in this assay compared to the EMSA results. In contrast, chromomycin was about 2.5 times more effective in inhibiting transcription than in preventing TC formation. Overall, the presence of additional proteins and a higher amount of DNA with greater sequence complexity do not seem to greatly interfere with the ability of these drugs to inhibit cell-free transcription. This is in contrast to previous studies in which the MGB distamycin was used to inhibit the TF E2F from binding to the dihydrofolate reductaste (DHFR) promoter and to inhibit DHFR promoter-driven cell-free transcription (*29*). Here, 200 times more drug was needed to inhibit transcription as compared to inhibition of E2F/DHFR promoter complex formation. However, studies carried out using mithramycin (which is chemically related to chromomycin) demonstrated that similar levels of drug were needed to inhibit both TF complex formation and cell-free transcription from the c-myc promoter (*40*). The ability of any given drug to inhibit TF complex formation and to maintain an equivalent level of activity in a cell-free environment may therefore be dependent on the particular TFs studied and the DNA sequence used as a target. The results obtained here may also stem from the drugs' effects on other sequences in the c-fos promoter. By interfering with the binding of other TFs, recruitment of a functional RNA polymerase complex may be inhibited and levels of transcription will drop. The TFs bound to the c-fos promoter may be more sensitive to chromomycin than the other drugs analyzed. This may explain chromomycin's greater potency in inhibiting cell-free transcription and endogenous c-fos expression, as discussed below. None of the drugs tested resulted in the detectable production of shorter transcripts, which suggests that these agents are acting on the level of transcription initiation, rather than elongation. This is supported by previous work where transcriptional elongation inhibition was not observed except at high drug concentrations in some systems (*14, 41*).

The serum inducibility of the c-fos promoter and the rapid turnover of its mRNA facilitated assessment of immediate or short-term drug effects on gene expression in NIH3T3 cells. In Northern blots, the order of the drugs' potency in inhibiting endogenous c-fos transcription following serum induction was chromomycin > nogalamycin > Hoechst 33342. The time course study, which demonstrated an approximately 40% inhibition after only 40 min of treatment with 1 μM chromomycin, demonstrates the fast-acting nature of this drug and suggests that it is able to enter cells quickly and effectively. These rapid effects, in addition to the cell-free transcription data discussed above, suggests that this drug is acting on the level of DNA by inhibiting TF association with the c-fos promoter. Higher concentrations of chromomycin were needed at shorter time points in order to achieve an equivalent level of inhibition. This drug's effects may therefore depend, at least in part, on accumulation within the cell. The fact that the drug still exhibits inhibitory effects after 16 h in cells suggests that it is relatively stable. Similar results were obtained in studies using mithramycin and chromomycin to inhibit the expression of a stably transfected c-myc gene in NIH3T3 cells (*41*). Here, expression of an exogenous gene was very effectively inhibited after a 24 h exposure to 1 μM of either drug.

Nogalamycin's pattern of inhibition of gene expression was similar to that obtained using chromomycin. Hoechst 33342, however, was more effective at shorter time points as evidenced by a lower IC_{50} for 1 h exposures. The

inhibition seen following 16 h exposures, although variable, was marginal at best (data not shown). Hoechst 33342 may therefore become unstable or inactivated in these cells over time. Because there are undetectable levels of c-fos mRNA prior to serum induction and because shorter transcripts cannot be detected, the presence of drug is likely preventing the initiation of transcription. No decrease in absolute G3 mRNA levels was noted after any drug treatment. In short-term drug exposures, this may be due to G3's longer mRNA half-life (8 h for G3 compared to 30 min for c-fos) (*42*). In addition, the lack of detectable shorter G3 transcripts following drug treatment of cells is again consistent with the drugs' inhibition of transcription initiation. If the drugs were causing transcript degradation or inhibition of transcription elongation, partial transcripts or smearing of the RNA samples would have been visible.

The IC_{50}s for drug inhibition of c-fos expression as measured in the Northerns were less than the IC_{50}s calculated for the cell-free transcription assay. The largest difference of an order of magnitude was obtained for chromomycin. The process of transcription is far more complex on an endogenous promoter, where many other proteins and long-range changes in DNA conformation come into play to provide an intricately regulated cellular response. These drugs' abilities to bind to many other regions on the c-fos promoter is likely contributing to their increased potency in the whole cell environment. The complexity of the drugs' effects is further evidenced by the results obtained in the other whole cell analyses. The similarity in IC_{50}s for the cytotoxicity, RNA synthesis, and Northern blot assays following 4 h drug exposures suggests that the toxicity of these agents is reflected by their inhibition of general transcription.

Drug association with many sequences in the genome and the resultant toxic effects could potentially be avoided by developing more specific DNA-binding compounds. Designing more effective and potent DNA-binding drugs with the goal of disrupting specific TF/DNA complexes is an essential step in developing potentially therapeutic compounds. Our results demonstrate how the properties and DNA-binding characteristics of classical DNA-binding compounds are related to their biological consequences on a particular gene. Structural modification of classical drugs has yielded novel agents, such as microgonotropens and polyamides (*43, 44*). These agents will next be analyzed using the c-fos SRE target to determine which modifications result in potent and specific DNA-binding drugs with significant cellular activity.

ACKNOWLEDGMENT

We gratefully thank Drs. David Kowalski and Deborah Kramer for their comments and advice in preparing the manuscript.

REFERENCES

1. Phillips, D. R., White, R. J., Trist, H., Cullinane, C., Dean, D., and Crothers, D. M. (1990) *Anticancer Drug Des. 5*, 21−29.
2. McHugh, M. M., Woynarowski, J. M., Mitchell, M. A., Gawron, L. S., Weiland, K. L., and Beerman, T. A. (1994) *Biochemistry 33*, 9158−9168.
3. Beerman, T. A., McHugh, M. M., Sigmund, R., Lown, J. W., Rao, K. E., and Bathini, Y. (1992) *Biochim. Biophys. Acta 1131*, 53−61.
4. Latchman, D. S. (1997) *Int. J. Biochem. Cell Biol. 29*, 1305−1312.
5. Hurst, H. C. (1996) *Eur. J. Cancer. [A] 32A*, 1857−1863.
6. Geierstanger, B. H., and Wemmer, D. E. (1995) *Annu. Rev. Biophys. Biomol. Struct. 24*, 463−493.
7. Yang, X. L., and Wang, A. H. (1999) *Pharmacol. Ther. 83*, 181−215.
8. Utsuno, K., Kojima, K., Maeda, Y., and Tsuboi, M. (1998) *Chem. Pharm. Bull. (Tokyo) 46*, 1667−1671.
9. Fox, K. R., and Alam, Z. (1992) *Eur. J. Biochem. 209*, 31−36.
10. Fox, K. R., and Waring, M. J. (1986) *Biochemistry 25*, 4349−4356.
11. Fox, K. R., Brassett, C., and Waring, M. J. (1985) *Biochim. Biophys. Acta 840*, 383−392.
12. Chiang, S. Y., Welch, J., Rauscher, F. J., III, and Beerman, T. A. (1994) *Biochemistry 33*, 7033−7040.
13. Dorn, A., Affolter, M., Muller, M., Gehring, W. J., and Leupin, W. (1992) *EMBO J. 11*, 279−286.
14. Bellorini, M., Moncollin, V., D'Incalci, M., Mongelli, N., and Mantovani, R. (1995) *Nucleic Acids Res. 23*, 1657−1663.
15. Bianchi, N., Passadore, M., Rutigliano, C., Feriotto, G., Mischiati, C., and Gambari, R. (1996) *Biochem. Pharmacol. 52*, 1489−1498.
16. Treisman, R. (1992) *Trends Biochem. Sci. 17*, 423−426.
17. Greenburg, M. E., and Ziff, E. B. (1984) *Nature 311*, 433−438.
18. Treisman, R. (1985) *Cell 42*, 889−902.
19. Norman, C., Runswick, M., Pollock, R., and Treisman, R. (1988) *Cell 55*, 989−1003.
20. Shaw, P. E., Schroter, H., and Nordheim, A. (1989) *Cell 56*, 563−572.
21. Shore, P., Bisset, L., Lakey, J., Waltho, J. P., Virden, R., and Sharrocks, A. D. (1995) *J. Biol. Chem. 270*, 5805−5811.
22. Gille, H., Sharrocks, A. D., and Shaw, P. E. (1992) *Nature 358*, 414−417.
23. Janknecht, R., Ernst, W. H., Pingoud, V., and Nordheim, A. (1993) *EMBO J. 12*, 5097−5104.
24. Urness, L. D., and Thummel, C. S. (1990) *Cell 63*, 47−61.
25. Lee, D. K., Horikoshi, M., and Roeder, R. G. (1991) *Cell 67*, 1241−1250.
26. Heidenreich, O., Neininger, A., Schratt, G., Zinck, R., Cahill, M. A., Engel, K., Kotlyarov, A., Kraft, R., Kostka, S., Gaestel, M., and Nordheim, A. (1999) *J. Biol. Chem. 274*, 14434−14443.
27. Yang, C., Shapiro, L. H., Rivera, M., Kumar, A., and Brindle, P. K. (1998) *Mol. Cell. Biol. 18*, 2218−2229.
28. Blake, M. C., Jambou, R. C., Swick, A. G., Kahn, J. W., and Azizkhan, J. C. (1990) *Mol. Cell. Biol. 10*, 6632−6641.
29. Chiang, S. Y., Azizkhan, J. C., and Beerman, T. A. (1998) *Biochemistry 37*, 3109−3115.
30. Hipskind, R. A., Rao, V. N., Mueller, C. G., Reddy, E. S., and Nordheim, A. (1991) *Nature 354*, 531−534.
31. Rao, V. N., and Reddy, E. S. (1992) *Oncogene 7*, 65−70.
32. Smith, C. K., Davies, G. J., Dodson, E. J., and Moore, M. H. (1995) *Biochemistry 34*, 415−425.
33. Pellegrini, L., Tan, S., and Richmond, T. J. (1995) *Nature 376*, 490−498.
34. Sharrocks, A. D., and Shore, P. (1995) *Nucleic Acids Res. 23*, 2442−2449.
35. Welch, J. J., Rauscher, F. J., III, and Beerman, T. A. (1994) *J. Biol. Chem. 269*, 31051−31058.
36. Spink, N., Brown, D. G., Skelly, J. V., and Neidle, S. (1994) *Nucleic Acids Res. 22*, 1607−1612.
37. Abu-Daya, A., and Fox, K. R. (1997) *Nucleic Acids Res. 25*, 4962−4969.
38. Hogan, M., Dattagupta, N., and Crothers, D. M. (1979) *Nature 278*, 521−524.
39. Fox, K. R., and Waring, M. J. (1984) *Nucleic Acids Res. 12*, 9271−9285.

40. Snyder, R. C., Ray, R., Blume, S., and Miller, D. M. (1991) *Biochemistry 30*, 4290−4297.
41. Ray, R., Thomas, S., and Miller, D. M. (1990) *Am. J. Med. Sci. 300*, 203−208.
42. Dani, C., Piechaczyk, M., Audigier, Y., El Sabouty, S., Cathala, G., Marty, L., Fort, P., Blanchard, J. M., and Jeanteur, P. (1984) *Eur. J. Biochem. 145*, 299−304.
43. Dervan, P. B., and Burli, R. W. (1999) *Curr. Opin. Chem. Biol. 3*, 688−693.
44. Bruice, T. C., Sengupta, D., Blasko, A., Chiang, S. Y., and Beerman, T. A. (1997) *Bioorg. Med. Chem. 5*, 685−692.

BI001427L

ELSEVIER

Biochimica et Biophysica Acta 1574 (2001) 100–108

BIOCHIMICA ET BIOPHYSICA ACTA
BBA

www.bba-direct.com

Inhibiting transcription factor/DNA complexes using fluorescent microgonotropens (FMGTs)

Christine M. White [a], Alexander L. Satz [b], Loretta S. Gawron [a], Thomas C. Bruice [b], Terry A. Beerman [a,*]

[a] *Department of Pharmacology and Therapeutics, Roswell Park Cancer Institute, Elm and Carlton Streets, Buffalo, NY 14263, USA*
[b] *Department of Chemistry, University of California, Santa Barbara, CA 93106, USA*

Received 12 July 2001; accepted 22 October 2001

Abstract

Fluorescent microgonotropens (FMGTs) are A/T selective, minor groove-binding bisbenzimidazole ligands. Basic side chains extending from these agents electrostatically contact the major groove side of the phosphodiester backbone of DNA, endowing them with high binding affinity. Here, we evaluate the potential of these agents as inhibitors of transcription factor (TF) binding to DNA and explore whether their ability to contact both grooves enhances their inhibitory activity. A series of FMGTs (**L2–L5**), with polyamine tails of varying lengths and degrees of branching, were compared to an analog lacking these basic side chains (**L1**), and the classical bisbenzimidazole Hoechst 33342 for effects on TF complex formation on the c-fos serum response element (SRE). Although **L1** could not inhibit TF/SRE interactions, **L2–L5** did so at submicromolar concentrations. Moreover, the FMGTs were up to 50 times more potent than Hoechst 33342 in inhibiting TF complex formation in electrophoretic mobility shift assays. The FMGTs also inhibited c-fos promoter-driven cell-free transcription and topoisomerase II activity in nuclei. These studies establish the potential of FMGTs as TF/DNA complex inhibitors in cell-free systems, provide insight into the relationship between their structure and biological activities, and demonstrate the benefits of functionalizing minor groove binding-agents with major groove-contacting groups.

Keywords: DNA-binding drug; Hoechst 33342; Bisbenzimidazole; Transcription factor; Minor groove; Microgonotropen

1. Introduction

The design, synthesis and evaluation of DNA-binding agents as inhibitors of biologically relevant activities continue to be areas of intense research. Small molecule DNA-binding ligands are capable of interfering with the function of proteins that interact with DNA, including transcription factors (TFs) and topoisomerases (topos) [1,2]. For example, the activity of TFs, proteins that play an integral role in the coordinated and regulated expression of genes by recognizing and binding to specific sequences in gene promoters, can be inhibited by a variety of DNA-binding drugs [3,4]. Increasing focus has been made on using drugs to interfere with TF recognition of target sites in order to inhibit gene expression.

Drugs that reversibly bind DNA can be categorized according to their mode of binding, their groove selectivity and their sequence preference. For example, the minor groove-binding drug family includes the naturally occurring oligopeptide distamycin and the synthetic bisbenzimidazole Hoechst compounds, both of which show preference for A/T rich sites. Previous work showed that these agents effectively inhibit TF/DNA interactions in cell-free systems [2]. Such studies indicated that the sequence and groove preferences of both TFs and drugs are important factors to consider when designing novel agents to disrupt desired TF/DNA complexes. This is reflected by the ability of distamycin to inhibit the TATA binding protein from binding to its A/T rich target sequence in the minor groove in cell-free assays but its ineffectiveness in preventing complex formation between early growth response factor and its G/C rich target sequence in the major groove [5]. However, the ability of distamycin to successfully inhibit major groove-binding TF complexes was demonstrated in assays

Abbreviations: TF, transcription factor; MGT, microgonotropen; FMGT, fluorescent microgonotropen; SRE, serum response element; SRF, serum response factor; TC, ternary complex; EMSA, electrophoretic mobility shift assay; oligo, oligonucleotide; topo II, topoisomerase II

* Corresponding author. Fax: +1-716-845-8857.
E-mail address: terry.beerman@roswellpark.org (T.A. Beerman).

0167-4781/01/$ – see front matter
PII: S0167-4781(01)00351-7

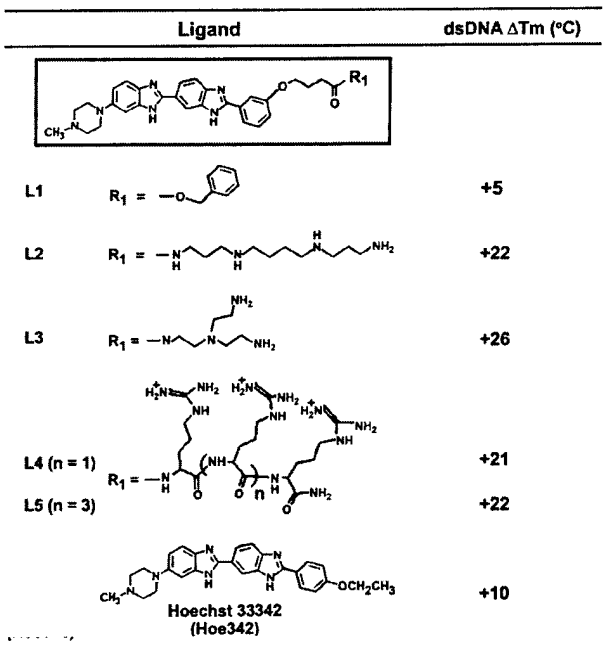

Fig. 1. Chemical characteristics of the ligands analyzed. The bisbenzimidazole and linker combination of the novel, rationally designed FMGTs is boxed. **L1** lacks basic side chains, but polyamine tails of varying lengths and degrees of branching extend from the FMGT moiety in **L2–L5**. Hoe342, a control agent, is a classical bisbenzimidazole. The T_m of ligand/DNA complexes was determined from thermal denaturation experiments employing 0.8 μM dsDNA oligo 5′-GCGACTGCAATTTC-GACGTCC-3′ in 10 mM NaCl and 10 mM potassium phosphate buffer, pH 7.0, in the presence of 2.8 μM ligand [18]. The T_m values are expressed relative to the T_m for ligand-free oligo (55°C).

employing homeodomain peptides, which primarily contact the major groove at A/T rich sites [6].

The majority of DNA-binding proteins interact with the major groove, presumably because it bears most of the recognizable nucleotide functional groups [7]. Many other proteins utilize both grooves [8,9]. Because of limited success at creating compounds targeting both grooves, many drug design strategies have focused on improving the specificity and affinity of minor groove-binding drugs [10]. Their ability to approach DNA from the opposite groove and to change the conformation of the double helix upon binding allows them to inhibit TF complex formation with the major groove as discussed above. While agents that bind solely to the minor groove are successful in inhibiting various TF/DNA complexes, drugs that extend into both grooves with increased affinity might have the potential to be more effective inhibitors of a wider range of TFs.

Microgonotropens (MGTs), developed by the Bruice laboratory, are novel agents that bind selectively to A/T rich sequences in the minor groove, but make electrostatic, major groove contacts with the phosphodiester backbone via basic side chains [11]. This allows these ligands to bind DNA with very high affinity ($K_a = 10^9$ M^{-1} or greater) and results in gross conformational changes of the helix [12,13]. The structures of the first generation of MGTs consisted of a tripyrrole moiety with polyamine tails of varying lengths and degrees of branching extending from the central pyrrole. Cell-free experiments revealed that the most successful ligand, MGT-6a, was several orders of magnitude more potent than distamycin in preventing the TF E2F1 from binding to its target sequence [14]. E2F1 contacts both grooves of DNA at a mixed A/T and G/C rich site, a mode of binding that proved to be a uniquely sensitive target for the action of these ligands. While the inhibitory potencies of the MGTs primarily correlated with their DNA-binding affinities, their effectiveness was also dependent upon the structure and length of their polyamine tails, suggesting that both factors are important determinants to consider when designing such agents to interfere with TF complex formation.

The success of first generation MGT design led to modification of alternative minor groove-binding moieties in order to improve their effectiveness as inhibitors of TF binding. The ease of synthesis and functionalization of bisbenzimidazoles made this class of agents a convenient starting point for the covalent attachment of major groove-binding functional groups. Additionally, classical bisbenzimidazoles, such as Hoechst 33342 (Hoe342, Fig. 1), have been shown to inhibit TF/DNA complex formation in a variety of systems [15,16]. Attaching polyamine tails to the *meta* position of the terminal benzene ring of a bisbenzimidazole resulted in fluorescent microgonotropens (FMGTs) (**L2–L5** in Fig. 1) [17,18]. These agents bind A/T rich sequences in the minor groove and like their tripyrrole MGT predecessors have the potential to electrostatically interact with phosphate groups on the major groove side of the phosphodiester backbone. Moreover, the FMGTs bind dsDNA with vastly superior affinity compared to Hoe342, as evidenced by the significantly higher melting temperatures of oligonucleotide (oligo) duplexes in the presence of the novel ligands (Table 1) [17]. This new application of the MGT design concept therefore has the potential to enhance the ability of bisbenzimidazoles to inhibit certain TF/DNA associations.

A model system using the serum response element (SRE) of the human c-fos promoter as a target was established to analyze the abilities of DNA reactive ligands to inhibit TF binding to their target sites [19]. The transcrip-

Table 1
Comparison of ligand effects on topo II activity in HeLa nuclei

Agent	Percent reduction in DNA–protein crosslinks
L2	60.1
L3	15.3
L4	36.1
L5	65.8
Hoe342	49.3

HeLa cells were labeled with ^{14}C-thymidine prior to nuclei isolation. The crosslinking agent VM-26 was co-incubated with radiolabeled nuclei in the presence of 20 μM of each agent for 10 min at 37°C. DNA–protein crosslinks were quantitated following SDS precipitation. Results are from three experiments.

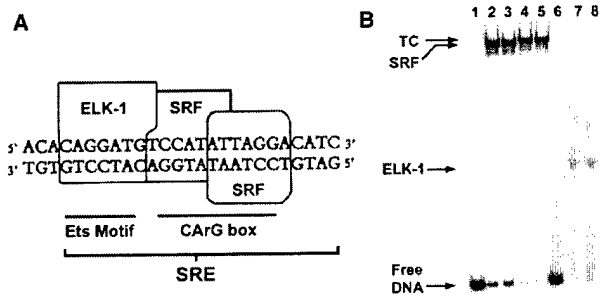

Fig. 2. Components of the c-fos promoter. (A) Binding of TFs to the human c-fos SRE. A homodimer of SRF must be bound before recruitment of Elk-1 can occur to form a TC. (B) Complex formation between purified TFs and radiolabeled probes in EMSAs. TFs and ^{32}P-labeled oligos are co-incubated 30 min before being electrophoresed on a polyacrylamide gel and autoradiographed. The 24 bp oligos contain sequences from the c-fos SRE or the *Drosophila* E74 promoter. Lane 1, free SRE probe; lanes 2 and 3, SRE plus SRF; lanes 4 and 5, SRE plus Elk-1 and SRE yields the TC; lane 6, free E74 probe; lanes 7 and 8, Elk-1 plus E74 probe.

tional upregulation of c-fos depends upon the activation of TFs constitutively bound to the SRE in a ternary complex (TC) (reviewed in [20]). The binding of a homodimer of serum response factor (SRF) to an A/T rich CArG box is required for recruitment of Elk-1 to a GGA-containing *ets* motif (see Fig. 2). Activation of the TC through phosphorylation of Elk-1 is necessary and sufficient for c-fos transcription [21]. The mode of binding of SRF and Elk-1 makes these factors amenable for targeting by FMGTs. Both factors primarily contact their consensus sequences in the major groove, but also make contact with surrounding bp and the phosphodiester backbone in the minor groove [22,23]. Occupation and deformation of the A/T rich SRF-binding site in the minor groove by FMGTs combined with the extension of their polyamine tails into the neighboring major groove may therefore lead to effective disruption of both SRF and Elk-1 binding.

While the concept of equipping minor groove-binding ligands with major groove-associating functional groups proved useful in improving the ability of the polypyrrole-based MGTs to inhibit TF/DNA interactions, biological analysis of these novel class of compounds has been somewhat limited [14,24], and the biological activities of the FMGTs have not yet been tested. Our lab has therefore undertaken to further analyze and characterize the FMGTs to determine whether applying the above strategy to bisbenzimidazoles can enhance their TF inhibitory ability. An FMGT analog lacking basic side chains, **L1**, was synthesized and compared to a series of FMGTs (**L2–L5**) functionalized with polyamine tails of varying lengths and structures (Fig. 1). The well-studied Hoe342 was used as a control. The c-fos model allowed us to evaluate these ligands in a more rigorous fashion compared to previous MGT evaluations, since it involves assessing drug effects on more than one TF in increasingly complex environments. The ability of the agents to inhibit SRF and Elk-1 complex formation on the SRE was determined using electrophoretic mobility shift assays (EMSAs). Their effects on c-fos promoter-driven cell-free transcription assay were also analyzed. Since the cellular activity of the novel FMGTs have never been investigated, we determined their effects on endogenous c-fos expression in whole cells using Northern blots. Our lab previously showed that minor groove-binding agents, including bisbenzimidazole analogues, are capable of decreasing topoisomerase II (topo II)-mediated activities in isolated nuclei. This system allowed us to examine the general effects of FMGTs on DNA template function without the complications of cellular uptake. Our findings can potentially be used as a basis for future FMGT structural modifications that may improve their potency and effectiveness. Additionally, these studies suggest that this drug design concept may be extended to other classes of minor groove-binding ligands as a means to enhance their potential as TF/DNA inhibitors.

2. Materials and methods

2.1. Agents

Stocks of 20 mM Hoe342 (Aldrich Chemical Co., Milwaukee, WI, USA) were prepared in distilled water. FMGT synthesis is described elsewhere [17,18]. Lyophilized FMGT aliquots were stored at −20°C and resuspended in 25% dimethyl sulfoxide to 1 mM before use. All drug solutions were stored in the dark at −20°C and diluted into distilled water immediately before use.

2.2. EMSAs

Oligos preparation, protein purification, and reaction conditions were as described [19]. Briefly, for the forward EMSAs, 1 nM radiolabeled oligo and varying concentrations of drug were incubated in binding buffer (see below) at room temperature for 30 min before purified TFs were added. The double-stranded oligo sequences were designated SRE (5′-ACACAGGATGTCCATATTAGGACA-3′) and E74 (5′-GATACCGGAAGTCCATATTAG-GAC-3′). After a subsequent 30 min incubation, the complexes were electrophoresed at 200 V in 0.5×TBE (44.6 mM Tris base, 44.5 mM boric acid, and 10 mM EDTA) on a 5% polyacrylamide gel for up to 2 h, with adequate separation of complexed and free DNA occurring by a minimum of 30 min. Dried gels were exposed to a phosphorimager cassette (Molecular Dynamics, Sunnyvale, CA, USA) and scanned with a Molecular Dynamics phosphorimager. Autoradiographs were quantitated using the manufacturer's ImageQuant program.

2.3. Cell culture

NIH3T3 cells were maintained as described previously

[19]. Logarithmically growing HeLa cells were maintained in suspension cultures in Joklik-modified minimal essential medium (S-MEM) supplemented with 5% fetal bovine serum and 5% horse serum at 37°C.

2.4. Cell-free transcription

Nuclear extracts were prepared from NIH3T3 cells and stored at −80°C until use [19]. In brief, the reaction was carried out by combining 0.5 μg of an *Sph*I-digested plasmid containing the full length human c-fos promoter (pFosLuc19) with drug and 5 μl buffer D (20 mM HEPES/KOH, pH 7.9, 100 mM KCl, 20% glycerol, 0.2 mM EDTA, 12.5 mM $MgCl_2$, 2 mM DTT, and 1 mM PMSF) to a final volume of 9 μl. After 30 min at 30°C, 15 μg of NIH3T3 nuclear lysate was added, the final volume was adjusted to 19 μl with buffer D and the reaction was incubated an additional 15 min. Addition of a reaction mixture containing [α-^{32}P]CTP and the subsequent purification and electrophoresis of the resulting radiolabeled 750 base transcript were accomplished using the protocol by Chiang et al. [25]. A radiolabeled, 250 base T3 transcript of pGEM4z (Promega) was used as an internal control. Autoradiography and quantitation were as described for the EMSAs. The c-fos transcript was normalized to the internal control in each lane before comparisons between drug-treated samples and controls were made.

2.5. Topo II activity assay

Nuclei isolation and subsequent topo II assays were carried out as described by Beerman, et al., and Woynarowski, et al., respectively, with some modification [26,27]. In brief, HeLa suspension cultures were radiolabeled with [^{14}C]thymidine (0.03 μCi/ml) for 24 h. All subsequent centrifugations were done at 4°C. Cells were pelleted for 4 min at 100×*g* and rinsed with cold nuclei isolation buffer (NIB: 2 mM KH_2PO_4, 150 mM NaCl, 1 mM EGTA, and 5 mM $MgCl_2$, pH 6.9). After repelleting as above, cells were resuspended in NIB containing 0.3% Triton X-100 and incubated on ice for 20 min. Following centrifugation at 300×*g* for 10 min, the pellet was resuspended in NIB to 10^6 nuclei/ml. In each reaction, 20 μM drug was incubated with 0.5 ml of prepared nuclei for 10 min at 37°C. VM-26 to a final concentration of 20 μM was added, followed by a 15 min incubation at the same temperature. No drug was added to controls. Reactions were carried out in the absence of VM-26 in order to test the ability of the agents themselves to induce precipitable complex formation. The reaction volume was brought to 1 ml with NIB before 1 ml 2× buffer (3% SDS, 40 mM EDTA, and 0.4 mg/ml salmon sperm DNA) was added. After a 15 min incubation at 65°C, the samples were cooled to room temperature and vortexed for 30 s. Addition of 0.5 ml 0.325 M KCl, followed by a 30 min incubation on ice, began precipitation of the topo II/DNA complexes. Following centrifugation at 1570×*g* for 15 min, 4 ml wash solution (10 mM Tris, 1 mM EDTA, 0.1 mg/ml salmon sperm DNA and 100 mM KCl) was added to each pellet and they were heated to 65°C for 5 min, cooled on ice for 15 min, then centrifuged at 1570×*g* as above. This washing step was repeated twice before the final pellet was hydrolyzed in 2 M perchloric acid for 1 h at 70°C. Precipitated complexes were quantitated through liquid scintillation counting and results were expressed as percent of total DNA co-precipitable with protein. Percent inhibition was then calculated by comparing drug-treated samples to controls.

3. Results

3.1. Components of the c-fos model

The binding sites for SRF and Elk-1 on the c-fos SRE are shown in Fig. 2A. These TFs were purified following expression as 6-histidine-tagged proteins in bacteria and combined with radiolabeled dsDNA oligos to establish optimal binding conditions in EMSAs. SRF alone can bind to the SRE (Fig. 2B: compare free SRE in lane 1 with the shifted SRF complex in lanes 2 and 3). While Elk-1 cannot autonomously bind to the SRE, it can bind to the high affinity *ets* motif on the *Drosophila* E74 promoter [28], as seen in Fig. 3B, lanes 1 and 2. Combining SRF and Elk-1 on the SRE (Fig. 2B, lanes 4 and 5) forms the TC, which can be distinguished from the SRF complex on the basis of its slight difference in mobility. This difference can be maximized by electrophoresing the complexes longer than illustrated, a condition that results in free probe running off the gel (not shown).

3.2. Ligand structures and characteristics

The TF/DNA complexes of the c-fos system were targeted using the six agents shown in Fig. 1. While **L1–L5** share bisbenzimidazoles as their minor groove-binding moieties and linkers at the *meta* position for attachment of functional groups, **L1** lacks positively charged polyamine tails. Hoe342 is chemically distinct because it lacks the *meta*-substituted linker and instead has an ethyl ether group substituted in *para*. Previously determined melting temperatures (T_m) using a dsDNA oligo containing the sequence 5′-AATTT-3′ provide a measure of relative stability of the ligand:DNA complexes. Equipping the bisbenzimidazole with polyamine side chains significantly increases the ability of these ligands to stabilize dsDNA as evidenced by the large T_m differences between **L1** and the FMGTs.

3.3. Ligand effects on complex formation in EMSAs

To determine if the presence of the polyamine tails at-

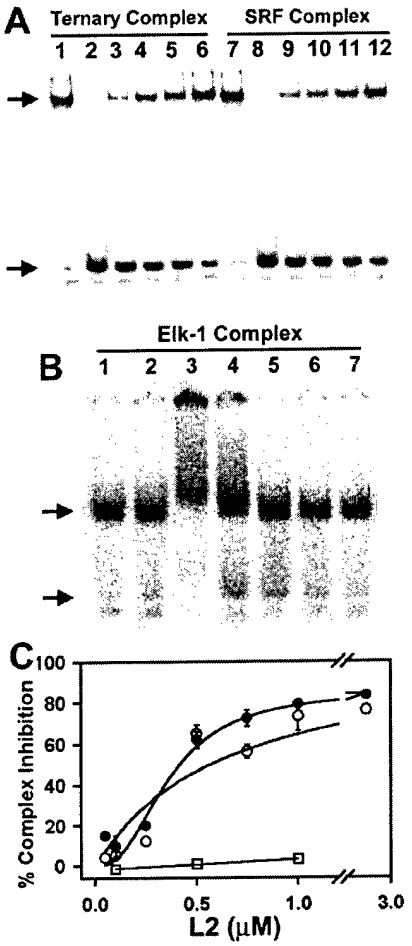

Fig. 3. Ligand effects on complex formation in EMSAs. For (A) and (B), FMGT-2 was co-incubated with radiolabeled probe for 30 min before purified TFs were added. Electrophoresis and autoradiography followed as described in Fig. 2. In each panel, upper arrows: TF/DNA complexes; lower arrows, free DNA. (A) Inhibition of complex formation on the SRE by **L2**. Lanes 1–6: Inhibition of TC formation. Lanes 7–12: Inhibition of SRF complex formation. Lanes 1 and 7, control, no drug; lanes 2 and 8, 10 μM; lanes 3 and 9, 1 μM; lanes 4, 5,10 and 11, 0.5 μM; lanes 6 and 12, 0.1 μM. (B) Inhibition of complex formation on E74. Lanes 1 and 2, control; lane 3, 10 μM; lane 4, 5 μM, lane 5, 1 μM; lane 6, 0.5 μM; lane 7, 0.1 μM. (C) Quantitation of **L2** inhibition. The percent DNA shifted in each drug-treated lane was compared to controls to calculate percent inhibition of SRF (●), Elk-1 (□) or TC (○) formation. Results are from four experiments (mean value ± standard error).

tributes different properties to the novel agents, their ability to inhibit complex formation in EMSAs was first evaluated. Increasing concentrations of ligand and radiolabeled oligos were co-incubated for 30 min. After addition of purified TFs, the samples were incubated for an additional 30 min to allow complex formation to reach equilibrium. Representative results of subsequent electrophoresis and autoradiography are shown for **L2** in Fig. 3A,B. The TC bound to the radiolabeled SRE is evident as a shifted complex in the untreated control (Fig. 3B, lane 1). 10 μM **L2** in lane 2 fully prevents complex formation while decreasing ligand concentrations in lanes 3–6 results in the return of TC complex formation to near control levels. Similar results were obtained in the same concentration range of **L2** for inhibition of SRF complex formation (Fig. 3A, lanes 7–12).

To determine if the FMGTs inhibited Elk-1 binding alone, EMSA evaluations were repeated using purified Elk-1 and a radiolabeled E74 probe (Fig. 3B). No inhibition of Elk-1 complexes occurred at low ligand levels up to 1 μM (lane 5). However, at 5 μM **L2** or higher (lanes 3 and 4), the probe smeared and became retained in the well of the gel, prohibiting accurate analysis at or above this concentration. This occurred regardless of the presence of Elk-1 protein (data not shown).

Densitometric analysis of autoradiograms as shown in Fig. 3A,B allowed the relative amounts of free and complexed DNA to be quantitated. After calculating percent complex formation for each sample, these values were expressed relative to ligand-free controls to yield percent inhibition of complex formation. Graphing these values against ligand concentration produced inhibition curves for effects of **L2** on each complex (Fig. 3C). **L2** inhibited

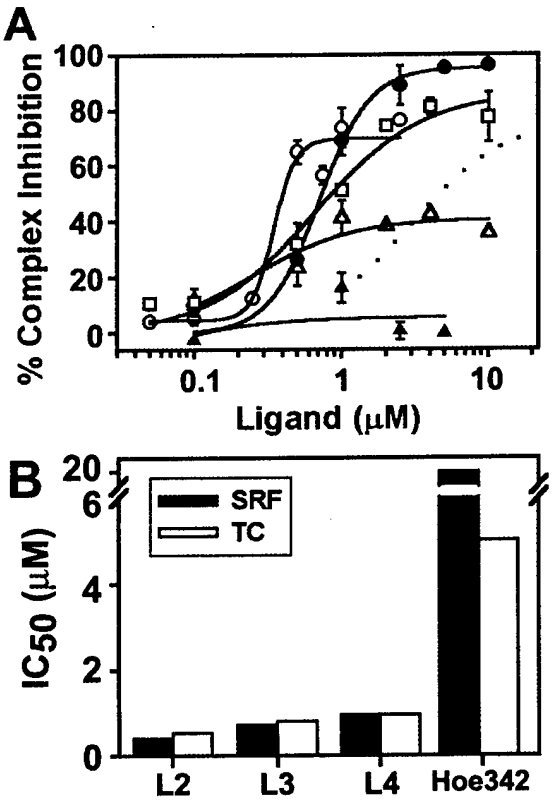

Fig. 4. Comparison of ligand effects on TF complex formation in EMSAs. (A) Drug inhibition of TC formation. Inhibition curves for each compound were plotted and quantitated as described in Fig. 3 for **L1** (▲), **L2** (○), **L3** (●), **L4** (□), **L5** (△) and Hoe342 (dotted line). Results are from four experiments (mean value ± standard error). (B) Summarized comparison of drug potencies in EMSAs. Drug concentrations required for 50% inhibition of complex formation (IC_{50}s) were calculated from inhibition curves as shown in (A) for TC and SRF complexes.

SRF and TC complex formation nearly equivalently, with maximal inhibition of 80% at about 1 μM. For Elk-1 complexes, only those lanes that clearly lacked visible smearing were analyzed. As seen in the representative gel in Fig. 3B, **L2** concentrations up to 1 μM could be successfully quantitated. As noted above, there is no measurable effect of **L2** on Elk-1 complex formation up to this concentration.

3.4. Comparing ligand inhibition of TF/DNA complex formation in EMSAs

The effectiveness of **L2** as an inhibitor of TF complex formation was compared to that of the remaining compounds. Inhibition curves for the effects of FMGTs on TC formation are shown in Fig. 4A. Results for Hoe342 are plotted as a dotted line.

Overall, **L2–L5** were all far more potent inhibitors of TC formation compared to **L1**. The most potent agent, **L2**, was over an order of magnitude more effective than the classical bisbenzimidazole Hoe342 in this assay and about twice as potent as either **L3** or **L4**. At 1 μM, the latter was able to effect 60% complex inhibition. In notable contrast, **L1** had no effect on TC formation even up to 5 μM. Although **L3** was not the most potent compound, it was the only agent analyzed to completely abolish complex formation by about 2 μM. In comparison, **L2** and **L4** reached a plateau of approximately 80% inhibition by 1 μM and 5 μM, respectively. At the highest concentration of Hoe342 tested (10 μM), complex formation was inhibited by 75%.

Of the FMGTs analyzed, **L5** was the least effective inhibitor of TC formation. Even at 10 μM **L5**, only 40% inhibition was attained. Above this concentration, the ligand caused oligo smearing similar to that observed in the earlier Elk-1 EMSAs, prohibiting further analysis. To note, **L4** and **L5** differ in length and complexity by two branched polyamine tail units attached to an amide-bonded backbone. This increased length therefore seems to reduce the ability of **L5** to inhibit TC formation on the SRE. However, **L5** was still much more effective than the analogue **L1**.

The inhibition of SRF complex formation by the ligands tested were similar to the profiles just discussed for TC inhibition (data not shown). None of the compounds inhibited Elk-1 complex formation and all caused well retention of the oligo at micromolar concentrations, as seen for **L2** (Fig. 3B).

The concentration of each agent required to inhibit complex formation by 50% (its IC_{50} value) was calculated from inhibition curves and used to compare drug potencies (Fig. 4B). L2 was the most potent inhibitor of SRF or TC formation with IC_{50} values of 0.4 μM and 0.5 μM, respectively. The other novel agents, **L3** and **L4**, also had submicromolar IC_{50} values. In contrast, approximately an order of magnitude more Hoe342 was required for the same level of SRF complex inhibition. Notably, whereas the FMGTs were equipotent in inhibiting TC or SRF complex formation, Hoe342 was a slightly more effective inhibitor of TC formation. However, despite this improved performance in the TC EMSAs, Hoe342 was still about an order of magnitude less potent than **L2**, **L3** or **L4**.

3.5. Ligand effects on c-fos promoter-driven cell-free transcription

Previous studies of DNA-binding drugs have demonstrated that agents often lose potency as assay conditions become more complex [19,25,29]. We therefore next wished to evaluate whether the FMGTs would also be able to inhibit c-fos promoter-driven transcription in cell-free assays and whether their ability to do so correlated with their EMSA potencies. Here, a more complex environment is achieved by placing the SRE into a longer piece of DNA with greater sequence variation and by adding a nuclear extract that contains cellular transcriptional machinery and an extensive array of additional proteins. The assay can therefore be carried out without nuclear uptake of the agents becoming a complicating factor. A plasmid containing the human c-fos promoter was linearized and incubated with drug for 30 min before being combined with nuclear extract from serum stimulated NIH3T3 cells, [α-^{32}P]CTP, and a mix of nucleotides to drive the production of a radiolabeled transcript. This 750 base transcript was subsequently purified, electrophoresed on a denaturing polyacrylamide gel, and visualized following autoradiography (Fig. 5A, upper arrow). Quan-

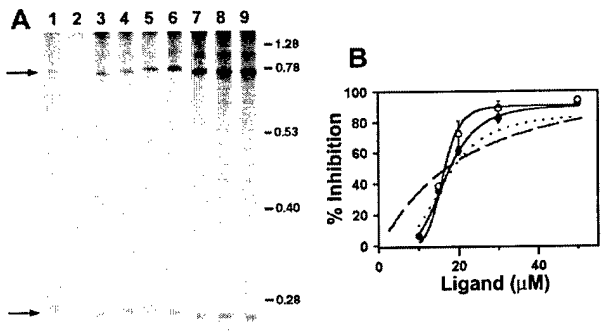

Fig. 5. Ligand effects on c-fos promoter-driven cell-free transcription. (A) Effect of **L2** on cell-free transcription. A plasmid containing the human c-fos promoter was linearized and incubated with drug for 30 min before nuclear extracts from serum-induced NIH3T3 cells were added. Following the reaction in the presence of [^{32}P]CTP, the radiolabeled, 750 base transcript (top arrow) is electrophoresed on a denaturing polyacrylamide gel. A radiolabeled 250 base transcript, used as an internal control (lower arrow), is added to each sample prior to loading. Positions of size markers, in kb, are indicated. Lanes 1 and 2, 30 μM; lanes 3 and 4, 20 μM; lanes 5 and 6, 15 μM; lane 7, 10 μM; lanes 8 and 9, controls, no drug added. (B) Quantitation of drug effects in this assay. All c-fos transcripts were normalized to internal controls before quantitation as in Fig. 4. Results from four experiments (mean value ± standard error) are shown for **L2** (○), **L3** (●), and Hoe342 (dotted line).

titation of the transcript and normalization to the internal control (lower arrow) allowed accurate comparisons between drug-treated and control samples.

Representative results for **L2** (Fig. 5A) show dose-dependent inhibition of transcription. A concentration of 30 μM **L2** nearly abolished transcript formation (lanes 1–2). As drug concentrations decrease to 10 μM in lane 7, transcripts are restored to near control levels (lanes 8 and 9). No change in transcript size was noted in any samples, indicating that inhibition of transcriptional elongation is unlikely. The disappearance of transcripts as drug concentrations increase therefore suggests that transcription initiation is primarily being affected.

The most potent agents in the EMSAs, **L2** and **L3**, were evaluated to determine their effectiveness in inhibiting cell-free transcription. **L1** was not tested because of its lack of activity in the former assay. Results for Hoe342, however, are plotted as a dotted line. Following densitometric quantitation of autoradiographs, transcript levels in drug-treated samples were expressed relative to controls and graphed against drug concentration (Fig. 5B). All the compounds were capable of inhibiting transcription at micromolar concentrations and each had an IC_{50} value of approximately 17 μM. This profile differed from that of the EMSAs, where there was a larger difference in potency between the FMGTs and Hoe342. However, like the EMSAs, slightly lower levels of the FMGTs compared to Hoe342 were needed to achieve complete inhibition of transcription as evidenced by their steeper inhibition curves. Over 90% inhibition of transcript formation was achieved at 30 μM **L2** or **L3**, while more than 50 μM Hoe342 was needed for equivalent inhibition.

3.6. Evaluation of ligand effects on topo II activity

As DNA-reactive agents that bind selectively to A/T rich sequences, the FMGTs may have additional effects on DNA, including the potential to affect other template-mediated activities. We wished to determine if the FMGTs could disrupt other DNA-associated activities in a cell-free environment, and how this activity related to their performance in the simpler EMSAs. As an enzyme responsible for maintaining correct DNA topology, topo II associates with the helix and nicks both strands, becoming covalently bound to the DNA ends formed in the process [30]. The DNA–topo II crosslink in this 'cleavable complex' can be induced by drugs such as the epipodophyllotoxins (i.e. VM-26 or VP-16) [31]. In the presence of minor groove-binding drugs such as netropsin or Hoechst 33258, the formation of these crosslinks in isolated nuclei is inhibited [27,32].

Nuclei isolated from ^{14}C-thymidine-treated HeLa cells were co-incubated with VM-26 and 20 μM of each of the ligands. The DNA–topo II crosslinks were then precipitated and quantitated. The percent inhibition calculated for each compound is listed in Table 1. The FMGTs varied greatly in their ability to inhibit crosslink formation, and this inhibition did not correlate to their observed potencies in inhibiting TF/DNA complex formation. Although these agents exhibited EMSA potencies in the order **L2** > **L3** > **L4** > Hoe342 > **L5**, their potencies in the topo II assay ranked **L5** > **L2** > Hoe342 > **L4** > **L3**. In the absence of VM-26, these agents were incapable of inducing crosslink formation (data not shown), demonstrating that they lacked the ability to induce cleavable complex formation themselves. Although no correlation between the EMSAs and the topo II assay was noted, the FMGTs were able to inhibit topo II activity in the more complex environment of isolated nuclei.

4. Discussion

The novel approach of adding basic side chains to bisbenzimidazole minor groove binders proved to be an effective method for enhancing their ability to inhibit TF complex formation on the c-fos SRE in cell-free assays. Whereas a bisbenzimidazole functionalized with a linker but no basic side chains (**L1**) was completely unable to inhibit TF complex formation in EMSAs, the FMGTs **L2**, **L3**, and **L4** were able to do so at submicromolar concentrations. Moreover, their potency was about 50-fold higher than Hoe342, a classical bisbenzimidazole that, like **L1**, lacks major groove-binding capability. **L2** and **L3** inhibited cell-free c-fos promoter-driven transcription. Additionally, the FMGTs affected general DNA template function as demonstrated by their ability to inhibit the formation of the topo II-cleavable complex in isolated nuclei.

The success of FMGT design and the significant role of the basic polyamine side chains is highlighted by their superior performance in the EMSAs as summarized in Fig. 4B. In marked contrast to the FMGTs, **L1**, without a basic side chain, was ineffective at inhibiting TF/DNA interactions. Furthermore, **L2** was over an order of magnitude more potent in inhibiting SRF complex formation than Hoe342. We also noted that while Hoe342 was more potent in inhibiting TC formation than SRF complex formation, the FMGTs were nearly equipotent on either complex. Thus, while the presence of Elk-1 in the TC may affect the ability of Hoe342 to prevent complex formation on the SRE, it appears to have little effect on the inhibitory activities of the FMGTs. Recruitment of Elk-1 to the TC alters helical conformation and bending [33]. This DNA conformational change may increase the affinity of Hoe342 for its binding site on the SRE, perhaps by altering groove width or shape. The maintenance of FMGT potency may be due to their higher affinity and their ability to clamp onto DNA by interacting with both grooves. This affinity may therefore persist regardless of the presence of a second TF.

The previously determined chemical characteristics of

the FMGTs may be related to their abilities to inhibit TF/DNA complexes [17,18]. The rank of FMGT potencies in inhibiting TF binding overall, **L2** > **L3** ~ **L4** > **L5** ≫ Hoe342 ≫ **L1**, may be due in part to the order in which they stabilize dsDNA, but these alone fail to completely explain the EMSA results. For example, in previous studies, **L3**, **L4** and **L5** bound an oligo containing five contiguous A/T bp with nearly equal affinities, supporting a prediction of nearly equal potencies in the EMSAs [18]. Although **L3** and **L4** were nearly equipotent, **L5** failed to reach even 50% inhibition of TC formation. The polyamine tail of **L5** is longer and contains two more branch points than **L4**. While these characteristics may increase the affinity of **L5** for isolated DNA, they fail to impart an improved ability to inhibit TF binding to the A/T rich site on the SRE oligo.

Extending this analysis to the remaining FMGTs, the polyamine tail of **L2** is about two times longer than that of **L3** and the observed potencies of these compounds in the EMSAs were similar. The additional branching on the polyamine tail of **L3** does not appear to improve the inhibitory potential of this agent. **L4** is nearly as long as **L2**, but more highly branched, and the former was slightly less potent in the EMSAs. It may be that a minimum tail length is required for these compounds to make adequate contact with the phosphodiester backbone, but that increasing the length or complexity of branching to the extent as found on **L5**, may interfere with the ability of these novel agents to inhibit TF/DNA association.

The addition of polyamine tails to bisbenzimidazoles did not compromise their ability to inhibit c-fos promoter-driven cell-free transcription in a more complex environment. **L2** and **L3** were chosen as representative FMGTs to be analyzed in this assay based on their high EMSA potencies, and they performed just as well as Hoe342. However, based solely upon the differences in potencies observed between the FMGTs and Hoe342 in the EMSAs, one would predict that the former agents would be more potent transcriptional inhibitors. As mentioned earlier, a decrease in the potency of DNA-binding drugs as assay conditions become more complex has been observed in many systems [19,25,29]. Additionally, previous studies of the polypyrrole-based MGTs focused mainly on their inhibition of TF/DNA complex formation in EMSAs. However, when evaluated in cell-free transcription assays, their potency was significantly reduced and became comparable to classical minor groove binders such as distamycin (S.Y. Chiang and T.A. Beerman, unpublished observations). In general, it appears that the ratio of improvement between drugs in simple EMSAs is not easily maintained in more complex environments.

The ability of the FMGTs to function in a more complex environment and inhibit other DNA template-associated processes was demonstrated by their inhibition of topo II activity in isolated nuclei. In this system, barriers to cellular or nuclear uptake do not exist and DNA template effects can be measured directly. Here, the order of potency of the compounds correlated with neither their DNA binding affinities nor their TF/DNA complex inhibitory potencies in the EMSAs. However, some similarities were noted between the ligand levels needed to inhibit topo II activity and those needed to inhibit cell-free transcription. For **L2** and Hoe342, 20 μM was sufficient to cause nearly equal levels of inhibition in both assays. However, 20 μM **L3** resulted in 4-fold higher inhibition of cell-free transcription. The characteristics that make the FMGTs good inhibitors of TF/DNA interactions may therefore differ from those needed to inhibit other DNA-related activities. This initial finding suggests that with additional modification, it may be possible to design an FMGT that selectively inhibits transcription over other DNA-related activities.

The potential of adding major groove-binding constructs to minor groove-binding compounds to enhance inhibition of TF/DNA complex formation is apparent from these studies, although further improvement is needed to attain more potent effects on transcription. Adding basic side chains to a bisbenzimidazole greatly improves its ability to inhibit TF binding to DNA in cell-free systems. The FMGTs, with their high DNA binding affinity and ability to interact with both grooves in higher order complexes, were more effective and potent inhibitors of TF/DNA interactions than **L1** or Hoe342, compounds without major groove-contacting ability. Importantly, these studies provide some initial insight into how polyamine tail length and branching can affect the inhibitory activity of these novel agents. We plan to further pursue whether additional changes to ligand structure and polyamine tail configuration may improve the activity of these agents in cell-free assays as well as whole cells.

In the field of drug design, minor groove-binding agents are playing increasingly significant roles in developing agents with improved abilities to distinguish between sequences. Achieving selective inhibition of desired TF/DNA complexes has potentially far-reaching implications in the molecular study of gene regulation as well as therapeutics. Perhaps most significantly, then, this study confirms that the novel drug design concept first employed in enhancing the DNA binding qualities of the tripyrrole MGTs can be applied to other sequence selective minor groove-binding agents and actually improves their ability to inhibit TF/DNA complexes.

Acknowledgements

We graciously thank Dr. Alfred Nordheim for providing the SRF expression vector (pILA-SRF) and pFos-Luc19 plasmid. We also thank Dr. Andrew Sharrocks for providing the Elk-1 expression vector (pAS278). This study was supported in part by National Cancer Institute Grant CA16056 (to T.A.B.), American Cancer Society

Grant DHP 158 (to T.A.B.), US Army Medical Research Grant BC980100 (to C.M.W.), and National Institutes of Health Grant 5R37DK0917136 (to T.C.B.)

References

[1] A.Y. Chen, C. Yu, B. Gatto, L.F. Liu, Proc. Natl. Acad. Sci. USA 90 (1993) 8131–8135.
[2] P.R. Turner, W.A. Denny, Mutat. Res. 355 (1996) 141–169.
[3] H.C. Hurst, Eur. J. Cancer [A] 32A (1996) 1857–1863.
[4] J.J. Welch, F.J. Rauscher 3rd, T.A. Beerman, J. Biol. Chem. 269 (1994) 31051–31058.
[5] S.Y. Chiang, J.J. Welch, F.J. Rauscher 3rd, T.A. Beerman, J. Biol. Chem. 271 (1996) 23999–24004.
[6] A. Dorn, M. Affolter, M. Muller, W.J. Gehring, W. Leupin, EMBO J. 11 (1992) 279–286.
[7] R. Schleif, Science 241 (1988) 1182–1187.
[8] J.A. Feng, R.C. Johnson, R.E. Dickerson, Science 263 (1994) 348–355.
[9] M.A. Schumacher, K.Y. Choi, H. Zalkin, R.G. Brennan, Science 266 (1994) 763–770.
[10] C. Hélène, Nature 391 (1998) 436–438.
[11] T.C. Bruice, Y.M. Houng, X.H. Gong, V. Lopez, Proc. Natl. Acad. Sci. USA 89 (1992) 1700–1704.
[12] K.A. Browne, X.H. Gong, T.C. Bruice, J. Am. Chem. Soc. 115 (1993) 7072–7079.
[13] H.G. Hansma, K.A. Browne, M. Bezanilla, T.C. Bruice, Biochemistry 33 (1994) 8436–8441.
[14] S.Y. Chiang, T.C. Bruice, J.C. Azizkhan, L. Gawron, T.A. Beerman, Proc. Natl. Acad. Sci. USA 94 (1997) 2811–2816.
[15] X.B. Zhang, F.L. Kiechle, Biochem. Biophys. Res. Commun. 248 (1998) 18–21.
[16] S. Wong, R.A. Sturm, J. Michel, X.M. Zhang, P. Danoy, K. McGregor, J.J. Jacobs, A. Kaushal, Y. Dong, I.S. Dunn, P.G. Parsons, Biochem. Pharmacol. 47 (1994) 827–837.
[17] A.L. Satz, T.C. Bruice, Bioorg. Med. Chem. Lett. 9 (1999) 3261–3266.
[18] A.L. Satz, T.C. Bruice, Bioorg. Med. Chem. 8 (2000) 1871–1880.
[19] C.M. White, O. Heidenreich, A. Nordheim, T.A. Beerman, Biochemistry 39 (2000) 12262–12273.
[20] R. Treisman, Trends Biochem. Sci. 17 (1992) 423–426.
[21] R. Marais, J. Wynne, R. Treisman, Cell 73 (1993) 381–393.
[22] Y. Mo, B. Vaessen, K. Johnston, R. Marmorstein, Nat. Struct. Biol. 7 (2000) 292–297.
[23] L. Pellegrini, S. Tan, T.J. Richmond, Nature 376 (1995) 490–498.
[24] T.C. Bruice, D.D. Sengupta, A. Blasko, S.-Y. Chiang, T.A. Beerman, Bioorg. Med. Chem. 5 (1997) 685–692.
[25] S.Y. Chiang, J.C. Azizkhan, T.A. Beerman, Biochemistry 37 (1998) 3109–3115.
[26] J.M. Woynarowski, R.D. Sigmund, T.A. Beerman, Biochim. Biophys. Acta 950 (1988) 21–29.
[27] T.A. Beerman, M.M. McHugh, R. Sigmund, J.W. Lown, K.E. Rao, Y. Bathini, Biochim. Biophys. Acta 1131 (1992) 53–61.
[28] V.N. Rao, E.S. Reddy, Oncogene 7 (1992) 65–70.
[29] S.Y. Chiang, R.W. Burli, C.C. Benz, L. Gawron, G.K. Scott, P.B. Dervan, T.A. Beerman, J. Biol. Chem. 275 (2000) 24246–24254.
[30] D.A. Burden, N. Osheroff, Biochim. Biophys. Acta 1400 (1998) 139–154.
[31] G.L. Chen, L. Yang, T.C. Rowe, B.D. Halligan, K.M. Tewey, L.F. Liu, J. Biol. Chem. 259 (1984) 13560–13566.
[32] T.A. Beerman, J.M. Woynarowski, R.D. Sigmund, L.S. Gawron, K.E. Rao, J.W. Lown, Biochim. Biophys. Acta 1090 (1991) 52–60.
[33] A.D. Sharrocks, P. Shore, Nucleic Acids Res. 23 (1995) 2442–2449.

Double-Stranded DNA Binding Characteristics and Subcellular Distribution of a Minor Groove Binding Diphenyl Ether Bisbenzimidazole†

Alexander L. Satz,‡ Christine M. White,§ Terry A. Beerman,*,§ and Thomas C. Bruice*,‡

Department of Chemistry and Biochemistry, University of California at Santa Barbara, Santa Barbara, California 93106, and Department of Pharmacology and Therapeutics, Roswell Park Cancer Institute, Elm and Carlton Streets, Buffalo, New York 14263

Received February 16, 2001; Revised Manuscript Received March 23, 2001

ABSTRACT: The interactions of Hoechst 33377 (H1) with 20 different oligomeric duplexes have been investigated via spectrofluorometric titrations and/or thermal denaturation experiments. H1 is shown to form 2:1 complexes with dsDNA binding sites of at least four contiguous A/T base pairs. H1 is also shown to possess the rare ability to meaningfully distinguish between different A·T rich sequences. For example, the combined equilibrium constants for complexation of the oligomeric duplex 5′-GCAATTGC-3′ (**15**) by H1 are found to be 110-fold greater than for the duplex 5′-GCTTAAGC-3′ (**16**). It is believed that the 5′-TpA-3′ dinucleotide step in **16** disrupts the rigid "A-tract" conformation of **15** and discourages minor groove binding by agents capable of recognizing longer dsDNA sequences. Molecular models are presented which elucidate the structure of the $(H1)_2$−dsDNA minor groove complex. The two H1 molecules bind to an A/T rich sequence of 6 bp in a slightly staggered, side-by-side, and antiparallel arrangement. Evidence suggests that the piperazine rings of the H1 side-by-side complex are capable of resting in the minor groove of G/C base pairs. Fluorescence microscopy studies using NIH3T3 cells indicate that H1 is capable of traversing the cytoplasmic membrane and selectively localizing to nuclear DNA. H1 also demonstrated the ability to inhibit endogenous transcription of the c-fos gene in NIH3T3 cells at micromolar concentrations. Cytotoxicity studies employing the same cell type show H1 to possess an LD_{50} of 3.5 μM.

Interest in the control of transcription at the molecular level has spurred efforts toward the development of new minor groove binding agents with greater sequence selectivity (*1*−*7*). Increased selectivity can be achieved by increasing the number of base pairs recognized by a DNA-binding agent. An alternative is to develop agents capable of distinguishing among all four DNA bases (*1*). Recently, we reported a novel tripyrrole peptide−bisbenzimidazole conjugate capable of recognizing 9 bp in the minor groove of dsDNA[1] (*8*). In a continuing effort to develop bisbenzimidazole-type compounds with increased specificity, we investigated the dsDNA binding characteristics of a diphenyl ether bisbenzimidazole H1 (*9*). H1 held the potential for recognizing dsDNA sequences longer than other bisbenzimidazole-type compounds such as H2 due to its increased length while still maintaining a crescent-shaped curvature. A crescent shape is a characteristic of bisbenzimidazoles that allows them to maintain optimal contact in the minor groove.

Although H3 is the most widely investigated of the bisbenzimidazole-type compounds, both H1 and H2 are known to be significantly more cytotoxic (*10*, *11*). It has been suggested that these agents exhibit greater cytotoxicity due to their greater cellular permeability (*11*). Minor groove binding agents can inhibit the binding of regulatory proteins to their DNA consensus sites in cell-free studies (*7*, *12*, *13*). This may be the mechanism by which H1 and H2 contribute to cell death. The cytotoxicity of H1 suggests that it possesses some type of biological activity. Previous studies did not investigate the ability of H1 to traverse the cell membrane and reach its nuclear DNA target. Quantitative determination of its ability to inhibit gene transcription in whole cells, in combination with the knowledge that it selectively localizes in nuclear DNA, would provide a much stronger link between its ability to bind DNA and its cytotoxicity.

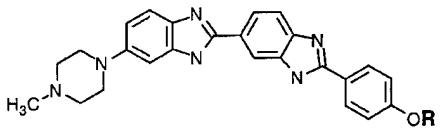

Hoechst 33377 (H1) R = -phenyl
Hoechst 33342 (H2) R = -ethyl
Hoecsht 33258 (H3) R = -H

Here we employ a combination of cell-free and cellular assays to determine if H1 would make a good lead compound for the pursuit of new minor groove binding agents with increased binding selectivity and potency. We have investigated the binding of H1 to the 18 bp oligomeric duplex 5′-GCGGTATAAAATTCGACG-3′ (**1**) and nine other related duplexes (**2**−**10**) in an effort to characterize H1's

† This work was supported by grants from the National Institutes of Health to T.C.B. (5R37DK09171-36) and the American Cancer Society to T.A.B. (RPG-96-034-04-CDD).

‡ University of California at Santa Barbara.

§ Roswell Park Cancer Institute.

[1] Abbreviations: H1, Hoechst 33377; H2, Hoechst 33342; H3, Hoechst 33258; dsDNA, double-stranded DNA; HPLC, high-pressure liquid chromatography; DMSO, dimethyl sulfoxide; Ar, aromatic; ssDNA, single-stranded DNA; TF, transcription factor; SRE, serum response element; SRF, serum response factor; EMSA, electrophoretic mobility shift assay; oligo, oligonucleotide.

10.1021/bi0103415 CCC: $20.00
Published on Web 05/04/2001

Table 1: Stoichiometries and Equilibrium Association Constants for $(Ligand)_x$−dsDNA Complexes and Relative Fluorescence Intensities[a]

oligomeric duplex[b]	H1	H2	H3
5′-GCGACTGCAATTTCGACGTCC-3′ (**11**)			
$(ligand)_x$−**11** stoichiometry	2:1	1:1	1:1
fluorescence intensity	5400	6400	6900
equilibrium association constant[d]	$K_1K_2 = 8.4 \times 10^{16}\ M^{-2}$	$K_1 = 1.2 \times 10^{9}\ M^{-1}$	$K_1 = 4.2 \times 10^{8}\ M^{-1}$
5′-GCGACTGCAATTCGACGTCC-3′ (**12**)			
$(ligand)_x$−**12** stoichiometry	2:1	1:1	1:1
fluorescence intensity	4400	5600	6400
equilibrium association constant[d]	$K_1K_2 = 2.6 \times 10^{16}\ M^{-2}$	$K_1 = 1.5 \times 10^{8}\ M^{-1}$	$K_1 = 1.8 \times 10^{8}\ M^{-1}$
5′-GGACGTCGATTGCAGTCGTC-3′ (**13**)			
$(ligand)_x$−**13** stoichiometry	no clear binding[c]	2:1	2:1
fluorescence intensity	140−190	4000	2500
equilibrium association constant[d]	no clear binding	$K_1K_2 = 2.3 \times 10^{14}\ M^{-2}$	$K_1K_2 = 4.7 \times 10^{14}\ M^{-2}$
5′-GGACGTCGTTGCAGTCGTCG-3′ (**14**)	no binding	no binding	no binding
fluorescence intensity	22	35	150
buffer only (no DNA)	22	23	160

[a] Stoichiometries determined by spectrofluorometric titration (10 mM potassium phosphate pH 7.0 buffer, 150 mM NaCl, 26 °C). Relative fluorescence intensities stated in arbitrary fluorescence units (450 nm) × M^{-1}. [b] Potential A·T rich binding sites are underlined. [c] The relative fluorescence intensity of the ligand−**13** complex is too weak to accurately measure the level of complex formation. [d] Determined by nonlinear least-squares fitting of an isothermal binding curve. Isothermal binding curves were generated using 10 mM potassium phosphate pH 7.0 buffer and 150 mM NaCl at 26 °C. Equilibrium constants are given as the product K_1K_2 for 2:1 ligand:DNA stoichiometries since separation of individual equilibrium constants is not possible. The stated equilibrium constants have a standard deviation of ±80%.

Table 2: Melting Temperatures for Ligand−18-mer Complexes (°C)[a]

		Δt_m		
18 bp oligomeric duplex	t^0_m	H1	H2	H3
5′-GCGGTATAAAATTCGACG-3′ (**1**)	57	6	5	3
5′-GCGGCATAAAATTCGACG-3′ (**2**)	62	4	4	2
5′-GCGGTGTAAAATTCGACG-3′ (**3**)	60	5	5	1
5′-GCGGTACAAAATTCGACG-3′ (**4**)	60	5	5	1
5′-GCGGTATGAAATTCGACG-3′ (**5**)	58	6	6	1
5′-GCGGTATAGAATTCGACG-3′ (**6**)	57	5	6	2
5′-GCGGTATAAGATTCGACG-3′ (**7**)	57	2	2	1
5′-GCGGTATAAAGTTCGACG-3′ (**8**)	58	1	0	1
5′-GCGGTATAAAACTCGACG-3′ (**9**)	58	3	2	1
5′-GCGGTATAAAATCCGACG-3′ (**10**)	58	5	3	2

[a] t_m values for complexes were determined by first-derivative analysis. t^0_m values are melting temperatures of oligomeric duplexes (0.15 μM) in 10 mM potassium phosphate pH 7.0 buffer containing 150 mM NaCl in the absence of ligand. Δt_m values are differences in melting temperatures for oligomeric duplexes in the absence and presence (0.3 μM = 2 equiv) of ligand. The standard deviation for Δt_m values is ±1 °C.

Table 3: Melting Temperatures for Oligomeric Duplexes of the Type d(-A_xT_x-) and d(-T_xA_x-) and Their Ligand Complexes (°C)[a,b]

		Δt_m			
oligomeric duplex[c]	t^0_m	H1	H2	H3	netropsin
5′-GCAATTGC-3′ (**15**)[b]	40	12	11	8	6
5′-GCTTAAGC-3′ (**16**)[b]	30	0	11	9	4
Δt_m(**15**) − Δt_m(**16**)		12	0	−1	2
5′-GAAAATTTTC-3′ (**17**)	29	19	18	14	14
5′-GTTTTAAAAC-3′ (**18**)	24	12	16	13	12
Δt_m(**17**) − Δt_m(**18**)		7	2	1	2
5′-GAAAAAATTTTTTC-3′ (**19**)	42	15	16	13	10
5′-GTTTTTTAAAAAAC-3′ (**20**)	39	16	15	13	9
Δt_m(**19**) − Δt_m(**20**)		−1	1	0	1

[a] t_m values for oligomer complexes were determined by first-derivative analysis. All t_m values were determined by employing 1.5 μM oligomeric duplex and 3 μM ligand. t^0_m values are melting temperatures of oligomeric duplexes in the absence of ligand. Δt_m values are differences in melting temperatures for oligomeric duplexes in the absence and presence of ligand. The standard deviation for Δt_m values is ±1 °C. [b] All experiments employed 10 mM potassium phosphate pH 7.0 buffer and 150 mM NaCl except for those involving **15** and **16**, for which equivalent buffer of 1 M NaCl was used. [c] 5′-TpA-3′ dinucleotide steps are underlined.

sequence selectivity (Table 2). The oligomeric duplex **1** contains the TATA box, which in eukaryotes consists of the consensus sequence 5′-TATAAAA-3′, and is recognized by the TATA binding protein (TBP) subunit of TFIID of the RNA polymerase II transcription initiation complex. One benefit of studying bisbenzimidazoles such as H1 is that they form highly fluorescent dsDNA complexes. This makes it possible to determine dsDNA complex stoichiometries and equilibrium association constants via spectrofluorometric titrations (*8*, *14*−*16*). $(H1)_x$−dsDNA complex stoichiometries and equilibrium association constants are reported for a series of oligomeric duplexes which differ in the size of their A/T rich binding sites (Table 1). The ability of H1 to distinguish among different A/T rich oligomeric duplexes of the type d(-A_xT_x-) versus d(-T_xA_x-) (x = 2, 4, and 6) is discussed (Tables 3 and 4). Comparisons are made between H1, H2, H3, and netropsin. Additionally, we report the ability of H1 to inhibit endogenous transcription of the c-fos gene in NIH3T3 cells and describe the use of fluorescence microscopy in determining the subcellular distribution of the agent.

To determine if H1 is able to bind to nuclear DNA, the subcellular localization of H1 was explored using fluorescence microscopy. Localization to the nucleus may be connected to an agent's ability to affect DNA-related functions. Recently, H2 was demonstrated to inhibit the endogenous expression of the c-fos gene in NIH3T3 cells at micromolar concentrations (*17*). The c-fos gene, an immediate-early response gene, is tightly regulated at the level of transcription (*18*, *19*). The expression of c-fos requires a functional serum response element (SRE), a promoter region containing an A/T rich site, to which a dimer of the serum response factor (SRF) binds (*20*, *21*). This A/T rich site in the SRE is a potential target for binding by H1 and disruption of normal gene expression. Consequently, we investigate the ability of H1 to inhibit endogenous transcription of the c-fos gene in NIH3T3 cells. Finally, because the DNA binding activity of H1 may contribute to its ability to cause cell death, its cytotoxicity profile is compared to those of H2 and H3.

Table 4: Comparison of Equilibrium Association Constants for Complexation of d(GCA_2T_2GC) versus d(GCT_2A_2GC) for H1 and H3[a]

	H1	H3
5′-GCAATTGC-3′ (**15**)		
equilibrium constant	$K_1K_2 = 1.6 \times 10^{16}$ M^{-2}	$K_1 = 2.4 \times 10^8$ M^{-1}
(ligand)$_x$−**15** stoichiometry	2:1	1:1
fluorescence intensity (λ_{max} = 450 nm)	4260	7200
5′-GCTTAAGC-3′ (**16**)		
equilibrium constant	$K_1K_2 = 1.4 \times 10^{14}$ M^{-2}	$K_1 = 1.1 \times 10^8$ M^{-1}
(ligand)$_x$−**16** stoichiometry	2:1	1:1
fluorescence intensity (λ_{max} = 480 nm)	1280	500
factor change in equilibrium constant given as K_{15}/K_{16}	110	2

[a] Determined by nonlinear least-squares fitting of an isothermal binding curve. Isothermal binding curves were generated using 10 mM potassium phosphate pH 7.0 buffer and 1 M NaCl at 16.5 °C. Equilibrium constants are given as the product K_1K_2 for 2:1 ligand:DNA stoichiometries since separation of individual equilibrium constants is not possible. The stated equilibrium constants have a standard deviation of ±80%. Complex stoichiometries were determined via spectrofluorometric titrations. Fluorescence intensities are provided in arbitrary fluorescence units × M^{-1} (oligomeric duplex). Fluorescence emission was monitored at 450 or 480 nm depending on the wavelength of maximum signal intensity for the ligand−dsDNA complex (λ_{max}).

MATERIALS AND METHODS

Organic Synthesis. ^{1}H NMR spectra were obtained on a Varian Unity Inova 400 spectrometer. Fast atom bombardment mass spectra were obtained on a VG analytical, VG-70E double-focusing mass spectrometer, with an Ion Tech Xenon Gun FAB source, and an OPUS/SIOS data interface and acquisition system. High-pressure liquid chromatography was carried out using a Hewlett-Packard series 1050 HPLC system equipped with a diode array detector. For preparative separations, an Alltech Macrosphere 300A, C8, silica, 7 μm, 250 mm × 10 mm reverse phase column was used. For analytical separations, an Alltech Macrosphere 300A, C18, silica, 7 μm, 250 mm × 4.6 mm reverse phase column was used.

H1. 2-(3-Nitro-4-aminophenyl)-6-(4-methyl-1-piperazinyl)-benzimidazole (222 mg, 0.63 mmol) was hydrogenated according to literature procedure to form the reactive diortho amine 2-(3,4-diaminophenyl)-6-(4-methyl-1-piperazinyl)benzimidazole (*22*). The diortho amine was dried under vacuum for 30 min and then without purification added to 5 mL of nitrobenzene and 1 equiv of 4-phenoxybenzaldehyde (125 mg). The solution was stirred at 140 °C for 23 h. The product was precipitated out with hexanes and collected by filtration. The crude product was then purified by flash chromatography (silica, 70:30:1 ethyl acetate/methanol/triethylamine mixture). The product was then further purified via HPLC reverse phase chromatography (0.1% aqueous trifluoroacetic acid, acetonitrile mobile phase) to yield 9.25 × 10^{-6} mol of product. Quantification of product quantity was achieved via NMR spectroscopy using an internal standard. Product purity was shown by analytical HPLC analysis: R_f = 0.1 (silica, 70:30:1 ethyl acetate/methanol/triethylamine mixture); ^{1}H NMR (D_2O + DMSO-d_6) δ 2.85 (s, 3H, CH_3-NR_2), 3−3.1 and 3.14−3.26 [two multiplets, 4H, (-CH_2)$_2$NMe, piperazine], 3.54 and 3.84 [two doublets, 4H, -(CH_2)$_2$N-Ar, piperazine], 7.04 (m), 7.1 (m), 7.18 (m), 7.23 (m), 7.28 (m), 7.4 (m), 7.66 (m), 7.84 (m), 7.93 (m), 8.1 (m), 8.32 (m) (signals detected between 7 and 8.4 ppm are due to Ar protons); LRMS (FAB) 501 $(M + H)^+$.

DNA Binding Investigations. Purified DNA oligomers were purchased from the Biomolecular Resource Center, University of California at San Francisco (San Francisco, CA). H2, H3, 0.05 wt % 3-(trimethylsilyl)propionic-2,2,3,3-d_4 acid, sodium salt in D_2O, solvents, and other reagents were purchased from Aldrich Chemical Co. Oligomeric duplexes were formed by annealing complementary oligomers by heating equal molar mixtures to 95 °C for 10 min and slowly cooling them to ambient temperature. In the case of less thermally stable oligomeric duplexes, ssDNA oligomers were heated to 90 °C and slowly cooled to 5 °C at a rate of 2 °C/min by employing a temperature programmable cell block. Molar extinction coefficients for oligomeric duplexes were approximated using an A_{260} of 16 800 M^{-1} (G·C base pair)$^{-1}$ and an A_{260} of 13 600 M^{-1} (A·T base pair)$^{-1}$. Solutions of known ligand concentrations were prepared via peak integration of the ligand's NMR spectrum where the ligand samples that were used contained a known quantity of the internal standard 3-(trimethylsilyl)propionic-2,2,3,3-d_4 acid, sodium salt (*15*). UV−vis spectra were acquired on a Cary 100 Bio UV−vis spectrophotometer equipped with a temperature programmable cell block. Data points were taken every 1 °C with a temperature ramp of 0.5 °C/min. Thermal melting temperatures were calculated by first-derivative analysis. Fluorescence spectra were obtained on a Perkin-Elmer LS50B fluorimeter equipped with a constant-temperature water bath. Solutions were excited at 345 nm. Spectrofluorometric titrations were carried out by titrating a constant concentration of DNA, usually between 2 and 100 nM, with a relatively concentrated solution of ligand. All experiments were carried out in 10 mM potassium phosphate pH 7.0 buffer and 150 mM NaCl unless specifically stated otherwise. Buffer solutions were treated with Chelex and filtered (0.22 μm).

Following determination of ligand−dsDNA complex stoichiometries, equilibrium constants for dsDNA complexation were determined by generating isothermal binding curves via spectrofluorometric titrations (titration of a dilute dsDNA solution with ligand). Equilibrium constants for ligand−dsDNA stoichiometries were calculated by fitting isothermal binding curves using either eq 1 or 2 with eq 3 (Figure 1C) (*8*, *15*). Equations 1 and 2 were employed to fit plots of fluorescence versus concentration of unbound ligand ($[L]_f$) for cases of 1:1 and 2:1 binding stoichiometries, respectively. The $[L]_f$ is calculated using eq 3. The derivation and use of eqs 1−3 have been discussed previously (*8*, *15*, *16*).

$$F = \sum\Phi_f\left(\frac{K_1[L]_f}{1 + K_1[L]_f}\right) \quad (1)$$

$$F = \sum\Phi_f\left(\frac{0.5K_1[L]_f + K_1K_2[L]_f}{1 + K_1[L]_f + K_1K_2[L]_f}\right) \quad (2)$$

where $\sum\Phi_f$ is the total fluorescence intensity upon saturation of dsDNA binding sites with ligand while K_1 and K_2 are the equilibrium association constants for the first and second binding events, respectively.

$$F = \sum \Phi_f \frac{[L]_{bound}}{n[DNA]_T} \quad (3)$$

where $[L]_{bound}$ is the concentration of ligand bound to dsDNA, n is the stoichiometry of binding, and $[DNA]_T$ is the total concentration of duplex DNA in the sample. Equation 4 was only employed for investigation of the H3−**13** and H3−**16** complexes. It was used to calculate the fluorescence signal of the ligand−dsDNA complexes adjusted for background emission of the uncomplexed ligand (F_{adj}).

$$F_{adj} = F - [L]_f \Phi_{buffer} \quad (4)$$

where $[L]_f$ is calculated using eq 3 and Φ_{buffer} is the relative fluorescence intensity of ligand in buffer as listed in Table 1 in units of fluorescence × M^{-1}.

Model Building. The molecular modeling program SYBYL was used to construct plausible ligand−dsDNA complexes. For $(H1)_2$−dsDNA and $(H3)_2$−dsDNA complexes, ligand molecules were docked into the A/T rich minor groove of a model B-DNA helix. The 1:1 H2−, H3−, and netropsin−dsDNA complex models were derived from X-ray crystal structure coordinates (*23*, *24*). Estimates of binding site size were made by measuring the length of the bound ligand along the helix axis (angstroms) and dividing that value by 3.4 Å, the average distance that separates bases along the helix axis of B-DNA.

Cell Culture. Murine NIH3T3 fibroblasts [American Type Culture Collection (ATCC)] were passaged in Dulbecco's modified Eagle's medium (DMEM) containing high levels of glucose (4500 mg/L) and sodium pyruvate (110 mg/L), supplemented with 10% calf serum. Cells were maintained at 37 °C in 5% CO_2.

Drug Handling and Storage. H1 samples were stored as lyophilized, 10 nmol aliquots at −20 °C in a light-tight box. Samples were resuspended in dH_2O (pH 3) to a final working concentration of 1 mM and stored at −20 °C until they were used. Resuspended drug was warmed to room temperature and mixed well before further dilutions into dH_2O as noted below. H2 (Aldrich Chemical Co.) was prepared in dH_2O and treated similarly.

Fluorescence Microscopy and Visualization of Drug Localization in Live NIH3T3 Cells. A total of 3.7 × 10^4 NIH3T3 cells were seeded onto 18 mm round coverslips in flat-bottomed 12-well plates and allowed to grow for 48 h. The growth medium was replaced with 0.8 mL of starvation medium (0.5% calf serum in DMEM), to which was added 10 μL of drug appropriately diluted in sterile dH_2O. After 16 h, the coverslips were pried from their wells and dip-rinsed in phosphate buffered saline. They were placed onto glass slides and observed immediately using an Olympus BX40 epifluorescence microscope equipped with a universal reflected light fluorescence vertical illuminator (Olympus, Inc.). An Olympus U-MNU filter cube was chosen to visualize the cells. Images were captured using an RT-SPOT color digital camera (Diagnostic Instruments, Inc.). Initially, the exposure time was manually set to 100 ms to accommodate the best visualization of the brightest image, and all subsequent images were captured using this exposure for any given experiment. Monochrome and color fluoromicrographs and their respective phase contrast images were captured. Duplicate coverslips for each drug exposure were evaluated in three separate experiments, and three images of different fields in each coverslip were captured to obtain representative results. Semiquantitative assessment of comparative drug intensity in the monochrome images was achieved using Diagnostic Instrument's ImagePro Plus program. The integrated optical density (IOD) of the cells was quantified and expressed per cell number in the field of view. IOD values for the three images captured per coverslip were then averaged.

Northern Blot Analysis. A total of 2.5 × 10^5 NIH3T3 cells were seeded into 60 mm plates and allowed to grow for 48 h. Following removal of growth medium and a PBS rinse, starvation medium was added. Drug dilutions were made into sterile dH_2O, and 20 μL of these dilutions was added to duplicate plates. At least three controls, which received dH_2O only, were used in each experiment. After 16 h, the cells were induced for c-fos by adding calf serum directly to the plates to a final concentration of 15% and incubating the cells at 37 °C for 30 min (previously determined to be optimal for c-fos mRNA expression). Total RNA was then isolated using TRIzol (GIBCO BRL) and electrophoresed in 1× MOPS buffer [40 mM MOPS (pH 7.0), 10 mM sodium acetate, and 10 mM EDTA] on a 1.5% denaturing agarose gel (2.2 M formaldehyde and 1× MOPS) for 4.5 h at 80 V. RNA was transferred and UV cross-linked to a GeneScreen membrane (NEN Life Science Products), incubated at 60 °C for 1 h in pre-hybe buffer [0.5 M sodium phosphate (pH 7.2), 7% SDS, 1 mM EDTA, and 1% bovine serum albumin (BSA)], and then hybridized to radiolabeled probes under the same conditions overnight. The plasmid pGEM4z-Fos (Loftstrand Laboratories, Ltd.), containing the murine c-fos coding sequence, and a phagemid containing the coding sequence for glyceraldehyde-3-phosphate dehydrogenase (G3) (ATCC) served as the probes. Each was linearized with *Hin*dIII and radiolabeled with [α-^{32}P]dCTP using Ambion's DecaPrime II kit. Blots were given two 20 min washes each in buffer A [40 mM sodium phosphate (pH 7.2), 5% SDS, 1 mM EDTA, and 0.5% BSA] and buffer B [20 mM sodium phosphate (pH 7.2), 1% SDS, and 1 mM EDTA] before being exposed to a Molecular Dynamics phosphorimaging screen and scanned with the company's STORM phosphorimager. Quantitation using the company's ImageQuant program allowed percent growth inhibition to be calculated by comparing drug-treated samples to solvent controls.

Cytotoxicity Assay. A total of 1 × 10^4 NIH3T3 cells were seeded into each well of a 24-well plate and allowed to grow for 24 h. Growth medium was removed and replaced with 0.4 mL of fresh growth medium. Drug was diluted into sterile dH_2O, and 10 μL of appropriate dilutions was added to each well. Triplicate samples for each drug concentration per experiment were carried out. In total, three experiments were performed. Cells were allowed to grow for 72 h before being trypsinized and counted using a automated particle counter (Beckman Coulter, Inc.). Percent cell survival was calculated by comparing drug-treated samples to solvent controls.

RESULTS

Synthesis of H1. H1 was originally synthesized via two consecutive reactions of diortho amines with imino ethers

to form the molecule's two benzimidazole rings (*9*). Our slightly modified approach took advantage of a reaction pioneered by Lown and co-workers that involves condensation of a diortho amine with an aldehyde in nitrobenzene solvent to give the final product (*25*). The ^{1}H NMR data for H1, previously unreported, are included in Materials and Methods.

*Spectrofluorometric Titrations of Oligomeric Duplexes **11**−**14** (15).* Similar to that of H3 (*14*, *15*), the fluorescence emission intensities of H1 and H2 greatly increase upon complexation with dsDNA. When excited at 345 nm, H1− and H2−dsDNA complexes emit a broad fluorescence signal centered at 450 nm. Table 1 lists stoichiometries of (ligand)$_x$−dsDNA complexes and their relative fluorescence intensities at 450 nm.

H1 forms 2:1 ligand−dsDNA complexes with oligomeric duplexes **11** and **12**. H2 and H3 form complexes with the same oligomers with 1:1 stoichiometries. The fluorescence spectra of H1 and H2 in pH 7.0 buffer (no DNA present) consist of a featureless straight line between 410 and 490 nm. In contrast, the uncomplexed fluorescence spectrum of H3 has a broad plateau or peak which begins to increase at ~460 nm and reaches a maximum at wavelengths of ≥480 nm.

The fluorescence spectrum of H1 in the presence of **13** contains a broad peak centered at 450 nm, characteristic of an (H1)$_x$−dsDNA complex. However, the instability and weak fluorescence of the (H1)$_x$−**13** complex prevented its stoichiometry from being determined accurately. H2− and H3−**13** complexes were found to have 2:1 stoichiometries. Titration of **13** with 1 equiv of H3 effects a pronounced peak centered at 450 nm within the fluorescence spectrum, which is characteristic of H3−dsDNA complexes. Later in the titration, at points with >1 equiv of H3, the solution's fluorescence spectrum shifts to the red and begins to resemble that expected for uncomplexed H3. As shown in Figure 1A, the high background fluorescence of uncomplexed H3 obscures the fluorescence emission of the (H3)$_2$−**13** complex. The later part of the titration (Figure 1A) describes a straight line with a slope of 1.76×10^8 M^{-1}, roughly equivalent to the value of 1.6×10^8 M^{-1} determined for uncomplexed H3 in pH 7.0 buffer. The magnitude of the fluorescence signal due to uncomplexed H3 was subtracted from each data point (eq 4) to yield a plot of $F_{adjusted}$ versus $[H3]_0$ from which the stoichiometry of the complex was determined (Figure 1B). Additionally, an isothermal binding curve was plotted and the equilibrium constant for complexation of **13** calculated (Figure 1C). Relative fluorescence intensities for ligands in the presence of oligomeric duplex **14** are equivalent to those observed in buffer only (Table 1).

*Equilibrium Association Constants for Complexation of Oligomeric Duplexes **11**−**13**.* All three ligands formed complexes with **11** and **12** at near-nanomolar concentrations (Table 1). Comparison between equilibrium constants determined in units of M^{-2} and M^{-1} can be made by calculating the square root of K_1K_2 values to give approximate equilibrium constants for individual binding events in units of M^{-1}. By this approximation, the equilibrium constant for complexation of **12** by H1 (K_1) is ~1.6×10^8 M^{-1}, equivalent to the K_1 values for H2 and H3. Using this same method, K_1 values for complexation of **13** by H2 and H3 are ~1.5×10^7 and 2.2×10^7 M^{-1}, respectively. Hence, binding of H2 and H3 to the oligomeric duplex **13** yields a K_1 value that is 10-fold lower than that obtained with duplex **12**.

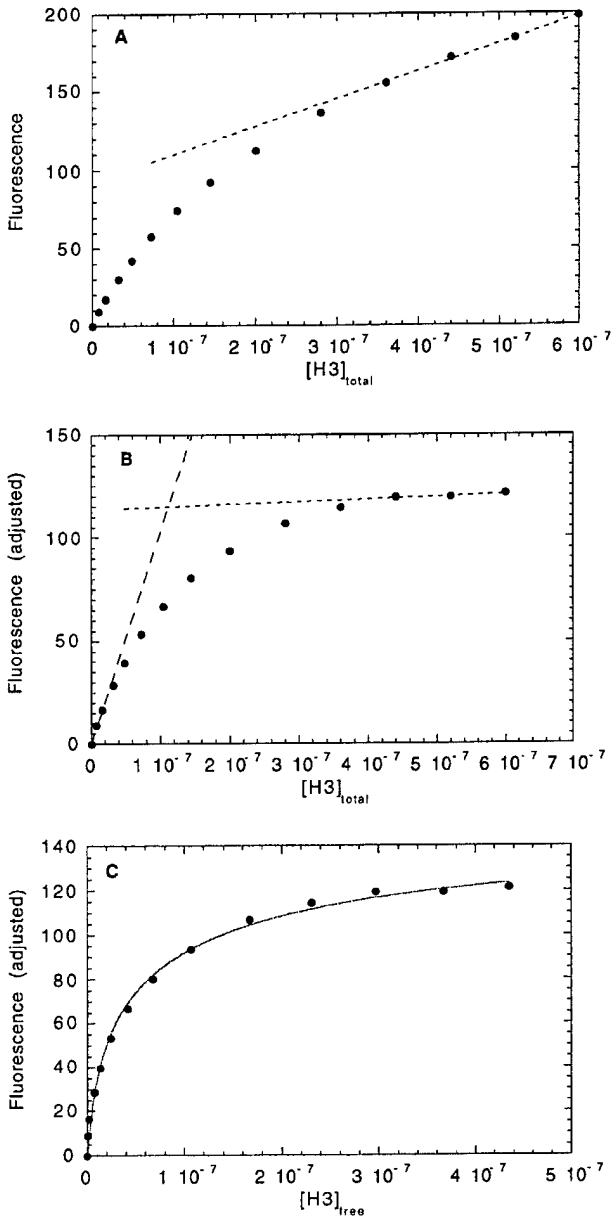

FIGURE 1: (A) Titration of 50 nM **13** with H3. The plot shows the relative fluorescence intensity at 450 nm in arbitrary units vs $[H3]_{total}$. The straight line was generated by linear least-squares fitting of data points late in the titration ($y = 92.51 + 1.77 \times 10^8$). (B) The fluorescence data from panel A have been adjusted to account for fluorescence due to uncomplexed (free) H3 using eq 4. The straight lines were generated by linear least-squares fitting of data points early and late in the titration. The two lines intersect at 100 nM, indicating formation of an (H3)$_2$−**13** complex. (C) The fluorescence data from panel B have been plotted vs $[H3]_{free}$ as calculated by eq 3. The data have been fit by a nonlinear least-squares fitting routine by employing eq 2 to determine the equilibrium association constant for complexation (for the fit shown in panel C, $R^2 = 0.99$).

The effects of ligands on the thermal stabilities of oligomeric duplexes **11**−**14** were investigated in an attempt to compare the effects with values ascertained via spectrofluorometric titrations. However, ligands had little effect on the thermal stabilities of **11**−**14** even when employing low-

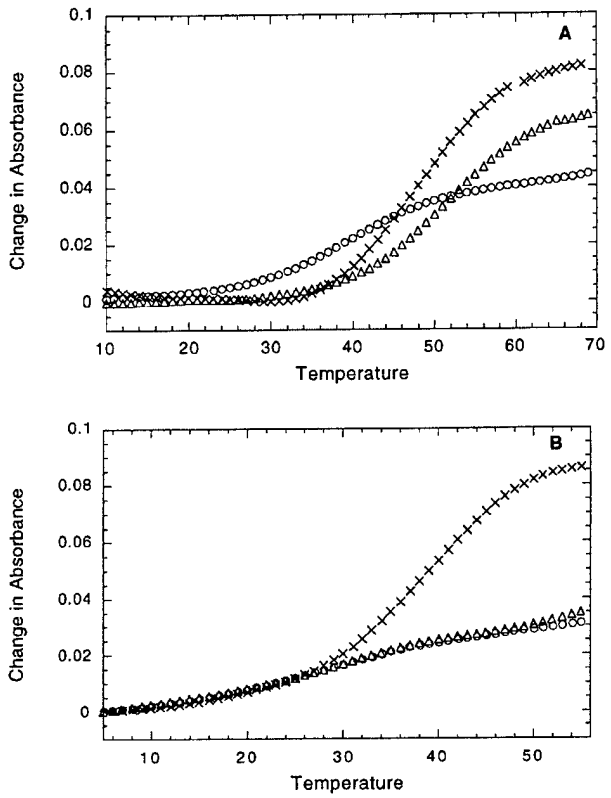

FIGURE 2: Thermal melting curves for oligomeric duplexes **15** (A) and **16** (B) and their ligand (2 equiv) complexes. Plots are shown as the change in absorption units vs degrees Celsius. Experiments were carried out using 1.5 μM duplex and 3 μM ligand, 10 mM potassium phosphate pH 7.0 buffer, and 1 M NaCl: DNA with H1 (△), DNA with H3 (×), and DNA with no ligand (○).

salt buffer (10 mM NaCl) due to intrinsically large t^0_m values (otherwise, thermal melting experiments employing **11**−**14** were carried out under the conditions provided in Table 2). H1−H3 each raised the melting point of **11** from 59 to 64 °C. Ligand Δt_m values were 1 °C or less for oligomeric duplexes **12**−**14**.

Thermal Stability of Ligand−18-mer Complexes. The thermal stabilities of (ligand)$_x$−dsDNA complexes for H1 are little affected by base pair changes of the type A/T → G/C within the TATAA region of **1** (Table 2). In contrast, H1 is very sensitive to A/T → G/C base pair changes in several other positions within **1** as illustrated by the small Δt_m values for oligomeric duplexes **7**−**9**. Thus, the increased thermal stability of the (H1)$_x$−**1** complex is attributed to complex formation between H1 and the duplex's AAATT region. Binding of **1**'s TATAA region by H1 appears to be so weak that A·T → G·C mutations have little effect on the overall thermal stability of the complexes. The Δt_m values for H2 show a similar trend to those for H1. Overall, The Δt_m values for H3 are too small to assess the ligand's sequence selectivity.

*Thermal Stability of Oligomeric Duplexes **15**−**20** and Their Ligand Complexes.* Thermal melting temperatures for a series of oligomeric duplexes are listed in Table 3 (Figure 2). Each pair contains an oligomeric duplex lacking a 5′-TpA-3′ step (**15**, **17**, and **19**) and a duplex containing a 5′-TpA-3′ dinucleotide in the middle of its A/T rich binding site (**16**, **18**, and **20**). H1 shows a tremendous preference for **15** over **16** and a significant preference for **17** over **18**. The (H1)$_2$−**15** complex has a Δt_m of 12 °C, and its melting curve shows a large increase in the hyperchromicity of the duplex. In contrast, the (H1)$_2$−**16** complex has a Δt_m of 0 °C and its melting curve shows no enhancement of the hyperchromicity of the duplex (Figure 2B). The Δt_m values for H1 complexes of **19** and **20** are equivalent. As shown in Table 3, neither H2, H3, nor netropsin demonstrates the selectively exhibited by H1.

*Equilibrium Constants for Complexation of **15** and **16** by H1 and H3.* As for oligomeric duplexes **11** and **12**, H1 formed 2:1 complexes with both **15** and **16** while H3 formed 1:1 complexes (Table 4). The K_1K_2 value for complexation of **15** by H1 was found to be 110-fold greater than for **16**. The fluorescence emission of the H3−**16** complex was found to be relatively weak. As was seen for the H3−**13** complex, the fluorescence signal of uncomplexed H3 obscured that of the H3−dsDNA complex such that it had to be subtracted out by employing eq 4. Fluorescence spectra for both H1 and H3 complexes with **16** displayed a peak with its maxima centered at ~480 nm, red-shifted approximately 30 nm compared to spectra of "normal" ligand−DNA complexes such as those for **11** and **12**. Spectrofluorometric titrations were conducted under conditions of high salt (1 M NaCl) and low temperature (16.5 °C) to stabilize the short oligomeric duplex **16**.

Estimation of Binding Site Size via Model Building. A plausible structure of a side-by-side (H1)$_2$−dsDNA complex was constructed, and its binding site size was measured to be 6.2 bp (Figures 3 and 4). With the piperazine rings not being counted, the side-by-side dimer was estimated to extend 14 Å along the helix axis and cover 4.1 bp. Binding site sizes for several other types of ligand−dsDNA complexes were also estimated (Figure 4).

Localization of H1 in Cells. To determine if H1 is able to enter nuclei, NIH3T3 cells were plated onto coverslips and exposed to the agent for 16 h in starvation medium (DMEM with 0.5% calf serum). Starvation conditions were chosen so that appropriate comparisons could be made to subsequent Northern blot experiments, which require starving NIH3T3 cells overnight in preparation for evaluation of drug effects on c-fos gene expression. Since H1 is a Hoechst analogue, cells were exposed to H2 under the same conditions to compare localization of the two compounds. The cells were not fixed or mounted following exposure to drug. Rather, the coverslips were simply transferred to glass slides and viewed immediately, when the cells were still alive. Representative fluoromicrographs (Figure 5A′,B′) of cells exposed to 1 μM H1 or 0.5 μM H2 show that both compounds localize exclusively to nuclei with similar staining patterns. While diffuse nuclear staining is observed, small regions of high drug concentrations exist as evidenced by areas of high fluorescence intensity. This speckled pattern for either drug does not always correspond to nucleoli, visible in the corresponding phase contrast micrographs. Overall, treatment of cells with 0.5 μM H2 yields nuclei that are slightly brighter than those treated with 1 μM H1. The staining on any given coverslip was fairly even, with little variation between viewing fields. These and additional images captured using a range of drug concentrations as well as semiquantitative analysis of the resulting fluoromicrographs (data not shown) demonstrated that approximately 4 times more H1 was

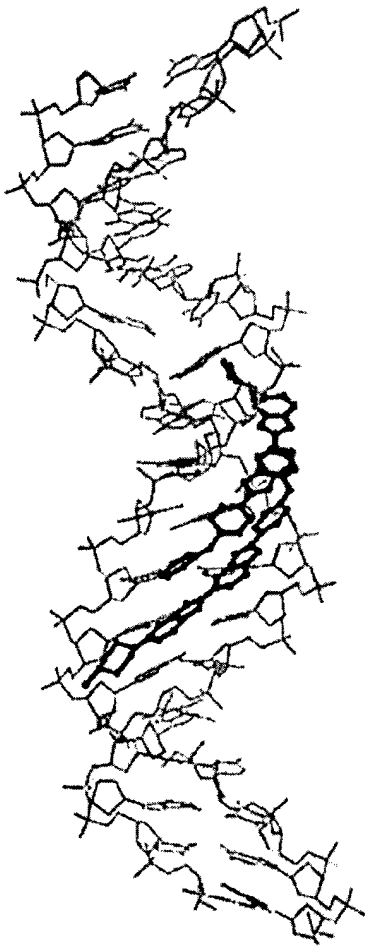

FIGURE 3: Computer-generated model of a plausible $(H1)_2$–dsDNA side-by-side antiparallel staggered complex.

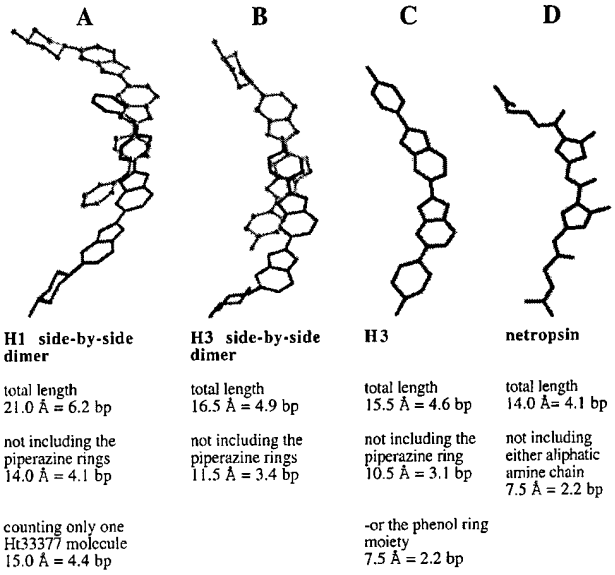

FIGURE 4: Ligands were extracted from computer-generated $(ligand)_x$–dsDNA models and are pictured in their dsDNA-bound conformations (DNA atoms are not shown so that ligand curvature can be better displayed). Estimated binding site sizes of $(ligand)_x$–dsDNA complexes are provided below the pictured ligands. Also generated but not pictured was the 1:1 H2–dsDNA complex whose binding site size was estimated to be 17.5 Å (5.1 bp).

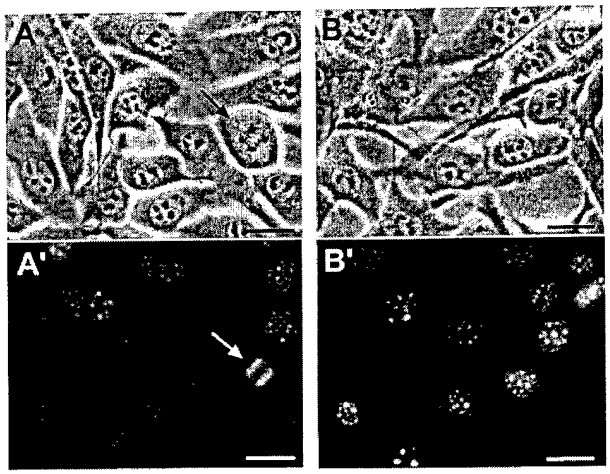

FIGURE 5: Localization of H2 and H1 to nuclei in live NIH3T3 cells. (A and A′) Representative phase contrast and fluoromicrographs, respectively, of NIH3T3 cells exposed to 1 μM H1 for 16 h. (B and B′) Representative phase contrast and fluoromicrographs, respectively, of NIH3T3 cells exposed to 0.5 μM H2 for 16 h. Images were captured immediately following transfer of coverslips of live cells to glass slides. H1 localizes to nuclear material, even in actively dividing cells (arrows). The bars are 10 μm in length.

required to attain the same level of H2 fluorescence intensity. A cell captured in the process of mitosis (Figure 5A,A′, arrows) shows that H1 associates with nuclear material even during division.

Effects of H1 on Endogenous c-fos mRNA Expression. The presence of H1 in the nucleus suggested that it may have DNA template effects in whole cells. The c-fos promoter has been established in the Beerman lab as a model system for evaluating the effect of DNA-binding drugs on transcription (*17*). Therefore, H1's effects on endogenous transcription of the c-fos gene in whole cells were evaluated. NIH3T3 cells were exposed to H1 for 16 h under starvation conditions before being serum induced for 30 min, which was previously determined to be an optimal time course for c-fos mRNA production. Control cells upregulate c-fos in response to serum stimulation, as detected in Northern blots (Figure 6A, first two lanes). Glyceraldehyde-3-phosphate dehydrogenase (G3), a constitutively expressed housekeeping gene, was used here as a loading control. The half-lives of G3 and c-fos mRNA are 8 h and 30 min, respectively. Therefore, drug effects on the total amount of G3 mRNA are expected to be minimal after only 16 h. Treatment of cells with H1 led to a dose-dependent inhibition of c-fos transcription, as evidenced by the loss in signal intensity (Figure 6A, lanes 3–6). There was no detectable drug effect on G3 expression, nor was there detection of shorter transcripts for either c-fos or G3. Quantitation of the Northern blot autoradiographs allowed drug-treated samples to be compared to controls, yielding a measurement of percent inhibition of c-fos expression (Figure 6B). A maximum concentration of 10 μM H1 was used, resulting in approximately 70% inhibition of expression. Inhibition of expression by 50% (the IC_{50} value) occurred at approximately 4 μM. To note, H2 had very little effect on c-fos expression at this time point, although inhibition was seen for shorter exposures of 1 and 4 h (*17*). In contrast, H1 had no effect on c-fos expression after these shorter exposures (data not shown).

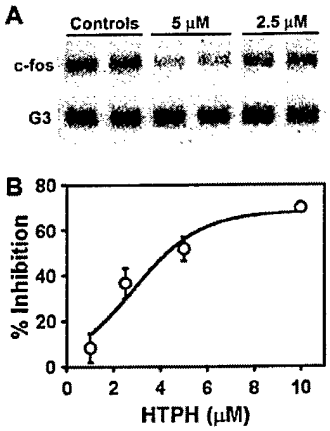

FIGURE 6: Effect of H1 on c-fos mRNA expression. (A) Representative Northern blot results from NIH3T3 cells exposed to H1 at the concentrations shown for 16 h under starvation conditions (0.5% serum). Following induction of c-fos by increasing the serum concentration to 15% for 30 min, 20 μg of total RNA was isolated and electrophoresed on a denaturing agarose gel. Subsequent blots were hybridized with radiolabeled probes for c-fos or G3. (B) Quantitation of H1's effects on c-fos cellular transcription was achieved through densitometric analysis of blots as shown in panel A. Comparison of drug-treated lanes to controls yielded percent inhibition for each treatment. The results are the means of four experiments (mean ± standard error).

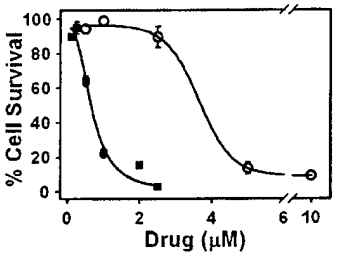

FIGURE 7: Cytotoxicity of H1 in NIH3T3 cells. Cells were allowed to grow in the presence of either H1 (○) or H2 (■) for 3 days before being trypsinized and counted. Percent cell survival was calculated by comparing the total cell number in drug-treated samples to solvent controls. The results are the means of triplicate samples in three separate experiments (mean ± standard error).

Cytotoxic Effects of H1. NIH3T3 cells were continuously exposed to a range of H1 or H2 concentrations for 3 days before being trypsinized and counted. Total cell numbers from each treatment were compared to appropriate solvent controls to yield percent cell survival. As shown in Figure 7, the concentration of H1 needed to kill 50% of the cells (LD_{50}) was 3.4 μM. By 10 μM H1, more than 90% cell death was observed. In comparison, the LD_{50} of H2 was 0.6 μM, and more than 95% of the cells died by 2.5 μM. Treatment of cells with 100 μM H3 over the same time period effected approximately 50% cell death.

DISCUSSION

Spectrofluorometric titrations were employed in an effort to determine the dsDNA binding characteristics of H1 (Table 1). H1 is shown to form $(H1)_2$–dsDNA complexes and to require a minimum binding site of 4 A/T bp. In contrast, H2 and H3 will form complexes with 3 A/T bp, although both ligands do prefer larger sites. The requirement of only 3 A/T bp for strong binding is an interesting observation since it is commonly reported that these agents require at least 4 A/T bp (*1*, *26*). Additionally, the $(H3)_2$–**13** complex stoichiometry of 2:1 is rather uncommon since such a stoichiometry has been previously reported only once for H3 (*16*). The difference in binding stoichiometries between H1 and H3 for normal size binding sites (4–5 bp) is not unexpected. It has been previously noted by this laboratory that changes in the terminal phenyl ring of H3 can alter the stoichiometries of its dsDNA complexes (*15*). The possibility that ligand–dsDNA stoichiometries determined via spectrofluorometric titrations might be misleading due to alternative modes of ligand binding has also been considered. H3 is know to interact with dsDNA by a secondary form of binding [probably intercalation (*27*)] which occurs at relatively high ligand:base pair ratios, shows no apparent base pair specificity, and is weakened considerably with increasing ionic strength (*28*). Relative fluorescence intensities for ligands in buffer with and without **14** were compared to determine if secondary forms of binding could be affecting our fluorescence measurements. The relative fluorescence intensities of H1–H3 were found to be unaffected by the addition of **14**. Thus, either no secondary form of dsDNA binding occurs at the concentrations of dsDNA that are employed, or they occur but are not detected by fluorescence spectroscopy. Either way, secondary forms of binding by H3 can only affect the observed stoichiometries if they occur in competition with H3's primary form of dsDNA binding (minor groove binding of A/T rich sites). This is unlikely since H3's secondary form of binding is roughly 100–1000-fold weaker than its primary form (*28*, *29*). Additionally, our observed stoichiometries (Table 1) are inconsistent with a competitive but nonspecific secondary form of binding.

A plausible $(H1)_2$–dsDNA complex constructed via model building illustrates the curvature of the two H1 molecules when placed in a slightly staggered, side-by-side, and antiparallel arrangement within the minor groove (Figure 3). This type of side-by-side arrangement within the minor groove has precedence since monocationic minor groove binders such as distamycin-based compounds have a propensity to complex dsDNA in this manner (*2*, *30*–*32*). When the molecules are staggered, the placement of the phenoxy ether ring of one H1 molecule adjacent to the bulky piperazine ring of the other is avoided. Structural investigations of side-by-side complexes of other minor groove binders such as polyamides with dsDNA consistently show the two polyamide molecules of the trimeric complex to be both antiparallel and staggered (*2*, *30*–*32*).

Inspection of the $(H1)_2$–dsDNA model suggests a binding site size of 6.2 bp versus an experimentally determined minimum binding site of 4 A/T bp (Figure 4). The 2 bp difference is interpreted as a lack of binding specificity on the part of H1's piperazine rings. Some X-ray crystal structures of H3–dsDNA complexes show the bisbenzimidazole rings of H3 bound to an A/T rich binding site while the piperazine ring rests against an adjacent G·C base pair (*24*, *33*). When the piperazine rings are excluded, the H1 side-by-side complex covers 4.1 bp, in agreement with the experimentally determined minimum A·T rich binding site size.

If the piperazine rings of $(H1)_2$–dsDNA complexes are capable of resting in the wider minor groove of G/C base pairs, it stands to reason that the piperizine rings of H2 and H3 might also. The binding site size of an $(H3)_2$–dsDNA

side-by-side complex was estimated to be 4.9 bp versus an experimentally determined minimum binding site size of 3 A/T bp. When the piperazine rings are excluded, the H3 side-by-side complex covers ~3.4 bp, roughly equivalent to the experimentally determined minimum A/T rich binding site size. The side-by-side $(H3)_2$−dsDNA complex was constructed in a manner similar to that of the $(H1)_2$−dsDNA complex with the two H1 molecules placed in a slightly staggered, side-by-side, and antiparallel arrangement within the minor groove.

As shown in Table 2, H1 selectively stabilizes those oligomeric duplexes which contain 4 bp A/T rich binding sites free of a 5′-TpA-3′ dinucleotide step (i.e., 4 bp "A-tracts"). A similar trend was observed for H2. It has been suggested that the 5′-TpA-3′ step produces a DNA structural alteration which discourages minor groove binding (*23*, *34*). Dickerson and co-workers have reported that A/T rich regions of dsDNA usually adopt poly(dA)/poly(dT)-like structures (termed A-tracts) (*35*, *36*). A-tracts consist of successive adenine bases which stack in a rigid and unbent column. Dickerson and co-workers emphasize that the A-tract structure can incorporate 5′-ApT-3′ steps, but is broken by 5′-TpA-3′ steps.

It was previously reported that the terbenzimidazole 5PTB was capable of selectively stabilizing **17** relative to **18** (*37*). The duplex **17** (5′-GA_4T_4C-3′) contains an uninterrupted 8 bp A tract, assumes a rigid A-tract conformation, and exhibits an anomalously slow migration in a polyacrylamide gel (*38*). The other duplex, **18** (5′-GT_4A_4C-3′), contains two 4 bp A tracts separated by a TpA dinucleotide, assumes a normal "B-like" conformation, and, on the basis of its molecular weight, migrates normally. The duplexes have also been shown to possess differential thermodynamic properties (**17** possesses a larger t^0_m than **18**) (*37*). These complexes have identical base compositions, yet evidence suggests that **17** is conformationally distinct from **18**. It was argued that the origin of 5PTB's selectivity was an entropically driven preference for highly solvated A-tracts such as those found within **17** (*37*). We have found that H1 also selectively stabilizes **17** relative to **18** (Table 3). We have also employed two additional pairs of oligomeric duplexes differing in the lengths of their A·T tracts: the pair **15** (5′-GCA_2T_2GC-3′) and **16** (5′-GCT_2A_2GC-3′), and the pair **19** (5′-GA_6T_6C-3′) and **20** (5′-GT_6A_6C-3′). Both previously uncharacterized pairs of duplexes exhibit differential thermodynamic properties similar to those of **17** and **18**. As shown by the values listed in Table 3, those duplexes containing a 5′-TpA-3′ dinucleotide have lower t^0_m values than those without. The $\Delta\Delta t_m$ values listed in Table 4 are unimpressive for all the ligands investigated except for H1 which selectively stabilizes **15** and **17** over **16** and **18** with $\Delta\Delta t_m$ values of 12 and 7 °C, respectively. The equilibrium constants for complexation of **15** with H1 were determined to be 110-fold larger than those for **16** (Table 4).

The selectivities of the different ligands can be explained in terms of the number of bases covered by their sequence selective moieties. As discussed earlier, the piperazine rings of the H1 side-by-side dimer are incapable of differentiating between A/T and G/C base pairs. Presumably, they are also incapable of selecting against 5′-TpA-3′ steps. When the piperazine rings are excluded, the H1 side-by-side dimer is estimated to have a sequence selective binding region which covers about 4.2 bp and prefers A-tracts over A/T rich sites containing 5′-TpA-3′ steps. H1 does not selectively stabilize **19** over **20** since H1 side-by-side complex formation may occur with an A-tract on either side of the dinucleotide 5′-TpA-3′ located within the middle of **20**. When the piperazine ring is not included, H2 is estimated to cover roughly 3.7 bp. The lack of selectivity of H2 for **17** over **18** can perhaps be explained in that the ligand can bind an A-tract on either side of the dinucleotide 5′-TpA-3′ located in the middle of **18**. However, this same rationale fails to explain H2's lack of selectivity between the shorter duplexes **15** and **16** unless the sequence selective moieties of H2 cover significantly less than 3.7 bp. The phenolic group of H3 has been shown by NMR spectroscopic investigations to rapidly rotate (at a rate of $>10^3$ s^{-1}) while the molecule is still bound within the minor groove (*39*, *40*). We propose that the phenol ring of H1 may not significantly contribute to the ligand's sequence selectivity. Alone, the bisbenzimidazole rings of H2 and H3 cover roughly 2.2 bp. Thus, H2 may complex **16** with its bisbenzimidazole rings on one side or the other of the 5′-TpA-3′ step. Netropsin's lack of selectivity between duplexes **15** and **16** can also be rationalized in terms of the size of its sequence selective binding site. When the agent's highly flexible aliphatic moieties are not included, netropsin is also estimated to recognize roughly 2.2 bp.

The subcellular distribution of H1 was investigated in an effort to determine if H1 was capable of associating with DNA in live cells (Figure 5). Visualization of H1 by fluorescence microscopy shows that this compound selectively localizes in the nucleus. H1 is therefore capable of traversing both the cytoplasmic and nuclear membranes and accumulating in the nucleus in a pattern suggestive of DNA binding. As previously mentioned, DNA binding agents such as H1 have the potential to act as template poisons by preventing the binding of various nuclear proteins to their DNA target sites (*7*, *41*). However, the ability of a ligand to bind DNA in vitro does not ensure its cellular activity. We demonstrate here that H1 inhibits endogenous transcription of the c-fos gene in whole cells at micromolar concentrations (Figure 6). These results suggest that H1 possesses the ability to reach its cellular target and is capable of inhibiting the binding of regulatory proteins. Our finding that H1 causes cell death at micromolar concentrations demonstrates that it is capable of disrupting normal cell function. The results of our cellular investigations for H1 and H2 were fairly similar. H3 showed little cellular activity in accord with literature reports (*10*, *11*). Apparently, alkylation of the terminal phenoxy moiety of H3 imparts upon both these molecules a superior ability to traverse the cell membrane and reach its DNA target.

CONCLUSIONS

The formation of a side-by-side complex with dsDNA appears to impart upon H1 a rare degree of sequence specificity. This may be due to the aromatic rings of the H1 side-by-side complex being held more rigidly in comparison to a 1:1 complex as for H2 or H3. Only two other types of minor groove binding agents are capable of distinguishing between different A/T rich sequences, and of the three, the mechanism by which H1 achieves its specificity is unique. The previously mentioned terbenzimidazole 5PTB forms only 1:1 complexes with **15** and **16** (*37*). Dervan and co-workers

have investigated a series of heteropolyamide hairpin-type molecules which contain various combinations of pyrrole, imidazole, and hydroxypyrrole subunits (*42*, *43*). These types of heteropolyamide molecules have, in some cases, demonstrated the ability to distinguish between A·T and T·A base pairs. However, the mechanism of heteropolyamide specificity is intrinsically different from that for H1 since heteropolyamide specificity is not related to the presence of A-tracts (heteropolyamides target sites which contain both A/T and G/C base pairs).

Evaluation of H1's biological potential revealed that it possesses many characteristics that are desirable for a DNA-reactive drug, including cellular permeability and nuclear localization, and an ability to decrease the level of gene expression. We believe that the unique mechanism of H1's specificity, combined with its ability to localize in nuclear DNA and inhibit RNA transcription, makes it a valuable starting point for the development of other sequence selective agents.

REFERENCES

1. Reddy, B. S. P., Sondhi, S. M., and Lown, J. W. (1999) *Pharmacol. Ther. 84*, 1−111.
2. Sharma, S. K., Tandon, M., and Lown, J. W. (2000) *J. Org. Chem. 65*, 1102−1107.
3. Xuereb, H., Maletic, M., Gildersleeve, J., Pelczer, I., and Kahne, D. (2000) *J. Am. Chem. Soc. 122*, 1883−1890.
4. Zimmer, C., and Wähnert, U. (1986) *Prog. Biophys. Mol. Biol. 47*, 31−112.
5. Boger, D. L., and Johnson, D. S. (1996) *Angew. Chem., Int. Ed. 35*, 1438−1474.
6. Bailly, C., and Chaires, J. B. (1998) *Bioconjugate Chem. 9*, 513−538.
7. Chiang, S. Y., Bruice, T. C., Azizkhan, J. C., Gawron, L., and Beerman, T. A. (1997) *Proc. Natl. Acad. Sci. U.S.A. 94*, 2811−2816.
8. Satz, A. L., and Bruice, T. C. (2001) *J. Am. Chem. Soc. 123*, 2469−2477.
9. Loewe, V. H., and Urbanietz, J. (1974) *Arzneim.-Forsch. 24*, 1927−1933.
10. Harapanhalli, R. S., Howell, R. W., and Rao, D. V. (1994) *Nucl. Med. Biol. 21*, 641−647.
11. Finlay, G. J., and Baguley, B. C. (1990) *Eur. J. Cancer 26*, 586−589.
12. Bruice, T. C., Sengupta, D., Blasko, A., Chiang, S. Y., and Beerman, T. A. (1997) *Bioorg. Med. Chem. 5*, 685−692.
13. Dorn, A., Affolter, M., Muller, M., Gehring, W. J., and Leupin, W. (1992) *EMBO J. 11*, 279−286.
14. Loontiens, F. G., Regenfuss, P., Zechel, A., Dumortier, L., and Clegg, R. M. (1990) *Biochemistry 29*, 9029−9039.
15. Satz, A. L., and Bruice, T. C. (2000) *Bioorg. Med. Chem. 8*, 1871−1880.
16. Browne, K. A., He, G. X., and Bruice, T. C. (1993) *J. Am. Chem. Soc. 115*, 7072−7079.
17. White, C. M., Heidenreich, O., Nordheim, A., and Beerman, T. A. (2000) *Biochemistry 39*, 12262−12273.
18. Nigg, E. A., and Treisman, R. (1994) *Curr. Opin. Cell Biol. 6*, 333−334.
19. Inada, K., Okada, S., Phuchareon, J., Hatano, M., Sugimoto, T., Moriya, H., and Tokuhisa, T. (1998) *J. Immunol. 161*, 3853−3861.
20. Treisman, R. (1985) *Cell 42*, 889−902.
21. Norman, C., Runswick, M., Pollock, R., and Treisman, R. (1988) *Cell 55*, 989−1003.
22. Ebrahimi, S. E. S., Bibby, M. C., Fox, K. R., and Douglas, K. T. (1995) *Anti-Cancer Drug Des. 10*, 463−479.
23. Ward, B., Rehfuss, R., Goodisman, J., and Dabrowiak, J. C. (1988) *Biochemistry 27*, 1198−1205.
24. Carrondo, M., Coll, M., Aymami, J., Wang, A. H. J., Vandermarel, G. A., Vanboom, J. H., and Rich, A. (1989) *Biochemistry 28*, 7849−7859.
25. Yadagiri, B., and Lown, J. W. (1990) *Synth. Commun. 20*, 955−963.
26. Harshman, K. D., and Dervan, P. B. (1985) *Nucleic Acids Res. 13*, 4825.
27. Moon, J. H., Kim, S. K., Sehlstedt, U., Rodger, A., and Norden, B. (1996) *Biopolymers 38*, 593−606.
28. Jorgenson, K. F., Varshney, U., and van de Sande, J. H. (1988) *J. Biomol. Struct. Dyn. 5*, 1005−1023.
29. Rao, K. E., and Lown, J. W. (1991) *Chem. Res. Toxicol. 4*, 661−669.
30. Kopka, M. L., Goodsell, D. S., Han, G. W., Chiu, T. K., Lown, J. W., and Dickerson, R. E. (1997) *Structure 5*, 1033−1046.
31. Wemmer, D. (1998) *Nat. Struct. Biol. 5*, 169−171.
32. Kielkopf, C. L., Baird, E. E., Dervan, P. B., and Rees, D. C. (1998) *Nat. Struct. Biol. 5*, 104−109.
33. Pjura, P. E., Grzeskowiak, K., and Dickerson, R. E. (1987) *J. Mol. Biol. 197*, 257−271.
34. Chen, F. M., and Sha, F. (1998) *Biochemistry 37*, 11143−11151.
35. Goodsell, D. S., Kaczorgrzeskowiak, M., and Dickerson, R. E. (1994) *J. Mol. Biol. 239*, 79−96.
36. Dickerson, R. E., Goodsell, D., and Kopka, M. L. (1996) *J. Mol. Biol. 256*, 108−125.
37. Pilch, D. S., Xu, Z. T., Sun, Q., LaVoie, E. J., Liu, L. F., and Breslauer, K. J. (1997) *Proc. Natl. Acad. Sci. U.S.A. 94*, 13565−13570.
38. Chen, J.-H., Seeman, N. C., and Kallenbach, N. R. (1988) *Nucleic Acids Res. 16*, 6803−6815.
39. BostockSmith, G. E., Laughton, C. A., and Searle, M. S. (1998) *Nucleic Acids Res. 26*, 1660−1667.
40. Embrey, K. J., Searle, M. S., and Craik, D. J. (1993) *Eur. J. Biochem. 211*, 437−447.
41. Mote, J., Ghanouni, P., and Reines, D. (1994) *J. Mol. Biol. 236*, 725−737.
42. Urbach, A. R., Szewczyk, J. W., White, S., Turner, J. M., Baird, E. E., and Dervan, P. B. (1999) *J. Am. Chem. Soc. 121*, 11621−11629.
43. Melander, C., Herman, D. M., and Dervan, P. B. (2000) *Chem. Eur. J. 6*, 4487−4497.

BI0103415

Inhibition of transcription factor-DNA complexes and gene expression by a microgonotropen

Christine M. White*, Alexander L. Satz†, Thomas C. Bruice†, and Terry A. Beerman*‡

*Department of Pharmacology and Therapeutics, Roswell Park Cancer Institute, Elm and Carlton Streets, Buffalo, NY 14263; and †Department of Chemistry, University of California, Santa Barbara, CA 93106

Contributed by Thomas C. Bruice, July 19, 2001

Developing minor groove-binding drugs to selectively inhibit transcription factor (TF)/DNA interactions and accompanying gene expression is a current goal in drug development studies. Equipping minor groove-binding agents with positively charged, major groove-contacting side chains yields microgonotropens (MGTs). Previously, we demonstrated that MGTs were superior inhibitors of TF/DNA complexes in cell-free assays compared with "classical" groove binders, but MGTs showed limited ability to inhibit gene expression. To determine what chemical characteristics contribute to or improve activity, we evaluate five MGTs for their effectiveness in inhibiting TF complex formation and resultant transcription by using the c-fos serum response element (SRE) as a target. MGT L1 binds DNA via a bisbenzimidazole equipped with a tripyrrole moiety. It is compared with analog L2, which has been functionalized with propylamines on each of the three pyrroles. L2, which binds DNA at subpicomolar concentrations, was at least three orders of magnitude more potent than L1 at inhibiting TF binding to the c-fos SRE in cell-free assays. Unlike L1 and previous MGTs, L2 also inhibited endogenous c-fos expression in NIH 3T3 cells at micromolar levels. Structure/activity relationships suggest that, although the tripyrrole/polyamine functional group of L2 may be largely responsible for its inhibition of TF complexes in cell-free assays, its bisbenzimidazole moiety appears to impart improved cellular uptake and activity. These findings make L2 a promising lead candidate for future, rational MGT design.

Rational design of DNA-binding ligands to inhibit targeted gene expression has widespread implications in understanding the molecular mechanisms of gene regulation and in ultimately developing novel therapeutics. The binding of transcription factors (TFs) to their target sites on gene promoters is essential for proper regulation of transcription. Selectively inhibiting the formation of TF/DNA complexes may therefore potentially decrease expression of a target gene of interest.

Recently, approaches using minor groove-binding agents to inhibit TF/DNA complex formation and transcription in a variety of cell-free systems have been explored (reviewed in ref. 1). The effectiveness of these agents as inhibitors is often closely related to their mode of binding and sequence selectivity, and it appears that many types of TF/DNA complexes can be targeted. For example, the A/T-selective minor groove-binding agent distamycin prevented the TATA binding protein from binding to its A/T-rich target site in the minor groove, but it was unable to inhibit the major groove-binding TF EGR from binding to its G/C-rich sequence (2). However, distamycin could prevent major groove-binding homeodomain peptides from binding to their A/T-rich sites (3).

Most TFs associate with high affinity primarily to their consensus binding sites on the major groove, but they gain increased specificity through simultaneous minor groove contacts (4). This suggests that high-affinity DNA binders capable of contacting both grooves may be more effective inhibitors of TF/DNA complexes than agents that bind solely to a single groove. The microgonotropens (MGTs) were designed with this goal in mind. The first generation of MGTs consisted of minor groove-binding, A/T-selective tripyrrole moieties with protonated polyamine tails attached to the central pyrrole (5). These tails allow MGTs to electrostatically contact the phosphodiester backbone on the major groove side of the helix, endowing them with high DNA-binding affinity (K_a values $\approx 10^{10}$ M^{-1}) and the ability to bend DNA, characteristics that may help them to more effectively compete with TFs for binding to target sites (6, 7). Indeed, initial studies demonstrated that MGTs could be orders of magnitude more potent than distamycin in inhibiting the TF E2F1 from binding to DNA (8). Further exploration into designing agents with similar capabilities led to the development of fluorescent MGTs (9, 10). These agents selectively bind A/T-rich sites in the minor groove via a bisbenzimidazole moiety, but polyamine tails linked in *meta* to the terminal phenyl ring allow electrostatic contact with the phosphodiester backbone. The DNA-binding affinities of these agents are significantly greater than "classical" bisbenzimdazoles like Hoechst 33258 (9).

The well defined serum response element (SRE) of the human c-fos promoter was used as a target to evaluate these agents as TF complex inhibitors in increasingly complex assay environments. The binding of a dimer of serum response factor (SRF) to an A/T-rich site and subsequent recruitment of the *ets* factor Elk-1 to a GGA core sequence to form a ternary complex (TC) is required for c-fos transcription (11). Both TFs primarily bind DNA in the major groove but make minor groove contacts (12, 13). This mode of binding and the presence of an A/T-rich site make these TFs potential targets for MGTs. We found that, whereas a bisbenzimidazole possessing a linker without basic side chains was completely ineffective at inhibiting TC formation in cell-free assays, fluorescent MGTs functionalized with polyamine tails of various lengths and degrees of branching could do so at micromolar concentrations and were up to 50 times more potent than the classical bisbenzimidazole Hoechst 33342 (Hoe342). However, although these fluorescent MGTs also inhibited c-fos promoter-driven cell-free transcription, they, like the first generation of MGTs, were inactive in cells (C.M.W. and T.A.B., unpublished data).

Because enhanced inhibition of TF/DNA complexes was observed when simple minor groove-binding agents were equipped with phosphodiester backbone-contacting polyamine tails, we further explored this drug design strategy and structure/activity relationships in an effort to create more potent agents that were also capable of decreasing gene expression. Past studies have shown that DNA-binding drugs lose relative potency as assay conditions become more complex (that is, in cell-free expression assays, where additional proteins and DNA

Abbreviations: TF, transcription factor; MGT, microgonotropen; SRE, serum response element; SRF, serum response factor; TC, ternary complex, dsDNA, double-stranded DNA; GAPDH, glyceraldehyde 3-phosphate dehydrogenase; EMSA, electrophoretic mobility shift assay; oligo, oligonucleotide; topo II, topoisomerase II.

‡To whom reprint requests should be addressed. E-mail: Terry.Beerman@Roswellpark.org.

The publication costs of this article were defrayed in part by page charge payment. This article must therefore be hereby marked "*advertisement*" in accordance with 18 U.S.C. §1734 solely to indicate this fact.

www.pnas.org/cgi/doi/10.1073/pnas.191374698

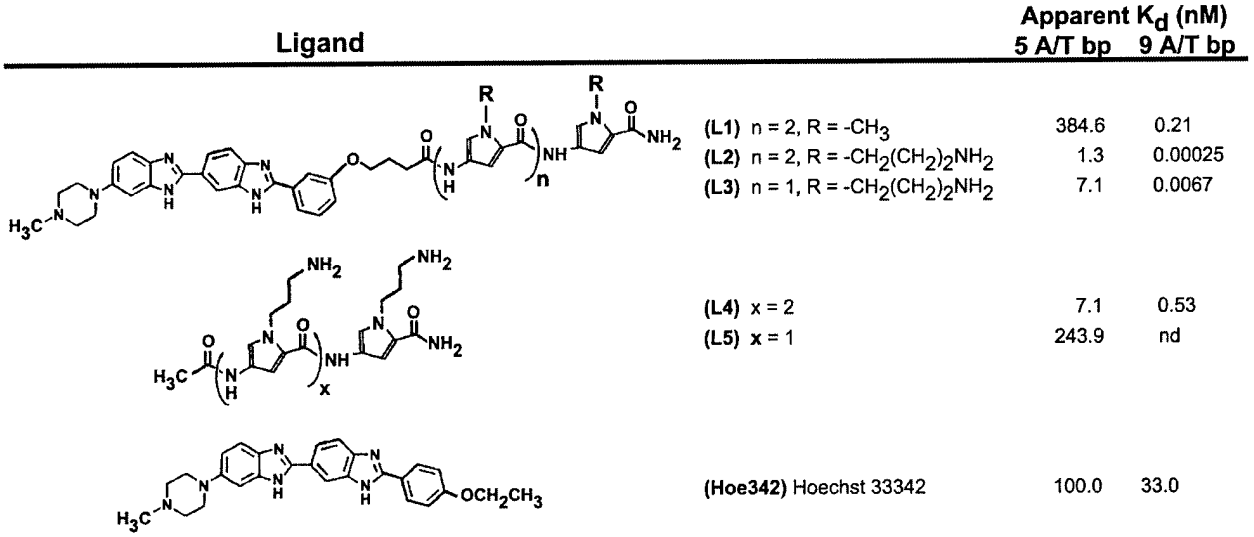

Fig. 1. Chemical structures of the DNA-binding agents used in this study. Previously determined apparent equilibrium dissociation constants (K_d values) were determined from melting curves of ligand:dsDNA complexes using 0.3 μM of the oligos 5′-CGCAAAAACGCACC-3′ and 5′-CGCAAAAAAAAACGC-3′ in 10 mM potassium phosphate buffer, pH 7.0, and 150 mM NaCl in the presence of 0.6 μM ligand. nd, not determined.

are added) (14, 15), and we wished to determine whether such limitations could be overcome by improved rational design.

Recent chemical characterization of the novel tripyrrole-bisbenzimidazole agent **L1** (Fig. 1) showed that it possessed interesting double-stranded DNA (dsDNA) binding characteristics, including recognition of 9 contiguous A/T bp at nanomolar levels and the ability to form antiparallel 2:1 complexes in the minor groove of DNA (16). Because attaching a single polyamine tail to tripyrrole compounds led to orders of magnitude increases in potency in inhibiting TF complexes in cell-free assays, each pyrrole subunit of **L1** was equipped with propylamines to yield **L2**. **L2** was found to have sequence selectivity and discrimination for 9-bp, A/T-rich sites similar to those of **L1**, but it binds dsDNA with a remarkable 1,000-fold higher affinity (16).

We now analyze the ability of these agents to inhibit TF/DNA complex formation on the c-fos SRE and subsequent gene expression in increasingly complex assays. Moreover, the activities of **L2** analogs are also evaluated to better determine how MGT structure and activity relate. These compounds include **L3**, which is similar to **L2** but possesses one less pyrrole subunit, and **L4** and **L5**, the pyrrole/polyamine moieties of **L2** and **L3**, respectively. A representative classical bisbenzimidazole, Hoe342, is used as a control minor groove binder. Besides comparing their potencies in inhibiting TF/DNA complex formation and transcription in cell-free assays, we explored how selective these agents were for inhibiting DNA template-related activities by using a topoisomerase II (topo II) assay. Their abilities to inhibit endogenous c-fos expression in whole cells and to cause cell death were also evaluated. Our studies reveal that equipping bisbenzimidazoles with phosphodiester backbone-contacting functional groups leads to increased inhibitory effectiveness by orders of magnitude in cell-free assays and also results in the first demonstration of MGT cellular activity. Importantly, the potency and cellular activity of **L2** make it a promising lead compound for future drug design.

Methods

DNA-Binding Ligands. MGTs were synthesized as described (16) and reconstituted in 25% DMSO. Hoe342 (Aldrich) was prepared in ddH_2O. Drug stocks were stored at −20°C and were diluted into ddH_2O before use.

Cell Culture. NIH 3T3 cells were maintained as described (14). HeLa cells were maintained in suspension cultures in Joklik-modified MEM (S-MEM) with 5% FBS and 5% horse serum at 37°C.

Electrophoretic Mobility Shift Assay (EMSA). The 24-bp oligonucleotides (oligos) derived from the human c-fos SRE (5′-ACACAGGATGTCCATATTAGGACA-3′) and the *Drosophila* E74 promoter (5′-GATACCGGAAGTCCATATTAGGAC-3′) were synthesized, purified, and end-labeled as previously described (14). Purification of 6-histidine-tagged SRF and Elk-1 following expression in bacteria, the assay reaction conditions, and subsequent autoradiogram analysis have also been described in detail (14). In brief, drug and oligo were allowed to incubate 30 min before addition of purified TFs and subsequent electrophoresis on a polyacrylamide gel.

Cell-Free Transcription. HeLa nuclear extracts were prepared following published protocol and stored at −80°C until use (14). The reaction was carried out and the results analyzed as previously described (14, 17). In brief, a linearized plasmid containing the full-length c-fos promoter was incubated with drug for 30 min at 30°C before the addition of 15 μg of nuclear extract and a subsequent 15-min incubation. After a 60-min incubation in the presence of [α-^{32}P]CTP, the resulting 750-base transcript was purified and electrophoresed on a denaturing polyacrylamide gel. A radiolabeled 250-base T3 transcript of pGEM4z (Promega) was used as an internal control. Normalization of the c-fos transcript to the internal control allowed accurate comparisons between samples.

Topo II Activity Assay. The isolation of HeLa nuclei and the subsequent assay reactions were as described (18, 19). Briefly, HeLa cells radiolabeled for 24 h with [^{14}C]thymidine were lysed in the presence of detergent and nuclei were pelleted by centrifugation. Nuclei were incubated with 20 μM drug for 10 min at 37°C before the addition of 20 μM VM-26, a topo II/DNA

crosslinking agent. After 15 min at 37°C, the topo II/DNA crosslinks were precipitated by hot K^+/SDS. The washed pellets were hydrolyzed in perchloric acid before precipitated counts were measured by scintillation counting.

Northern Blot Assay. Following published protocol (14), NIH 3T3 cells were treated with drugs for 16 h under starvation conditions (growth media with 0.5% serum) before c-fos expression was induced by raising serum concentration to 15%. Total RNA was isolated, electrophoresed on a denaturing agarose gel, transferred to a nylon membrane, and hybridized with radiolabeled cDNA probes to c-fos and glyceraldehyde 3-phosphate dehydrogenase (GAPDH). Densitometric analysis of autoradiographs allowed comparison between drug-treated samples and controls and calculation of percent inhibition of expression.

Cytotoxicity Assay. A total of 1×10^4 NIH 3T3 cells were seeded into 24-well plates and allowed to grow 24 h before being exposed to drug in triplicate. Controls received solvent only. Cells were incubated under normal growth conditions for 72 h. The medium was removed, and cells were rinsed once with PBS before being trypsinized and counted with a particle counter (Coulter). Drug-treated samples were compared with controls to calculate percent control growth.

Results

Design of the Novel DNA-Binding Ligands. To explore whether adding basic side chains to novel minor groove binders by using a rational design approach would improve their ability to inhibit TF/DNA interactions, **L1** was used as a starting compound (Fig. 1). Previously determined K_d values show that **L1** binds with high affinity to A/T-rich sites and can distinguish between 5 and 9 A/T bp. Adding propylamine tails to each of **L1**'s pyrroles yields **L2**, which has vastly improved binding affinity and greater sequence selectivity. The effect of side chain length on inhibitory activity was assessed by synthesizing **L3**, which has one less pyrrole than **L2**. The contribution of the pyrrole/propylamine tails to activity was explored by using the analogs **L4** and **L5**, which correspond to the basic side chains of **L2** and **L3**, respectively. Hoe342, a well studied classical bisbenzimidazole chemically and structurally distinct from the MGTs, was used as a control and as a reference compound to which the former agents were compared.

Effect of the Agents on TC Formation in EMSAs. The ability of these agents to inhibit TF/DNA complex formation was first analyzed by using EMSAs, a system consisting of purified TFs and a radiolabeled 24-bp oligo. In a representative gel (Fig. 2*A*), SRF and Elk-1 added to the SRE forms the TC, visible as a "shifted" complex (lanes 1 and 2, top arrow). Incubating the oligo with DNA-binding ligand before adding TFs inhibits TC formation in a dose-dependent manner, as shown for both **L5** and **L4** (lanes 3–5 and 6–9, respectively). Quantitation of the percent complexed DNA in each lane and subsequent comparison of ligand-treated samples to controls allows calculation of percent inhibition of complex formation. Plotting these values against ligand concentration yields inhibition curves for each agent (Fig. 2*B*). The most potent agent, **L2**, inhibited TC formation completely by 0.25 μM, while two orders of magnitude more **L1**, the least potent compound, did not even attain 20% inhibition. Compared with **L5**, which also performed poorly and was less effective than Hoe342, **L4** was about 50-fold more potent. To note, the bisbenzimidazoles **L2** and **L3** were 8 and 91 times more effective, respectively, than their polyamide/propylamine analogs **L4** and **L5** in this assay. Results are summarized and potencies of the agents are compared in Table 1, which lists IC_{50} values (the ligand concentration needed to inhibit the observed activity by 50%).

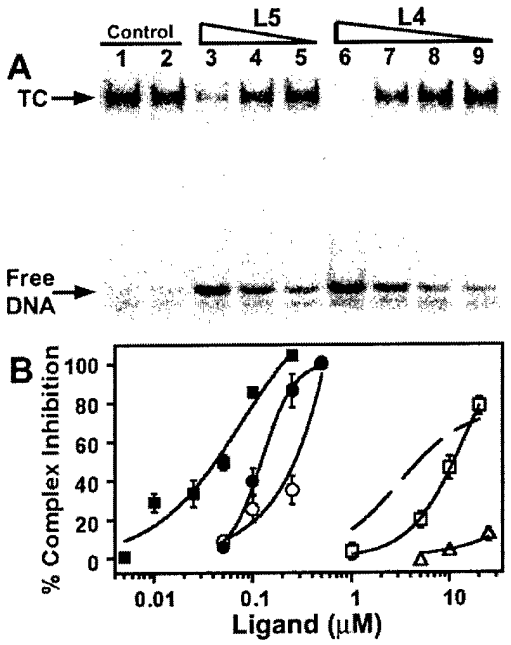

Fig. 2. Effect of agents on complex formation in EMSAs. (*A*) Representative EMSA showing drug inhibition of TC formation on the SRE. DNA-binding agent and oligo were co-incubated 30 min at room temperature before the addition of purified TFs, followed by another 30-min incubation and electrophoresis on a polyacrylamide gel. Lanes: 1 and 2, controls; 3, 4, and 5, 20 μM, 10 μM, and 5 μM **L5**, respectively; 6, 7, 8, and 9, 0.5 μM, 0.25 μM, 0.1 μM, and 0.05 μM **L4**, respectively. (*B*) Inhibition curves for drug effects on TC formation. Quantitation of autoradiographs as in *A* allowed percent inhibition to be plotted against drug concentration for: **L1** (△), **L2** (■), **L3** (●), **L4** (○), **L5** (□), and Hoe342 (– – –). Results are from three experiments (mean value ± SE).

Inhibition of Cell-Free Transcription. In general, although minor groove-binding agents may successfully inhibit TF/DNA interactions in simple EMSAs, many are known to lose relative potency as assay conditions become more complex and are less effective as inhibitors of gene expression (14, 17, 20). To determine whether the five MGTs exhibited similar characteristics, their ability to inhibit cell-free expression in the presence of additional DNA and proteins was analyzed next. In the cell-free transcription assay, a linearized plasmid containing the full-length human c-fos promoter is co-incubated with DNA-binding ligand before a nuclear lysate and radiolabeled nucleotides are added. The resulting transcript is isolated and electro-

Table 1. Comparison of agent potencies on inhibiting TF complexes on the c-fos promoter

	IC_{50} values, μM		
Compound	EMSA: TC formation	Cell-free transcription	N. blot: c-fos expression
L1	>10	nd	*
L2	0.041	0.62	9
L3	0.12	3.15	*
L4	0.32	4.8	*
L5	10.9	27.3	*
Hoe342	4.8	16.8	*

IC_{50} values were obtained from inhibition curves as in Figs. 2*B* and 3*B*. N., Northern; nd, not determined.
*No inhibition was noted at 10 μM.

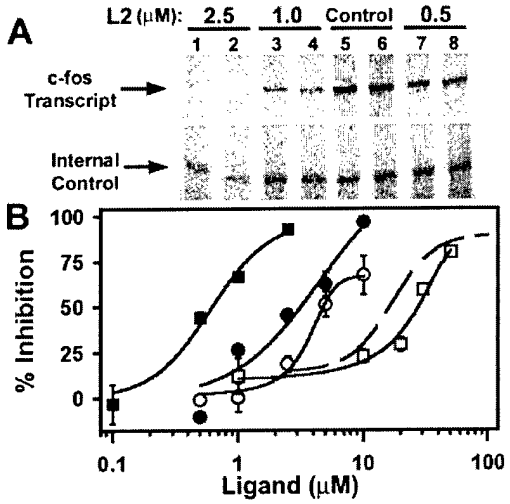

Fig. 3. Effect of agents on c-fos promoter-driven cell-free transcription. (*A*) Representative autoradiograph of assay results using **L2**. A linearized plasmid containing the full-length human c-fos promoter was co-incubated with DNA-binding agent before nuclear lysate, and a mix of radiolabeled nucleotides were added. Analysis of the purified transcript (upper arrow) was as described in the text. A radiolabeled, 250-base transcript (lower arrow) served as a loading control. **L2** concentrations are indicated. (*B*) Effect of agents on cell-free transcription. Normalizing transcripts to internal controls allowed percent inhibition to be calculated and plotted against drug concentration for: **L2** (■), **L3** (●), **L4** (○), **L5** (□), and Hoe342 (– – –). Results are from three experiments (mean value ± SE).

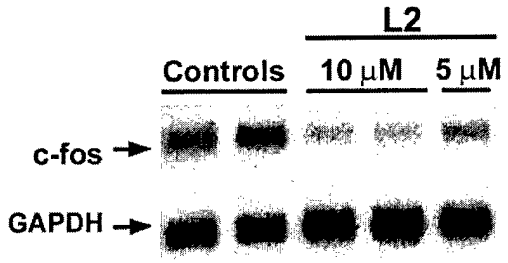

Fig. 4. Effects of **L2** in NIH 3T3 cells. (*A*) **L2** inhibits endogenous c-fos expression. NIH 3T3 cells were exposed to **L2** for 16 h in the presence of low (0.5%) serum. Expression of c-fos was induced by raising serum concentration to 15%. Total RNA was isolated 30 min later and processed as described in the text. Hybridization to radiolabeled cDNA probes for c-fos and GAPDH followed. **L2** concentrations are indicated.

phoresed on a denaturing polyacrylamide gel, where it is identified on the basis of its known size. In the absence of DNA-binding ligand, a high-intensity transcript is produced (Fig. 3*A*, lanes 5 and 6, upper arrow). Treating the plasmid with **L2** results in a dose-dependent decrease in transcript formation (lanes 1–4 and 7–8). After normalizing the transcripts to internal controls (lower arrow), percent inhibition was calculated and inhibition curves were plotted (Fig. 3*B*). Because **L1** exhibited such poor activity in the EMSAs, it was not analyzed in this assay. The inhibition curve profiles for the remaining agents were similar to the EMSAs: **L2** was most potent while **L5** exhibited the lowest potency. However, the gap between the least and most effective agents has narrowed appreciably. Overall, higher concentrations of the agents were needed to inhibit transcription as compared with the EMSAs, with the highest increase (≈26 fold) noted for **L3**. Notably, **L2** was significantly more effective than the other agents tested. Its potency exceeded that of its pyrrole/propylamine analog **L5** by 44-fold (Table 1).

Effect of the Agents on Cellular Gene Expression. Because the potency of **L2** in the cell-free transcription assay was promising, we analyzed this and the other compounds more rigorously by evaluating their effects on endogenous c-fos expression in NIH 3T3 cells. The dependence of c-fos transcription on the formation of a functional TC, its serum inducibility, and its 30-min mRNA half-life (21, 22) facilitated this analysis. Evaluation of the agents showed that only **L2** inhibited c-fos expression in NIH 3T3 cells after a 16-h exposure (Fig. 4 and Table 1). At 10 μM, **L2** inhibited c-fos expression by about 60%. The absolute level of GAPDH mRNA was unchanged. The remaining agents, at concentrations up to 10 μM for 16 h, failed to inhibit c-fos transcription here.

Collateral Effects of the Agents. Because the DNA-binding ligands proved to be effective inhibitors of transcription in cell-free assays and because we were interested in characterizing the biological activity of these agents more fully, we wished to explore whether other activities (unrelated to c-fos expression) were affected by their association with DNA. As an enzyme that maintains DNA topology, topo II induces a doublestrand break, becomes covalently attached to the free DNA ends, and passes the strands through the gap before resealing them (23). Its activity can be measured by trapping the covalent topo II/DNA complex in its intermediate form through the use of drugs such as VM-26, followed by precipitation and quantitation of the complexed DNA (see *Methods*). Minor groove-binding drugs have been found to inhibit the catalytic activity of topo II in this assay (18). The percent inhibition of topo II activity in isolated nuclei obtained at 20 μM for each agent are presented in Table 2. It was noted that the effectiveness of the agents did not correlate to their potencies in the EMSAs or cell-free transcription assays. For example, **L3** inhibited topo II less than would be expected based on its potency in the latter assays. Conversely, **L5**, which was the least potent compound in the previous cell-free evaluations, inhibited topo II activity better than Hoe342 and roughly as well as **L3**.

Because the agents demonstrated an ability to inhibit topo II activity in nuclei and because **L2** could decrease endogenous gene expression, we wondered whether they might affect cell survival. Representative results are shown for **L2** in Fig. 5. We found that **L2** decreased NIH 3T3 viability after a 3-day continuous exposure. Over 80% cell death was effected by 10 μM. Concentrations needed to kill 50% of the cells (LD_{50} values) are presented in Table 2. Analysis of the other agents revealed that

Table 2. Collateral effects of the agents

Compound	Topo II % inhibition*	Cytotoxicity LD_{50}†, μM
L1	49.9	7.0
L2	95.1	6.6
L3	59.6	>10
L4	91.0	‡
L5	61.9	‡
Hoe342	49.3	3.4

*Percent inhibition of topo II activity in HeLa nuclei at 20 μM drug. Nuclei from [^{14}C]thymidine-labeled HeLa cells were treated with 20 μM DNA-binding agent for 10 min at 37°C. The crosslinking agent VM-26 was added to a final concentration of 20 μM and reactions were incubated 15 min. DNA-protein crosslinks were quantitated following sodium dodecyl sulfate precipitation. Results are from three experiments.

†LD_{50} values were calculated from dose-response curves as shown in Fig. 5.

‡No effect at 10 μM.

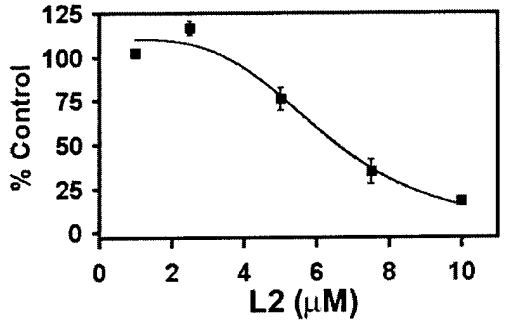

Fig. 5. L2 decreases cell viability. NIH 3T3 cells were continuously exposed to L2 under normal growth conditions for 3 days before being counted as described in the text. Percent control growth was calculated by comparing drug treated samples to controls. Results are from three experiments containing triplicate samples (mean value ± SE).

L3 was also able to kill cells, but required higher concentrations to achieve the same effects as the former compound. After 3 days, only 40% of the cells were killed by 10 μM L3. While Hoe342 was about 2-fold more potent than L2, the polypyrrole MGTs L4 and L5 were ineffective up to 10 μM. Interestingly, although L1 was unable to decrease endogenous c-fos expression, it was approximately as cytotoxic as L2.

Discussion

Much effort has been applied toward developing DNA-reactive agents that bind longer sequences with high affinity and greater selectivity. Designing such agents that inhibit DNA-related functions but still maintain cellular permeability can be a formidable task. We have demonstrated that these goals can be achieved by using a unique strategy of equipping minor groove-binding ligands with functional groups that allow for electrostatic contact with the phosphodiester backbone. When L1, chosen for its ability to preferentially bind long A/T sites at nanomolar concentrations, was functionalized with propylamines to yield L2, its ability to inhibit TF complexes was enhanced by at least 1,000-fold. It is the first MGT to maintain significantly improved potency relative to a classical minor groove binder in the cell-free transcription assay and is also the first MGT to inhibit endogenous gene expression in whole cells.

The structure/activity relationships apparent from our studies provide some insight into how MGT design plays a role in determining inhibitory profiles. Compounds lacking basic side chains (L1 and Hoe342) were poor inhibitors of TC formation in EMSAs. Although equipping a bisbenzimidazole with a tripyrrole improves its binding affinity and ability to distinguish between A/T-rich sites of different lengths, it appears that this alone is not enough to create an ideal TF complex inhibitor. The polyamine tails on each of L2's pyrroles apparently not only endow it with a capability to bind dsDNA at subpicomolar levels (25), but also impart a vastly improved TF inhibitory potency compared with L1. Although the SRE contains only six contiguous A/T bp rather than the optimal nine, this site was sufficient for L2 binding. TFs that bind longer A/T-rich sites may prove to be even better targets. Inhibitory potency, like DNA binding affinity, correlated with pyrrole/polyamine side chain length, because L3 and L5 were less potent than their longer analogs L2 and L4, respectively.

Although all of the agents are A/T selective and can potentially disrupt SRF binding and subsequent TC formation, their potencies in the cell-free assays may depend on their intrinsic chemistry and how well they bind to the SRE sequence provided. For example, the small size of L5 may prevent it from providing adequate steric hindrance or from altering DNA conformation enough to effectively inhibit TF binding. The increased length of L4 may improve these characteristics and make it nearly as effective as the bisbenzimidazoles L2 or L3. The latter agents, with their potential to provide more extensive distortion over a longer sequence, may overcome the limitations of the classical minor groove binders and even the polypyrrole-based MGTs, making them more effective and potent transcriptional inhibitors.

The EMSA trends noted above were also apparent in the cell-free transcription assay, where a more complex environment provides a more rigorous assessment of an agent's ability to inhibit TF/DNA interactions. While the order of potency was the same as that observed in the EMSAs, drastic drops in effectiveness were noted (Table 1). Loss of DNA-binding drug potency in this assay has been observed before (14, 15) and is expected, because the increased amount and length of DNA provide a greater number of potential drug binding sites. More DNA-binding proteins may also interfere with drug binding to the SRE. The ability of L3 to inhibit transcription was especially hindered, because a 26-fold higher concentration was required compared with the EMSAs. In notable contrast to the other compounds, L2 inhibited transcription by 50% at submicromolar levels, an order of magnitude improvement over L5 or Hoe342. Overall, the results suggest that conjugating pyrrole/polyamine constructs to bisbenzimidazoles not only enhances effectiveness in EMSAs, but also proportionately maintains potency in the presence of additional proteins and more DNA with greater sequence complexity.

Although L2 was designed to bind DNA, its effect on another template-related activity, topo II, was significantly less than its ability to decrease gene expression, suggesting that its collateral damage effects are minimal. We noted that higher drug concentrations were needed in the topo II activity assays, which may be partially attributable to increased amounts of DNA in the nuclear environment. The most effective agents in this assay, L2 and L5, both possessed tripyrrole/propylamine functional groups, but there was little correlation between potencies in the cell-free assays and the ability to inhibit topo II activity in nuclei. This suggests that topo II inhibition may rely on ligand characteristics that are different from those required for TF complex inhibition. Because topo II is a processive enzyme, it may not be affected by the agents in the same way that TFs are. At 20 μM Hoe342, both cell-free transcription and topo II activity are inhibited nearly equally. In contrast, 2 μM L2 completely inhibited cell-free transcription but had no effect on topo II (data not shown). This observation suggests that L2 might be more selective for inhibiting TF complexes compared with other DNA-template related activities. Because different Hoechst analogs inhibited topo II activity with varying degrees of potency in previous studies (18), it is reasonable to postulate that additional modification of the fluorescent MGTs may eventually yield compounds with improved selectivity for inhibiting other desired DNA template functions.

The superior potency of L2 was further demonstrated when it was found to be the only agent with the ability to inhibit endogenous gene expression. A 16-h exposure to 10 μM L2 was sufficient to inhibit c-fos transcription in NIH 3T3 cells by over 50%. Serum-starved cells have undetectable levels of c-fos mRNA and transcription is up-regulated only upon serum induction. Therefore, any decrease in c-fos mRNA is likely attributable to direct drug effects on transcription. The inhibition of c-fos transcription suggests that L2 is cell-permeable and can localize to the nucleus. There was no effect on total GAPDH mRNA levels. The longer half-life of GAPDH mRNA [8 h, compared with 30 min for c-fos (24)] may only partially account for this observation. If L2 was capable of down-regulating GAPDH immediately upon drug treatment, there should have been a detectable decrease in its mRNA. This observation has

been made for other DNA-binding drugs, suggesting that GAPDH may be relatively insensitive to down-regulation by such agents (14). The other MGTs may have no effect on gene expression because of lower bioavailability or because their potency in the whole cell environment is too weak. Additionally, binding of the agents to other A/T-rich sites in the genome may lower the effective concentration available to inhibit TF complex formation on the SRE. This nonspecific binding is likely contributing to the lower potency of **L2** in whole cells, because an order of magnitude more drug is required to inhibit endogenous c-fos transcription compared with cell-free assays (24).

The overall activity profile of **L2** is therefore consistent with its binding to DNA in whole cells, an event that affects gene regulation and might contribute to its cytotoxicity. Although **L3** was unable to decrease c-fos expression in NIH 3T3 cells after 16 h, it effected cell death after 3 days of continuous exposure, suggesting that it may take longer to accumulate to bioreactive levels in cells, or that its cytotoxic mechanism of action may not depend solely on its ability to bind DNA. This latter possibility may also apply to **L1**, which was cytotoxic, but unable to inhibit c-fos gene expression.

Earlier MGT studies demonstrated that rationally designed agents with the potential to contact both grooves are more potent inhibitors of TF/DNA interactions than agents that interact solely with a single groove (8). The current study corroborates these findings but also surpasses them, because the rationale used resulted in agents that inhibited TF complex formation in EMSAs as well as cell-free transcription assays and also decreased gene expression in whole cells. Specifically, combining the pyrrole/polyamine-based structure of the MGTs with a bisbenzimidazole moiety yielded agents (**L2**, **L3**, and **L4**) that were significantly more potent TF complex inhibitors than the classical minor groove-binder Hoe342. It is of interest to note that our work suggests that the polypyrrole/polyamine and bisbenzimidazole moieties may contribute separately to MGT activity characteristics. The tripyrrole/propylamine functional group was essential for potent inhibition of TC formation, because **L4** was an effective inhibitor and **L1** was not. Furthermore, this expands the possibilities for MGT design, because it has now been demonstrated that equipping each pyrrole with a polyamine does not compromise the agent's inhibitory activity in cell-free assays. A bisbenzimidazole attached to **L4** to yield **L2** was only slightly more potent than the former in the cell-free assays, but inhibited gene expression in whole cells. Thus, it appears that the bisbenzimidazole moiety is essential for cellular activity. The combination of bisbenzimidazole and tripyrrole/propylamine therefore seems particularly well suited for inhibiting TF/DNA contacts in both cell-free assays and cellular assays. In contrast, the *p*-OH bisbenzimidazole Hoechst 33258 shows little cellular activity, suggesting that the nature of terminal ring substituents may have profound effects on the cellular uptake and/or biological effects of these compounds.

The enhanced potency observed when minor groove-binding agents are equipped with constructs capable of electrostatically interacting with the phosphodiester backbone has implications for future drug design. Logical construction of a bisbenzimidazole functionalized with a tripyrrole/propylamine tail yielded a MGT, **L2**, with significantly improved ability to inhibit TF complex formation in cell-free assays and to decrease gene expression in the whole cell environment. Similar stimulation of activity may therefore be seen by endowing other minor groove-binding compounds with the ability to contact the DNA backbone. The correlations among pyrrole/polyamine subunit number, polyamine tail length, and potency can be investigated further to determine whether additional increases in subunit number and/or modified polyamine tails will create even more powerful and selective agents.

This work was supported by National Cancer Institute Grant CA16056 (to T.A.B.), American Cancer Society Grant DHP 158 (to T.A.B.), U.S. Army Medical Research Grant BC980100 (to C.M.W), and National Institutes of Health Grant 5R37DK0917136 (to T.C.B.)

1. Wemmer, D. E. & Dervan, P. B. (1997) *Curr. Opin. Struct. Biol.* **7,** 355–361.
2. Chiang, S. Y., Welch, J. J., Rauscher, F. J., 3rd, & Beerman, T. A. (1996) *J. Biol. Chem.* **271,** 23999–24004.
3. Dorn, A., Affolter, M., Muller, M., Gehring, W. J. & Leupin, W. (1992) *EMBO J.* **11,** 279–286.
4. Schleif, R. (1988) *Science* **241,** 1182–1187.
5. Bruice, T. C., Houng, Y. M., Gong, X. H. & Lopez, V. (1992) *Proc. Natl. Acad. Sci. USA* **89,** 1700–1704.
6. Browne, K. A., Gong, X. H. & Bruice, T. C. (1993) *J. Am. Chem. Soc.* **115,** 7072–7079.
7. Gong, X. H., Browne, K. A., Groppe, J. C., Blasko, A., Houng, Y. M. & Bruice, T. C. (1993) *J. Am. Chem. Soc.* **115,** 7061–7071.
8. Chiang, S. Y., Bruice, T. C., Azizkhan, J. C., Gawron, L. & Beerman, T. A. (1997) *Proc. Natl. Acad. Sci. USA* **94,** 2811–2816.
9. Satz, A. L. & Bruice, T. C. (1999) *Bioorg. Med. Chem. Lett.* **9,** 3261–3266.
10. Satz, A. L. & Bruice, T. C. (2000) *Bioorg. Med. Chem.* **8,** 1871–1880.
11. Treisman, R. (1992) *Trends Biochem. Sci.* **17,** 423–426.
12. Huang, K., Louis, J. M., Donaldson, L., Lim, F. L., Sharrocks, A. D. & Clore, G. M. (2000) *EMBO J.* **19,** 2615–2628.
13. Mo, Y., Vaessen, B., Johnston, K. & Marmorstein, R. (2000) *Nat. Struct. Biol.* **7,** 292–297.
14. White, C. M., Heidenreich, O., Nordheim, A. & Beerman, T. A. (2000) *Biochemistry* **39,** 12262–12273.
15. Bellorini, M., Moncollin, V., D'Incalci, M., Mongelli, N. & Mantovani, R. (1995) *Nucleic Acids Res.* **23,** 1657–1663.
16. Satz, A. L. & Bruice, T. C. (2001) *J. Am. Chem. Soc.* **123,** 2469–2477.
17. Chiang, S. Y., Azizkhan, J. C. & Beerman, T. A. (1998) *Biochemistry* **37,** 3109–3115.
18. Beerman, T. A., McHugh, M. M., Sigmund, R., Lown, J. W., Rao, K. E. & Bathini, Y. (1992) *Biochim. Biophys. Acta* **1131,** 53–61.
19. Woynarowski, J. M., Sigmund, R. D. & Beerman, T. A. (1988) *Biochim. Biophys. Acta* **950,** 21–29.
20. Chiang, S. Y., Burli, R. W., Benz, C. C., Gawron, L., Scott, G. K., Dervan, P. B. & Beerman, T. A. (2000) *J. Biol. Chem.* **275,** 24246–24254.
21. Greenberg, M. E. & Ziff, E. B. (1984) *Nature (London)* **311,** 433–438.
22. Treisman, R. (1985) *Cell* **42,** 889–902.
23. Burden, D. A. & Osheroff, N. (1998) *Biochim. Biophys. Acta* **1400,** 139–154.
24. Dani, C., Piechaczyk, M., Audigier, Y., El Sabouty, S., Cathala, G., Marty, L., Fort, P., Blanchard, J. M. & Jeanteur, P. (1984) *Eur. J. Biochem.* **145,** 299–304.
25. Satz, A. L. & Bruice, T. C. (2001) *Bioorg. Med. Chem.*, in press.